Stability of Exomoons Around Giant Planets

Ricardo Aparecido de Moraes

Ricardo Aparecido de Moraes

Stability of Exomoons Around Giant Planets

Relatório de Pós-doutorado realizado na Universidade Estadual Paulista (UNESP), Faculdade de Engenharia e Ciências, Guaratinguetá.

Supervisor: Prof. Dr. Othon Cabo Winter

CAPES PrInt - 88887.310463/2018-00

GUARATINGUETÁ
2025

Resumo

O presente relatório descreve as atividades do pesquisador no período de Janeiro de 2021 à Janeiro de 2023 durante a realização do projeto entitulado “Stability of Exomoons Around Giant Planets” (CAPES/PRINT). O relatório está organizado da seguinte maneira: No capítulo 1, fazemos um pequeno resumo do projeto original, descrevems as etapas cumpridas e apresentamos a produção acadêmica gerada a partir dos resultados obtidos. No capítulo 2, apresentamos nossa participação em projetos de extensão universitária. No capítulo 3, descrevemos as atividades didáticas realizadas. Nos anexos são apresentados os comprovantes das atividades descritas neste relatório.

Sumário

1 Atividades de pesquisa **4**

1.1 Resumo do projeto . . . 4

1.2 Descrição das atividades de pesquisa . . . 5

1.2.1 Etapa 1 - Estabilidade de múltiplas exomoons (2021) . . . 5

1.2.2 Etapa 2 - Estabilidade de exomoons co-orbitais (2022) . . . 6

1.3 Produção acadêmica . . . 8

1.3.1 Artigos publicados . . . 8

1.3.2 Artigos submetidos . . . 8

1.4 Participação em eventos e congressos . . . 8

2 Atividades de Extensão Universitária **11**

3 Atividades didáticas e de orientação **12**

3.1 Atividades didáticas . . . 12

3.2 Atividades de orientação . . . 12

3.2.1 Co-orientação de Mestrado . . . 12

3.3 Participação em bancas[1] . . . 13

4 Anexos **14**

4.1 Moraes et al., 2022 . . . 14

4.2 Moraes et al., 2023 - aceito na MNRAS . . . 29

4.3 Sfair et al., 2025 - submetido . . . 45

4.4 Certificado XXV Escola de Verão em Dinâmica Orbital e Planetologia . . . 55

4.5 Certificado XX Colóquio Brasileiro de Dinâmica Orbital . . . 57

4.6 Certificado XXVI Escola de Verão em Dinâmica Orbital e Planetologia . . . 59

4.7 Livro de resumos dos pôsteres XI Taller de Ciencias Planetarias . . . 61

4.8 Certificado 2nd International Stardust Conference - STARCON 2 . . . 65

4.9 Certificado XXI Colóquio Brasileiro de Dinâmica Orbital . . . 67

4.10 Comprovante de atividade didática . . . 69

4.11 Comprovante de orientação de Mestrado - Julio Cesar Monteiro dos Santos 71

[1]Apenas as participações como membro titular ou membro convidado são apresentadas, participações como membro suplentes foram omitidas

4.12 Comprovante de participação em banca de defesa de Mestrado - Julio Cesar Monteiro dos Santos 73
4.13 Comprovante de participação em banca de qualificação de Doutorado - Tiago Francisco Lins Leal Pinheiro 75

Referências **77**

Capítulo 1

Atividades de pesquisa

1.1 Resumo do projeto

O objetivo principal do nosso projeto era responder a seguinte pergunta: "Considerando a maré planetária como a fonte principal de perturbações, quais são as características dos sistemas favoráveis a hospedar *exomoons* detectáveis?". Dessa forma, nosso projeto tinha como foco estudar a estabilidade de satélites naturais hipotéticos ao redor de planetas extrassolares, considerando que esses satélites seriam perturbados por efeitos gravitacionais originários da deformação do planeta hospedeiro.

Apesar de diversos candidatos à *exomoons* serem propostos na literatura (Bennett et al., 2014; Ben-Jaffel and Ballester, 2014; Lewis et al., 2015; Hippke, 2015; Teachey et al., 2018; Heller et al., 2019; Oza et al., 2019; Fox and Wiegert, 2021; Kipping et al., 2022), luas ao redor de exoplanetas ainda não foram confirmadas. Isso se deve principalmente a falta de tecnologia suficiente para a detecção desses objetos. Desta forma, o primeiro desafio do nosso projeto é estabelecer o que seria uma *exomoon* detectável, dada a tecnologia atual. O projeto *Hunt for Exomoons with Kepler* (HEK) (Kipping et al., 2012) mostrou que *exomoons* com massas acima de 0.2 massas terrestres ($M_\oplus$) podem ser detectadas com a tecnologia e os métodos de detecção atuais, em especial o método de trânsito planetário. Essa estimativa é corroborada pela detecção de exoplanetas com massas inferiores ao limite de 0.2 $M_\oplus$, por exemplo o exoplaneta Kepler-37 b (Barclay et al., 2013) que é menor que o planeta Mercúrio. Contudo, atualmente os dois candidatos à *exomoons* mais favoráveis são ambos corpos com dimensões e massas comparáveis à planetas do tipo super-Terra ou Netuno (Teachey et al., 2018; Kipping et al., 2022). Assim, em nossos estudos iremos trabalhar com satélites com massas variando entre as massa do planeta Marte, 0.107 $M_\oplus$, e do planeta Netuno, 17.15 $M_\oplus$. Ao assumir esse intervalo de massa para os satélites, nós implicitamente também decidimos que estudaremos apenas sistemas contendo exoplanetas gigantes, com massas comparáveis a massa de Júpiter (M_{Jup}), nominalmente os sistemas Kepler-1625 e Kepler-1708, que são àqueles onde *exomoons* foram propostas.

A estabilidade de *exomoons* está especialmente ligada com a forma como esses corpos são afetados pela maré do planeta hospedeiro, especialmente os satélites localizados mais internamente (Barnes and O' Brien, 2002; Alvarado-Montes et al., 2017; Sucerquia et al., 2020). No entanto, o achatamento do planeta também pode interferir na estabilidade dos satélites (Greenberg, 1974). Dessa forma, um modelo mais robusto de estabilidade para *exomoons* deve levar em conta estes dois efeitos.

1.2 Descrição das atividades de pesquisa

Com o objetivo de estudar a estabilidades de *exomoons*, o projeto de pesquisa foi dividido em três etapas. A seguir descrevemos as atividades correspondentes a cada etapa.

1.2.1 Etapa 1 - Estabilidade de múltiplas exomoons (2021)

A primeira etapa do projeto era focada em: i) definir o tipo de recurso numérico utilizado para o tratamento do problema; ii) testar o recurso escolhido, comparando nossos com resultados da literatura; iii) escolher as condições iniciais que norteariam nosso estudo sobre estabilidade; iv) estudar a estabilidade de múltiplas *exomoons*.

Uma vez que o principal efeito perturbativo considerado em nosso trabalho é o efeito de maré, nós optamos por utilizar o pacote numérico POSIDONIUS (Blanco-Cuaresma and Bolmont, 2017). O pacote POSIDONIUS é o sucessor do tradicionalmente utilizado MERCURY-T (Bolmont et al., 2015), no qual foram corrigidos e aprimorados diversos aspectos acerca da implementação da maré planetária. Por ser uma ferramenta nova, diversos testes foram realizados utilizando como parâmetros alguns resultados conhecidos da literatura, especialmente os apresentados em Bolmont et al. (2015).

Motivados pelos resultados de Moraes and Vieira Neto (2020), na primeira etapa do projeto decidimos estudar estabilidade de um segundo satélite massivo no sistema Kepler-1625. Para isso, consideramos que o sistema seria composto pelo planeta, Kepler-1625 b, pelo candidato à satélite, Kepler-1625 b-I, e um satélite extra com as características da Terra, que estaria localizado entre os planeta e o candidato proposto. Dessa forma, estudamos como os efeitos de maré e do achatamento do planeta influenciariam a estabilidade desse segundo satélite. Nossos resultados mostram que um segundo satélite com as características da Terra pode ser estável nesse sistema, porém a posição e a excentricidade desse satélite seriam limitadas pelos efeitos de maré do sistema. Nós mostramos que, em geral, esse segundo satélite estaria localizado mais próximo do planeta em órbitas quase circulares, exceto no caso onde ressonâncias de movimento médio entre os satélites manteriam o satélite secundário mais afastado do planeta e em órbitas excêntricas.

Os resultados do nosso trabalho foram publicados no início de 2022 na revista *Monthly Notices of the Royal Astronomical Society* (MNRAS) com o título “On the stability of additional moons orbiting Kepler-1625 b" (Moraes et al., 2022). O artigo pode ser encontrado em doi.org/10.1093/mnras/stab3576 e no anexo 4.1 deste relatório.

Neste trabalho destaca-se a participação do pesquisador do exterior Dr. Gabriel Borderes-Motta, à época pós-doutorando na Universidade Carlos III de Madrid, Espanha e do aluno de Mestrado do Programa de Pós-Graduação em Física da FEG-UNESP, Julio Cesar Monteiro dos Santos.

1.2.2 Etapa 2 - Estabilidade de exomoons co-orbitais (2022)

Inicialmente, a segunda etapa do projeto previa o estudo da estabilidade de múltiplos satélites ao redor de exoplanetas gigantes mais distantes da estrela, os chamados planetas *cool-giants*. À época da proposta do projeto, não existiam candidatos à satélites identificados ao redor dessa classe de planetas, porém, recentemente Kipping et al. (2022) conduziram uma busca por satélites ao redor de mais de 80 planetas gigantes com massas comparáveis a massa de Júpiter, orbitando sua estrela hopedeira com um semieixo maior maior que 1 unidade astronômica (au). A partir dessa investigação, os autores encontraram sinais de uma lua com cerca de 2.61 raios da Terra ($R_{\oplus}$) ao redor do planeta Kepler-1708 b, dessa forma o candidato Kepler-1708 b-I foi proposto. Os próprios autores conduziram uma análise preliminar acerca da estabilidade do satélites e encontraram que o candidato seria estável. Ainda, esse satélite teria chegado a sua posição atual após forte interação com a maré planetária.

Tendo em vista o novo candidato e os resultados apresentados em Moraes et al. (2022), optamos por investigar a estabilidade de satélites co-orbitais aos candidatos propostos nos sistemas Kepler-1625 e Kepler-1708. Por simplicidade, desconsideramos quaisquer outros efeitos além da interação gravitacional mútua entre os corpos. Nós optamos por trabalhar com dois tipos de sistemas diferentes: i) um sistema composto pelo planeta e os dois satélites co-orbitais e; ii) um sistema composto pela estrela, planeta e os dois satélites co-orbitais. Para o satélite co-orbital nós variamos a massa e o tamanho desses corpos, sendo que o menor desses corpos tinha as características do planeta Marte e o maior corpo teria a mesma massa e raio do que a candidato à satélite proposto.

Para os sistemas onde a estrela foi negligênciada, nós encontramos que ambos os sistemas, Kepler-1625 and Kepler-1708, são capazes de hospedar satélites co-orbitais massivos. Ainda, encontramos que alguns resultados do problema restrito de três corpos também são aplicáveis para o caso não-restrito no estudo de corpos co-orbitais. Assim como no caso restrito, nós encontramos que o satélite co-orbital fica confinado ao redor do ponto de equilíbrio Lagrangiano L_4 descrevendo um movimento similar à uma órbita do tipo girino. O movimento do satélite co-orbital é composto por dois movimentos diferentes, o primeiro sendo um movimento de longo período do epicentro do satélite co-orbital ao redor de L_4. Ao redor do epicentro, um segundo movimento epicíclico de curto período também foi encontrado. Nossos resultados mostram que nos casos onde há ressonâncias entre os períodos de libração desses dois movimentos, a estabilidade do par co-orbital é comprometida.

Ao considerar a estrela nos sistemas, nós encontramos que os efeitos gravitacionais devido a proximidade da estrela no sistema Kepler-1625 impedem que satélites co-orbitais massivos sejam possíveis. Por outro lado, a adição da estrela não alterou os resultados para o sistema Kepler-1708, uma vez que a separação estrela-planeta é maior. Ainda, para o sistema Kepler-1708, fomos capazes de estudar os efeitos da presença de um satélite co-orbital na variação do tempo de trânsito (TTV) do planeta. Dessa forma, nosso trabalho pode ser utilizado para futuros estudos que almejam detectar *exomoons*.

Nossos resultados foram compilados em formato de artigo científico intitulado "The Dynamics of Co-orbital Giant Exomoon - Applications for the Kepler-1625 b and Kepler-1708 b Satellite Systems". O trabalho foi aceito para publicação na MNRAS em 2022 e mais posteriormente publicado em 2023, após o encerramento das atividades deste projeto. O artigo pode ser encontrado em doi.org/10.1093/mnras/stad314 e no anexo 4.2 deste relatório.

Neste trabalho, buscamos a colaboração da Profa. Dra. Daniela Cardoso Mourão do Departamento de Matemática da FEG-UNESP, dada a sua notada experiência no estudo de corpos co-orbitais.

Ainda durante a Etapa 2 do nosso projeto, foi iniciado um trabalho de exploração da origem do asteroide co-orbital da Terra, (469219) Kamo'oalewa (Chodas, 2016; de la Fuente Marcos and de la Fuente Marcos, 2016). Kamo'oalewa é um dos menores co-orbitais da Terra e tem uma órbita estável do tipo quasi-satélite. Ainda, ao analisar o espectro desse objeto, Sharkey et al. (2021) encontrou sinais de que Kamo'oalewa pode ter uma composição compatível com silicatos encontrados na Lua, tal que esse asteroide poderia ter sido no passado uma parte do satélite natural terrestre.

Nosso trabalho envolve pesquisadores da FEG-UNESP, da Universidade de Tübingen na Alemanha, do Instituto Sueco de Física Espacial (IRF), e do Instituto Astronômico da Academia Tcheca de Ciências (ASU-CAS) e tem como objetivo explorar a possibilidade de pequenos corpos serem ejetados da Lua e se tornarem co-orbitais da Terra, com maior atenção para corpos que porventura alcancem órbitas do tipo quasi-satélite. Nós consideramos um sistema formado por Sol, Terra, Lua e partícula, tal que as partículas são ejetadas de pontos aleatórios da superfície lunar com vetor velocidade normal à superfície, apontando para fora dela. A velocidade de ejeção das partículas foi variada entre 1 e 7 vezes a velocidade de escape da Lua e o sistema foi integrado numericamente utilizando o pacote REBOUND (Rein and Liu, 2012) por 1000 anos.

Nossos resultados mostram que diversas partículas evoluíram para órbitas heliocêntricas dentro da região co-orbital da Terra. Essas partículas apresentaram uma evolução complexa, tal que por vezes encontramos partículas com órbitas que se alternam entre tipo ferradura e tipo quasi-satélite. Ainda, encontramos que o número de partículas que entram na região co-orbital da Terra apresenta uma forte relação com a velocidade de ejeção da superfície da Lua, uma vez que quanto menor a velocidade de ejeção, maior o número de objetos co-orbitais. Resultados da literatura indicam que objetos com as dimensões de Kamo'oalewa podem ter sido de fato ejetados da Lua (Singer et al., 2020), o que reforça nossa hipótese inicial.

A maior parte das simulações numéricas e análise de resultados foi feita durante a vigência deste projeto, contudo sua finalização se deu apenas em 2025. Este trabalho encontra-se submetido ao periódico "The Open Journal of Astrophysics" com o título "The Moon as a possible source for Earth's co-orbital bodies". A versão atual do artigo é apresentada no anexo 4.3.

A Etapa 3 do nosso projeto, que consistiria em estudar a estabilidade de sistemas planetários compactos estava prevista para ser realizada em 2023.

1.3 Produção acadêmica

1.3.1 Artigos publicados

1. **MORAES, R A**; BORDERES-MOTTA, G ; WINTER, O C ; MONTEIRO, J. On the stability of additional moons orbiting Kepler-1625 b. **Monthly Notices of the Royal Astronomical Society**, v. 510, p. 2583-2596, 2022. (Anexo 4.1).

2. **MORAES, R A**; BORDERES-MOTTA, G ; WINTER, O C ; MOURÃO, D. The dynamics of co-orbital giant exomoons - applications for the Kepler-1625 b and Kepler-1708 b satellite systems. **Monthly Notices of the Royal Astronomical Society**, v. 520, p. 2163-2177, 2023. (Anexo 4.2).

1.3.2 Artigos submetidos

1. SFAIR, R; GOMES, L C; WINTER, O C; **MORAES, R A**; BORDERES-MOTTA, G; SCHÄFER, C M. The Moon as a possible source for Earth's co-orbital bodies. (Anexo 4.3).

1.4 Participação em eventos e congressos

A seguir apresentamos os congressos e eventos científicos aos quais participamos de maneira remota (online) ou presencial. Alguns congressos não emitiram certificado, para esses casos buscamos maneiras alternativas de comprovar nossa participação.

1. **Evento:** XXV Escola de Verão em Dinâmica Orbital e Planetologia
   Ano: 2021

Tipo da Apresentação: Oral
Modalidade: Online
Título da Apresentação: Exoplanetas
Certificado: Anexo 4.4.

2. **Evento:** XX Colóquio Brasileiro de Dinâmica Orbital
   Ano: 2021
   Tipo da Apresentação: Pôster
   Modalidade: Online
   Título da Apresentação: Stable Orbits In the Kepler 1625b Satellite System
   Certificado: Anexo 4.5.

3. **Evento:** XXVI Escola de Verão em Dinâmica Orbital e Planetologia
   Ano: 2022
   Tipo da Apresentação: Oral
   Modalidade: Online
   Título da Apresentação: Exoplanetas
   Certificado: Anexo 4.6

4. **Evento:** XI Taller de Ciencias Planetarias
   Ano: 2022
   Tipo da Apresentação: Pôster
   Modalidade: Online
   Título da Apresentação: Órbitas Estáveis no Sistema de Satélites de Kepler 1625b
   Certificado: O Congresso não emitiu certificados, mas segue no anexo 4.7 o livro de resumos dos pôsteres (Resumen 34). Adicionamos apenas a primeira página do livro e as páginas onde aparecem o nosso resumo.

5. **Evento:** 2nd International Stardust Conference - STARCON 2
   Ano: 2022
   Tipo da Apresentação: Oral
   Modalidade: Online
   Título da Apresentação: On the Possibility that 2016 HO3 Kamo'oalewa was a Piece of the Moon
   Certificado: Anexo 4.8.

6. **Evento:** XXI Colóquio Brasileiro de Dinâmica Orbital
   Ano: 2022
   Tipo da Apresentação: Oral
   Modalidade: Presencial

Título da Apresentação: The Dynamics of Co-orbital Giant Exomoons - Applications for the Kepler-1625 b and Kepler-1708 b Satellite Systems
Certificado: Anexo 4.9.

Capítulo 2

Atividades de Extensão Universitária

1. **Seminários GDOP (2021-)**
   Instituição: Universidade Estadual Paulista "Júlio de Mesquita Filho" - UNESP, Campuus de Guaratinguetá
   Função: Palestrante e responsável por convidar palestrantes
   Referência: https://www.youtube.com/channel/UC-8eTKrfxzta1M6EDoyVY2g.

2. **Escola de Verão de Dinâmica Orbital e Planetologia (2021-)**
   Instituição: Universidade Estadual Paulista "Júlio de Mesquita Filho" - UNESP, Campuus de Guaratinguetá
   Função: Palestrante
   Referência: Anexos 4.4 e 4.6.

3. **Asteroid Day Guaratinguetá Brasil (2022)**
   Instituição: Universidade Estadual Paulista "Júlio de Mesquita Filho" - UNESP, Campuus de Guaratinguetá
   Função: Palestrante
   Referência: https://www.dinamicaorbital.org/asteroid-day/.

Capítulo 3

Atividades didáticas e de orientação

Nosso projeto previa a atuação do proponente em atividades didáticas, lecionando disciplinas junto ao Programa de Pós-Graduação em Física da FEG-UNESP e também a orientação de alunos de Pós-graduação.

3.1 Atividades didáticas

- **Ensino de Pós-Graduação** (Anexo 4.10)
  Instituição: Universidade Estadual Paulista "Júlio de Mesquita Filho" - UNESP, Campuus de Guaratinguetá
  Função: Professor Responsável
  2021 - 2021: Tópicos Especiais "Formação de Satélites Regulares" (180h)
  2022 - 2022: Dinâmica Orbital (90h)

3.2 Atividades de orientação

3.2.1 Co-orientação de Mestrado

Concluída

- **Período:** 2020 - 2022 (Anexos 4.11 e 4.12)
  Aluno: Julio Cesar Monteiro dos Santos.
  Título da dissertação: Fluxo de Material para o Disco Circumplanetário Necessário para a Formação de Satélites de Planetas Gigantes.
  Orientador: Ernesto Vieira Neto.
  Apoio Financeiro: Fundação de Amparo à Pesquisa do Estado de São Paulo (FAPESP).

3.3 Participação em bancas[1]

- **Dissertação de Mestrado** (Anexo 4.12)
  Candidato: Julio Cesar Monteiro dos Santos.
  Título: Fluxo de Material para o Disco Circumplanetário Necessário para a Formação de Satélites de Planetas Gigantes.
  Membros: VIEIRA NETO, E; SOUSA R R; ROIG, F V; MORAES, R A.

- **Qualificação de Doutorado** (Anexo 4.13)
  Candidato: Tiago Francisco Lins Leal Pinheiro.
  Título: Constraining the nature of the nature of the possible extrasolar PDS110b ring system.
  Membros: SFAIR, R; MORAES, R A; BENEDETTI ROSSI, G.

[1] Apenas as participações como membro titular ou membro convidado são apresentadas, participações como membro suplentes foram omitidas

Capítulo 4

Anexos

4.1 Moraes et al., 2022

Monthly Notices of the ROYAL ASTRONOMICAL SOCIETY
MNRAS **510,** 2583–2596 (2022) https://doi.org/10.1093/mnras/stab3576

On the stability of additional moons orbiting Kepler-1625 b

R. A. Moraes ,[1]⋆ G. Borderes-Motta ,[2] O. C. Winter [1] and J. Monteiro [1]
[1]*UNESP, Universidade Estadual Paulista – Grupo de Dinâmica Orbital & Planetologia, Guaratinguetá, CEP 12.516-410, São Paulo, Brazil*
[2]*Bioengineering and Aerospace Engineering Department, Universidad Carlos III de Madrid, Leganés, 28911, Madrid, Spain*

Accepted 2021 December 4. Received 2021 December 3; in original form 2021 August 18

ABSTRACT
Since it was proposed, the exomoon candidate Kepler-1625 b-I has changed the way we see satellite systems. Because of its unusual physical characteristics, many questions about the stability and origin of this candidate have been raised. Currently, we have enough theoretical studies to show that if Kepler-1625 b-I is indeed confirmed, it will be stable. Regarding its origin, previous works indicated that the most likely scenario is capture, although conditions for in situ formation have also been investigated. In this work, we assume that Kepler-1625 b-I is an exomoon and study the possibility of an additional, massive exomoon being stable in the same system. To model this scenario, we perform *N*-body simulations of a system including the planet, Kepler-1625 b-I, and one extra Earth-like satellite. Based on previous results, the satellites in our system will be exposed to tidal interactions with the planet and to gravitational effects owing to the rotation of the planet. We find that the satellite system around Kepler-1625 b is capable of harbouring two massive satellites. The extra Earth-like satellite can be stable in various locations between the planet and Kepler-1625 b-I, with a preference for regions inside 25 R_p. Our results suggest that the strong tidal interaction between the planet and the satellites is an important mechanism to ensure the stability of satellites in circular orbits closer to the planet, while the 2:1 mean motion resonance between the Earth-like satellite and Kepler-1625 b-I would provide stability for satellites in wider orbits.

Key words: planets and satellites: dynamical evolution and stability – planets and satellites: individual: Kepler-1625 b-I.

1 INTRODUCTION

Natural satellites are common in our Solar system, and only two planets, Mercury and Venus, do not host any. The variety of satellites around planets is also remarkable. Regarding the size of satellites, there are larger satellites, such as the Galilean satellite Ganymede, which is larger than Mercury, and much smaller satellites, such as the inner Uranian satellites. Several special dynamical configurations are also found among the satellites of our Solar system; for example, there are satellites in resonance, most famously the three-body resonant chain, called the Laplace resonance, locking the motion of Io, Europa and Ganymede, and co-orbital satellites, such as the Janus–Epimetheus case around Saturn. In addition, it is not only planets that have satellites: in our Solar system, satellites are spotted around dwarf-planets, the famous Pluto–Charon binary system for example, and even around asteroids, such as in the case of the asteroid 65803 Didymos with its satellite Dimorphos (this system is the target of NASA's mission DART (Double Asteroid Redirection Test), launched on 2021 November 24).

The abundance and diversity of detected exoplanets suggest the possibility of an equally diverse population of extrasolar satellites, termed exomoons. To date, no exomoons are confirmed, even though many candidates have been proposed (Bennett et al. 2014; Ben-Jaffel & Ballester 2014; Lewis et al. 2015; Hippke 2015; Teachey, Kipping & Schmitt 2018; Heller, Rodenbeck & Bruno 2019; Oza et al. 2019; Fox & Wiegert 2021). The absence of confirmed exomoons is due mainly to the limitations of present technology and instruments. Given these constraints, only exomoons with masses greater than 0.1–0.5 Earth masses ($M_\oplus$) could be detected by transit (Heller et al. 2014), currently one of the most promising methods for the detection of exomoons. This lower limit for the mass covers bodies that are one order of magnitude more massive than the most massive satellite of our Solar system, Ganymede.

Exomoons are a subject of interest in part because they are potentially habitable. Heller et al. (2014) point out that, because of the number of Jupiter-like planets inside their respective stellar habitable zones, exomoons could be more likely to harbour biological life than exoplanets. Zollinger, Armstrong & Heller (2017) showed that Mars-like satellites around giant planets in low-mass star systems could be good candidates for habitability under certain assumptions. More recently, Ávila et al. (2021) explored the case of an Earth-like satellite around a 'free-floating' Jupiter-like planet and found that a significant amount of liquid water can be retained on the exomoon's atmosphere, and thus considered the simulated exomoons as capable of sustaining life.

Among the proposed exomoons, the most promising candidate is the one first presented by Teachey et al. (2018). These authors analysed the transit light curves from the *Kepler* telescope of the system Kepler-1625 and found signs of a Neptune-like satellite orbiting a giant planet. However, the analysis presented by Teachey et al. (2018) was based on only three transits of the planet. To confirm or refute the hypothesis of the exomoon's presence, Teachey & Kipping (2018) combined the transits from *Kepler* with one more

⋆ E-mail: ricardo.moraes07@gmail.com

transit signal from the *Hubble Space Telescope* (*HST*). They found that the new data supported the hypothesis of a moon around Kepler-1625 b. Furthermore, they were able to refine the possible semimajor axis of the candidate and the mass of the planet.

The exomoon candidate hypothesis was contested by Kreidberg, Luger & Bedell (2019), who presented a re-analysis of the *HST* observations using an independent data reduction method. They showed that the transit light curve was well fitted by a planet-only model, so that the addition of a moon did not improve the fit. Moreover, Kreidberg et al. (2019) concluded that the moon signal found by Teachey et al. (2018) were merely an artefact from data reduction.

Heller et al. (2019) also aimed to contribute to the debate. These authors presented an alternative interpretation for the *Kepler* and *HST* data previously analysed. Using an independent reduction method for the *HST* data and the transits from *Kepler*, Heller et al. (2019) found a solution that corroborated the planet–moon scenario initially proposed; however, they pointed out that this result should be viewed with caution because of the systematic errors in the data from *Kepler* and *HST*. It was suggested that the presence of an exomoon is not a secure detection and that alternative interpretations from the data could be considered; for example, that the later transit by Kepler-1625 b could be due to the presence of a non-detected inclined inner planet. In this case, the planet will be a hot Jupiter with its mass depending on the considered semimajor axis.

More recently, Teachey et al. (2020) applied different detrending models to the transit light curves presented in Teachey & Kipping (2018) and found that some reduction techniques are indeed capable of smoothing the moon signal. However, from a statistical point of view, the adoption of more flexible detrending models did not provide better evidence than simpler detrending models, pointing in favour of a planet–moon scenario. Furthermore, Teachey et al. (2020) investigated the differences between the analyses of Teachey & Kipping (2018) and Kreidberg et al. (2019) and could not find the source of the discrepancies between the two results. In this way, the authors argued that the noise properties from the two analyses were identical, such that the light curves presented by Kreidberg et al. (2019) are not better constrained than those published first.

All in all, the current status of the problem is undetermined, with the planet–exomoon model being a valid interpretation for the signal identified in the *Kepler* and *HST* data.

Despite having an exomoon candidate, the Kepler-1625 system seems very ordinary when compared with other exoplanetary systems. It is formed by a G-type star with mass $M_\star \sim 1.079\ \mathrm{M}_\odot$ and radius $R_\star \sim 1.793\ \mathrm{R}_\odot$ (Mathur et al. 2017). So far, only one planet has been detected in the system, Kepler-1625 b. The planet has a semimajor axis of $a_\mathrm{p} \sim 0.87$ au (Morton et al. 2016) and a radius of $R_\mathrm{p} \sim 1.18\ R_\mathrm{J}$. The planet's mass is not well constrained, but previous investigations suggested a planet with a few Jupiter masses. Recent estimations presented by Teachey et al. (2020) show a peak probability around $3\ M_\mathrm{J}$. However, as shown in fig. 10 in Teachey et al. (2020), the distribution encompasses a broad range of values. The characteristics of the satellite candidate Kepler-1625 b-I are also not well determined. According to Teachey & Kipping (2018), the candidate is a Neptune-like body. Several planet–satellite orbital separations have been proposed based on different analyses (Teachey et al. 2018; Teachey & Kipping 2018; Martin, Fabrycky & Montet 2019; Teachey et al. 2020). In this paper, we will adopt the canonical value of $40\ R_\mathrm{p}$. The exomoon candidate's orbit is usually assumed to be circular. The transit data indicate that the satellite would be in a very inclined configuration. Teachey & Kipping (2018) found that the inclination of the candidate is 42^{+15}_{-18} degrees for a linear detrending, 49^{+21}_{-22} degrees for a quadratic detrending, and 43^{+15}_{-19} degrees for an exponential detrending. As can be seen, the inclination varies depending on the model adopted, and the error bar for the values is also very significant.

Since the proposal of Kepler-1625 b-I, many theoretical models have studied its stability (Heller 2018; Quarles, Li & Rosario-Franco 2020; Rosario-Franco et al. 2020) and origin (Hamers & Portegies Zwart 2018; Heller 2018; Hansen 2019; Moraes & Vieira Neto 2020). From the stability point of view, the satellite candidate is possible and stable, because its orbit is well inside the planet's Hill sphere but not close enough for it to be dragged towards the planet as a result of tidal forces. The origin of this candidate, however, remains mysterious. Most papers focus on capture mechanisms for its origin, which is a fair assumption based on the satellite's size, mass and inclination. Moraes & Vieira Neto (2020) found that formation in a circum-planetary disc is also possible, and the authors set a lower limit for the number of solids needed for the formation of such a massive body and studied its post-formation evolution. Their conclusion points towards in situ formation in a supermassive circum-planetary disc. However, the origin of the material was not discussed in their paper.

Based on the features of our Solar system, systems with multiple satellites are expected to be abundant around giant planets. The question is whether this pattern holds for exomoons around giant planets and how big these bodies could be. Many authors have studied the stability of single planet-sized satellites (Heller et al. 2014; Heller & Pudritz 2015a, b; Barr 2016), with most studies showing that Mars-like exomoons could be stable around super-Jovian planets. However, is this true for systems with multiple satellites?

Kollmeier & Raymond (2019) and Rosario-Franco et al. (2020) explored this issue when they discussed the feasibility of the moon's moons, or submoons, around Kepler-1625 b-I. Even though submoons are not found in our Solar system, the size and orbital characteristics of Kepler-1625 b-I motivated Kollmeier & Raymond (2019) to study the stability around the satellite candidate and under what conditions a submoon would be stable. The authors found that the existence of submoons strongly depends on the mass of the host moon and its orbital separation from the planet, because of the intense tidal interactions between the submoon and the moon. They found that submoons are possible around Kepler-1625 b-I and that the largest possible submoon would have the Vesta-to-Ceres size. Later, Rosario-Franco et al. (2020) found that submoons around Kepler-1625 b-I will orbit inside a 0.33 Hill radius of the satellite (see their table 1 for more details), and the mass of the stable submoons would be 70 per cent of the mass of the asteroid Vesta.

Moraes & Vieira Neto (2020) showed that even in an extreme system like Kepler-1625 b, multiple satellites could be stable for long periods in certain locations around the host planet. However, the authors did not explore in detail the locations of these bodies or the gravitational interaction between the surviving satellites.

Kipping (2021) identified a phenomenon that would be produced by the presence of one exomoon over the transit timing variation (TTV) of an exoplanet, the 'exomoon corridor'. According to this author, the analysed TTVs induced by an exomoon will peak near two cycles. In addition, the author estimated that almost half of the exomoons would manifest themselves in short TTV periods of two to four cycles, regardless of the exomoon's semimajor axis distribution (see fig. 1 from Kipping 2021). If this is the case, the exomoon corridor phenomenon will help to distinguish the TTVs induced by exomoons from those induced by planet–planet interactions. However, the exomoon corridor was developed for only one exomoon around a planet.

A recent study by Teachey (2021) expanded the exomoon corridor method to systems with multiple satellites and found that such an

Table 1. Canonical values of the mass, radius and semimajor axis adopted for the planet Kepler-1625 b and the satellite Kepler-1625 b-I (the data for the satellite describe a Neptune-size body at 40 R_p).

	Mass $[M_J]$	Radius $[R_J]$	Semimajor axis [ua]
Kepler-1625 b	3	1.18	0.87
Kepler-1625 b-I	0.05395	0.3522	0.02206

effect holds for systems with up to five satellites in both resonant and non-resonant configurations.

Motivated by the aforementioned works, we propose to investigate in more detail the regions around the planet Kepler-1625 b considering the presence of the satellite Kepler-1625 b-I, searching for orbits where other massive satellites would be stable.

We refer to 'stable orbits' in our systems as orbits where a secondary satellite can be placed and survive both the gravitational effects of the planet and the primary satellite (Kepler-1625 b-I) and the non-gravitational effects, such as tidal interactions with the central planet and the rotational deformation on the shape of the host body. We chose to take into account tides raised by the planet in the satellites and vice versa, and the rotational flattening effects from the planet, where such effects will be modelled by an estimation of the J_2 coefficient of the body (Hussmann et al. 2019; Moraes & Vieira Neto 2020).

The paper is organized as follows. In Section 2, we detail the characteristics of the system and the equations of motion, and present a deeper discussion about the tidal and the rotational flattening models. Our models and results regarding the stability of the satellites are presented in Section 3; the analysis of the dynamical evolution of our system is given in Section 4; and in Section 5 we summarize our findings and draw our conclusions.

2 MODEL

Our main goal is to find stable orbits for massive satellites around Kepler-1625 b, considering that the satellite candidate Kepler-1625 b-I is already present. In this case, we will refer to Kepler-1625 b-I as the 'primary satellite', while the satellite for which we will study the stability will be identified as the 'secondary satellite'.

The study proposed here is supported by previous studies targeting the possibility of finding multiple extrasolar satellites (Heller et al. 2016; Moraes & Vieira Neto 2020; Teachey 2021). Also, from the point of view of the origins of Kepler-1625 b-I, three scenarios have been proposed so far: tidal capture by the planet (Hamers & Portegies Zwart 2018); 'pull-down capture' from a co-orbital configuration (Hansen 2019); and in situ formation (Moraes & Vieira Neto 2020). In all cases, the hypothesis of having more satellites in the system is plausible. In the case of capture, Kepler-1625 b-I could have destroyed an ancient family of satellites around the host planet, pushed the ancient exomoons to closer orbits or scattered those satellites in wide eccentric orbits, somewhat similar to the scenario proposed for the capture of Triton in the Neptune system (Agnor & Hamilton 2006). In the case of in situ formation, Moraes & Vieira Neto (2020) identified surviving satellites that formed at the same time as Kepler-1625 b-I and are stable in inner orbits.

Because of the many uncertainties regarding the values for the mass, radius and semimajor axis of both Kepler-1625 b and Kepler-1625 b-I, in this paper we will consider some canonical values, as summarized in Table 1, where the mass and the radius of the satellite are given in terms of the mass and radius of Neptune, $M_{\rm Nep}$ and $R_{\rm Nep}$, respectively. Because the information about the eccentricity and inclination of Kepler-1625 b-I is uncertain, we will consider the primary satellite to be in a circular and coplanar orbit around the central planet. Even though the analysis of the transits of Kepler-1625 b presented by Teachey & Kipping (2018) found that the exomoon candidate could be in a very inclined orbit, it is not yet possible to know if the planet is tilted on its axis, such that the exomoon's orbit is coplanar with its equator, or if the exomoon candidate is indeed significantly inclined with respect to the planet's equator. Here we have opted for the simpler case, where the exomoon is coplanar to the planet's equator, and leave the inclined case for future explorations.

For the secondary satellite, we opted to work with an Earth-like satellite (Table 1) because of the limitation imposed on the size of detectable satellites. In addition to Earth-like satellites, Ganymede- and Mars-like satellites were also tested in the early stages of our study. However, the differences in the size of these three types of satellites were not reflected in our results, and therefore we will only present the models with Earth-like bodies as the secondary satellites.

2.1 Equations of motion

To describe the motion of the primary and secondary satellites around the planet we use a coordinate system centred on the planet. The equations of motion of a satellite j with mass M_j at a distance r_j from the central body are given by

$$\ddot{\mathbf{r}}_j = -G(M_{\rm p} + M_j)\frac{\mathbf{r}_j}{|\mathbf{r}_j|^3} - GM_i\frac{\mathbf{r}_j - \mathbf{r}_i}{|\mathbf{r}_j - \mathbf{r}_i|^3} - GM_i\frac{\mathbf{r}_i}{|\mathbf{r}_i|^3} + \frac{\mathbf{F}_j^{\rm T} + \mathbf{F}_j^{\rm R}}{M_j} + \frac{\mathbf{F}_j^{\rm T} + \mathbf{F}_j^{\rm R}}{M_{\rm p}} + \frac{\mathbf{F}_i^{\rm T} + \mathbf{F}_i^{\rm R}}{M_{\rm p}}, \tag{1}$$

where $j = 1$, 2 and $i = 1$, 2, with $j \neq i$, are the satellite indexes, with 1 for the primary and 2 for the secondary. G is the gravitational constant, r_j is the distance from the planet to the jth satellite, M_j and $M_{\rm p}$ are the masses of the satellite j and the central planet, and $\mathbf{F}_j^{\rm T}$ and $\mathbf{F}_j^{\rm R}$ are, respectively, the tidal and rotational flattening forces acting on the satellite j (these effects are explained in Subsection 2.2). The terms on the right-hand side of equation (1) are divided into gravitational and tidal/rotational terms. The first three terms are, respectively, the gravitational force from the planet on satellite j, the mutual gravitational interaction between the satellites, and an indirect term due to the choice of the coordinate system. The next three terms are the tidal and rotational flattening accelerations due to the bulge induced by the planet on the satellite j, the bulge induced by the satellite j on the planet, and the bulge induced by the satellite i on the planet, respectively. It should be noted that the satellites do not raise tides in each other and that the tidal bulge induced in each satellite does not affect the motion of the other, and thus the fourth term on the right-hand side of equation (1) does not have a similar term for the satellite i (Fig. 1).

As can be seen from equation (1), the presence of the star is neglected. As shown by Moraes & Vieira Neto (2020), for the distances we are considering for the satellites, the effects of the star can be safely ignored, as the planet will be the gravitationally dominant body.

2.2 Tidal and rotational flattening models

In addition to the gravitational interaction between the bodies in the system, we also assume tidal forces and rotational flattening as sources of perturbation on the system.

2.2.1 Tidal model

To properly model the tides in the system, we consider the constant time-lag formalism proposed in Mignard (1979) and Hut (1981) (see also Bolmont et al. 2015 and references therein). In our models we consider that the central planet will generate a tidal bulge in each satellite and that each orbiting satellite will also generate a tidal bulge in the central planet, while the satellites do not generate tides in each other (Fig. 1). Also, the tidal bulge induced by the planet on one satellite does not affect the motion of the other. On the other hand, all the bulges generated by the satellites on the planet affect the motion of all the orbiting bodies.

To describe the tidal components of the acceleration (components that carry the tidal effects over satellite j in the equations of motion) we will adopt the notation used in Bolmont et al. (2015). Thus, we present the tidal forces acting on the satellite j decomposed into radial ($\mathbf{F}^{\mathrm{T}}_{\mathrm{rad}}$) and orthogonal ($\mathbf{F}^{\mathrm{T}}_{\mathrm{ort}}$) terms as follows:

$$\begin{aligned}\mathbf{F}^{\mathrm{T}}_{j} &= \mathbf{F}^{\mathrm{T}}_{\mathrm{rad}} + \mathbf{F}^{\mathrm{T}}_{\mathrm{ort}} \\ &= \left[F^{\mathrm{T}}_{\mathrm{rad},j} + F^{\mathrm{T}}_{\mathrm{rad,p}} + \left(F^{\mathrm{T}}_{\mathrm{ort},j} + F^{\mathrm{T}}_{\mathrm{ort,p}}\right)\frac{\mathbf{v}_j\cdot\hat{\mathbf{r}}_j}{|\mathbf{r}_j|}\right]\hat{\mathbf{r}}_j \\ &\quad + \left[F^{\mathrm{T}}_{\mathrm{ort},j}\left(\Omega_j - \dot{\theta}_j\right) + F^{\mathrm{T}}_{\mathrm{ort,p}}\left(\Omega_{\mathrm{p}} - \dot{\theta}_j\right)\right]\times\hat{\mathbf{r}}_j, \end{aligned} \tag{2}$$

where $\mathbf{v}_j$ and Ω_j are the velocity and the rotation vectors of the satellite j, Ω_{p} is the rotation vector of the planet, $\hat{\mathbf{r}}_j = \mathbf{r}_j/|\mathbf{r}_j|$ is a unit vector in the radial direction, and $\dot{\theta}_j$ is the instantaneous orbital angular velocity vector, which is a colinear vector with the orbital angular momentum of the satellite j (θ_j is the true anomaly of the respective satellite). Here, we consider the time evolution of the rotation vectors of the planet and the satellites, Ω_{p} and Ω_j respectively, through the integration of the torque equations given by the conservation of the total angular momentum (see sections 2.4.2 and 2.5 of Bolmont et al. 2015 for a complete analytic development of such equations). In our model, we are neglecting the evolution of the bodies, such that the physical radius and the radius of gyration of the planet and the satellites are kept constant, thus simplifying the evolution of the rotation vectors.

The terms $F^{\mathrm{T}}_{\mathrm{rad},j}$ and $F^{\mathrm{T}}_{\mathrm{rad,p}}$ refer to the radial tides, while $F^{\mathrm{T}}_{\mathrm{ort},j}$ and $F^{\mathrm{T}}_{\mathrm{ort,p}}$ refer to the orthogonal tides. The subscripts j and p are related to tides from the satellites j and the planet p, respectively. These terms are based on equation (5) from Bolmont et al. (2015) and are given by

$$\begin{aligned} F^{\mathrm{T}}_{\mathrm{rad},j} &= -3\frac{GM_{\mathrm{p}}^2 k_{2,j} R_j^5}{|\mathbf{r}_j|^7}\left(1 + 3\frac{|\mathbf{v}_j|}{|\mathbf{r}_j|}\tau_j\right), \\ F^{\mathrm{T}}_{\mathrm{rad,p}} &= -3\frac{GM_j^2 k_{2,\mathrm{p}} R_{\mathrm{p}}^5}{|\mathbf{r}_j|^7}\left(1 + 3\frac{|\mathbf{v}_j|}{|\mathbf{r}_j|}\tau_{\mathrm{p}}\right), \\ F^{\mathrm{T}}_{\mathrm{ort},j} &= 3\frac{GM_{\mathrm{p}}^2 R_j^5}{|\mathbf{r}_j|^7}k_{2,j}\tau_j, \\ F^{\mathrm{T}}_{\mathrm{ort,p}} &= 3\frac{GM_j^2 R_{\mathrm{p}}^5}{|\mathbf{r}_j|^7}k_{2,\mathrm{p}}\tau_{\mathrm{p}}, \end{aligned} \tag{3}$$

where R_j and R_{p} are the radii of the satellite j and the planet, respectively, $k_{2,j}$ and τ_j are the second-order potential Love number and the constant time lag of the satellite j, while $k_{2,\mathrm{p}}$ and τ_{p} have the same meaning, but for the central planet.

The tides have the effect of damping the eccentricity of the orbiting body while affecting its migration. The direction of the migration depends primarily on the eccentricity of the orbiting body and its semimajor axis.

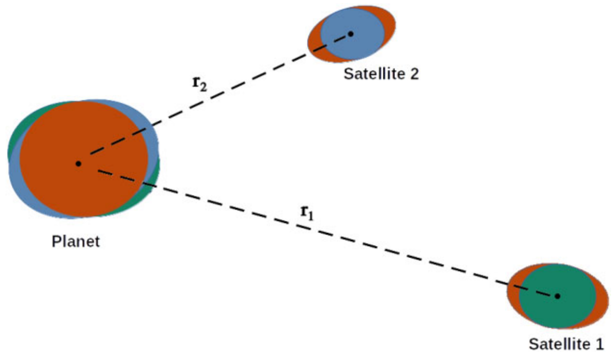

Figure 1. Illustration of how tides are considered in this paper. The central planet exerts tides on each satellite independently, and each satellite also exerts tides on the planet, but satellites do not generate tides in each other.

When the satellites have zero eccentricity and zero obliquity,their orbits are perfectly synchronized with the central planet; that is, the satellites' angular velocity are equal to the planet's rotational velocity, and thus only the tides of the planet are present. For small non-zero eccentricities, the tides from the central planet are dominant over the tides of the satellites. In this case, the direction of the migration of the satellites depends on their orbital position: if a satellite is located beyond its corotation radius (r_{corot}) then its angular velocity is smaller than the planet's rotation rate and the satellite migrates outwards; and if the satellite is located inside r_{corot} its angular velocity is greater than the planet's rotation rate, and thus the satellite migrates inwards. For a highly eccentric satellite, the tides from the satellite dominate and the satellite will always migrate inwards (Leconte et al. 2010; Sánchez, de Elía & Downes 2020). The rate at which the semimajor axis of a satellite in an eccentric orbit varies is given by (Leconte et al. 2010; Hansen 2010; Sánchez et al. 2020)

$$\begin{aligned}\frac{1}{a}\frac{\mathrm{d}a}{\mathrm{d}t} &= -\frac{1}{t_{\mathrm{sat}}}\left[f_1(e) - \frac{\Omega_{\mathrm{sat}}}{n}f_2(e)\right] \\ &\quad - \frac{1}{t_{\mathrm{p}}}\left[f_1(e) - \frac{\Omega_{\mathrm{p}}}{n}f_2(e)\right], \end{aligned} \tag{4}$$

with n being the mean motion of the satellite, and where t_{sat} and t_{p} are the dissipation time scales for circular orbits of the satellite and the planet, respectively, given by

$$\begin{aligned} t_{\mathrm{sat}} &= \frac{1}{6}\frac{1}{Gk_{2,\mathrm{sat}}\tau_{\mathrm{sat}}}\frac{M_{\mathrm{sat}}}{M_{\mathrm{p}}(M_{sat} + M_{\mathrm{p}})}\frac{a^8}{R_{\mathrm{sat}}^5}, \\ t_{\mathrm{p}} &= \frac{1}{6}\frac{1}{Gk_{2,\mathrm{p}}\tau_{\mathrm{p}}}\frac{M_{\mathrm{p}}}{M_{\mathrm{sat}}(M_{\mathrm{p}} + M_{\mathrm{sat}})}\frac{a^8}{R_{\mathrm{p}}^5}, \end{aligned} \tag{5}$$

and $f_1(e)$ and $f_2(e)$ are functions of the eccentricity of the satellite that appear for eccentric orbits, given by equation (6):

$$\begin{aligned} f_1(e) &= \frac{1 + (31/2)e^2 + (255/8)e^4 + (185/16)e^6 + (25/64)e^8}{(1-e^2)^{15/2}}, \\ f_2(e) &= \frac{1 + (15/2)e^2 + (45/8)e^4 + (5/16)e^6}{(1-e^2)^6}. \end{aligned} \tag{6}$$

For a more extensive analysis of the secular evolution of the semimajor axis, eccentricity and spin of a body being tidally disturbed, see Leconte et al. (2010), Hansen (2010) Bolmont, Raymond & Leconte (2011), Bolmont et al. (2013), and Sánchez et al. (2020).

As mentioned above, in all our models we will consider the central planet, the primary satellite Kepler-1625 b-I, and a secondary Earth-like satellite. To properly account for tides in the system,

Table 2. Tidal parameters for the planet Kepler-1625 b, the satellite Kepler-1625 b-I, and the secondary satellite. The columns present the body, the rotation period, the second-order potential Love number, and the constant time lag (Bolmont et al. 2015; Tokadjian & Piro 2020).

	Period [h]	k_2	τ [s]
Kepler-1625 b	10	0.380	1.842×10^{-3}
Kepler-1625 b-I	16	0.340	0.766
Secondary satellite	24	0.305	698

some important parameters must be set, namely the rotation period, the second-order potential Love number, and the constant time lag (hereafter referred to as tidal parameters) for each body. For simplicity, we will consider the central planet Kepler-1625 b to have tidal parameters equal to those of Jupiter (parameters taken from Bolmont et al. 2015). This choice is justified because the planet has a similar size to Jupiter and mass 3 M_J. For a more massive planet ($\geq 10\,M_\mathrm{J}$), brown-dwarf parameters could be considered. For Kepler-1625 b-I, we follow Tokadjian & Piro (2020) and set the potential Love number and constant time lag to describe an ice-giant planet like Neptune, with $k_{2,\,1} = 0.34$ and $\tau_1 = 0.766$ s. Also, the rotation period of the satellite was taken as 16 h, the same as for the planet Neptune. As the primary satellite is located farther out in the system, where the tides from the planet are weaker, a slower or faster rotating body will produce similar results. In the case of the secondary satellite, we are taking it to be an Earth-like body with the same tidal parameters as the Earth (values taken from Bolmont et al. 2015). We also tested an Earth-like satellite rotating faster (18 hours) and slower (30 hours); however, the results were very similar to those obtained with the typical rotation period of 24 h. A summary with the values of the tidal parameters for each body is presented in Table 2.

2.2.2 *Rotational flattening model*

Following Hussmann et al. (2019) and Moraes & Vieira Neto (2020), we chose to include in our models the effects of the non-sphericity of the simulated bodies due to their rotation.

In addition to the distortions on the surface of a body due to tides, the shape of this body will also change as a result of its rotation. The gravitational effects of this rotational deformation will change its gravitational field, thus affecting all the bodies in the system, especially those in closer orbits (Murray & Dermott 1999).

Here we consider the torques exerted by the planet on the satellites and the torques exerted by the satellites on the planet, while torques from one satellite are not felt by the other satellite. These gravitational effects will precess the orbit of eccentric satellites, causing the mean eccentricity and mean obliquity of the satellites to change (Bolmont et al. 2015).

We model the rotational deformation of a body using the parameter J_2, which defines how oblate instead of spherical a body is. For a given satellite j, $J_{2,\,j}$ can be calculated as (Bolmont et al. 2015)

$$J_{2,\,j} = k_{2f,\,j} \frac{\Omega_j^2 R_j^3}{3 G M_j}, \tag{7}$$

where $k_{2f,\,j}$ is the second-order fluid Love number of the satellite. The fluid Love number can be defined as the potential Love number for a perfect fluid body. For simplicity, we will consider the fluid Love number to be equal to the potential Love number (Bolmont et al. 2015); for a complete discussion about the differences between these two parameters, see Correia & Rodríguez (2013) and references therein. Equation (7) can be used to calculate $J_{2,\,\mathrm{p}}$ for the central planet simply by exchanging the subscript 'j' for 'p'.

As in the case of the tidal model, we will adopt a notation similar to Bolmont et al. (2015) and describe the rotational flattening force of a central planet and a satellite j over a satellite $j$as,

$$\begin{aligned}
\mathbf{F}_j^{\mathrm{R}} = & -\frac{3 G M_j M_\mathrm{p}}{2|\mathbf{r}_j|^5}\left(J_{2,\,j} R_j^2 + J_{2,\mathrm{p}} R_\mathrm{p}^2\right)\mathbf{r}_j \\
& + \frac{15 G M_j M_\mathrm{p}}{2|\mathbf{r}_j|^7}\left(J_{2,\,j} R_j^2 \frac{(\mathbf{r}_j\cdot\Omega_j)^2}{|\Omega_j|^2} + J_{2,\mathrm{p}} R_\mathrm{p}^2 \frac{(\mathbf{r}_j\cdot\Omega_\mathrm{p})^2}{|\Omega_\mathrm{p}|^2}\right)\mathbf{r}_j \\
& - \frac{3 G M_j M_\mathrm{p}}{|\mathbf{r}_j|^5}\left(J_{2,\,j} R_j^2 \frac{\mathbf{r}_j\cdot\Omega_\mathrm{p}}{|\Omega_\mathrm{p}|^2}\right)\Omega_\mathrm{p} \\
& - \frac{3 G M_j M_\mathrm{p}}{|\mathbf{r}_j|^5}\left(J_{2,\,p} R_\mathrm{p}^2 \frac{\mathbf{r}_j\cdot\Omega_j}{|\Omega_j|^2}\right)\Omega_j .
\end{aligned} \tag{8}$$

Now that we have defined all the forces acting in our system and can compute the total acceleration felt by a satellite j (equation 1), we will move on to describe our computational methods and our set-ups.

3 NUMERICAL SIMULATIONS

Our study is mainly numerical, and thus we start this section by presenting the numerical tools used in this work, followed by a discussion about the systems studied and the results of our simulations regarding the stability of the systems. The analysis of the dynamical evolution of the systems is presented in Section 4.

3.1 Numerical tools

In this work we will perform N-body simulations using the numerical package POSIDONIUS[1] (Blanco-Cuaresma & Bolmont 2017). POSIDONIUS is a new N-body code that allows the user to include dissipative effects such as tides, general relativity, rotational flattening, and the evolution of the bodies. The package is the second generation of the widely used MERCURY-T (Bolmont et al. 2015) written in RUST (see Blanco-Cuaresma & Bolmont 2016 for the advantages of using RUST in astrophysics) with a package of PYTHON scripts for the implementation of initial conditions and post-processing analysis. This new numerical tool ensures memory safety, can reproduce numerical N-body experiments, and improves the integration of the spin when compared with MERCURY-T. POSIDONIUS has been used in recent studies involving the evolution of planets and satellites in scenarios where tides are considered (Bolmont et al. 2019, 2020).

POSIDONIUS allows the user to choose between different integration schemes for the time evolution of the equations of motion. Here, we opted to use the IAS15 integration scheme (Rein & Spiegel 2015). The main reason for this choice is that in our problem we expect to find several close encounters between the satellites and between the satellites and the central planet . The IAS15 integrator can solve such close encounters with high accuracy while still being faster than most other high-order integration schemes (Rein & Spiegel 2015).

3.2 Initial conditions

As noted above, the systems we are studying are composed of the central planet (Kepler-1625 b), the primary satellite (Kepler-1625 b-I), and a secondary Earth-like satellite. The physical characteristics of the planet and the primary satellite are given in Table 1, while the secondary satellite has Earth's radius and mass. The primary

[1] https://www.blancocuaresma.com/s/posidonius

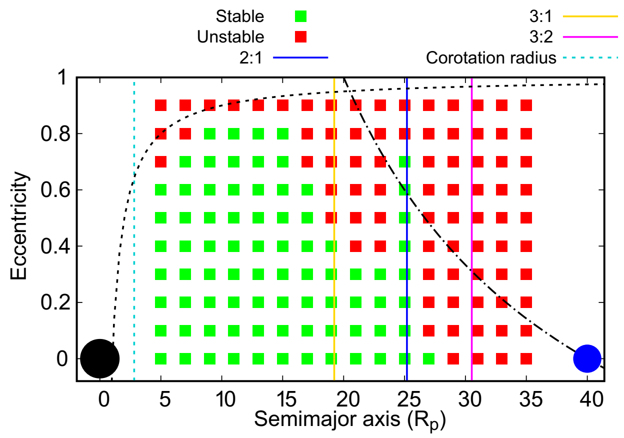

Figure 2. Grid with the initial conditions. Green denotes the conditions that end up being stable after 1 Myr, and red denotes the unstable cases. The vertical lines show the approximate locations of some mean-motion resonances, namely 2:1 (blue line), 3:2 (magenta line) and 3:1 (yellow line). The innermost dashed line shows the initial location of the corotation radius for the Earth-like moons. The black and blue circles represent the central planet and Kepler-1625 b-I, respectively. The black dashed line shows where the secondary satellites' pericentres crosses the radius of the planet, and the black dash-dotted line shows where the secondary satellites' apocentres crosses the orbit of the primary satellite.

satellite starts at 40 R_p from the planet for all cases, and in a circular and coplanar orbit. In order to find stable orbits for the secondary satellite, we simulate several cases with the initial semimajor axis of the satellites varying from $a_0 = 5$ to $a_0 = 35\ R_p$, considering $\Delta a_0 = 2\ R_p$. For each position we simulate 10 cases, varying the eccentricity of the secondary satellite from $e_0 = 0.0$ to $e_0 = 0.9$, with $\Delta e_0 = 0.1$. The satellites are taken to be coplanar in all cases. The angular orbital elements of both satellites and their obliquities are set to zero. Regarding the obliquity of the satellites, as we are considering the effects of tides and rotational flattening in addition to the usual gravitational interactions, Bolmont et al. (2015) showed for several cases that the obliquity of orbiting bodies under these dissipative effects decreases to zero very quickly, in about 100 yr. We used their results to justify our choice.

As we are considering additional effects to our model, we present the tidal parameters of all the bodies in the system in Table 2, recalling that we only consider tides generated by the planet on the satellites and the tides raised by the satellites on the planet, neglecting satellite–satellite tidal interactions. For the gravitational effects due to rotational flattening, the 'only' parameter needed is J_2, which is calculated for each satellite and the planet with equation (7). Each simulation is carried out for 1 Myr or until a collision or an ejection is detected. Satellites are ejected from the system if they reach 1 Hill radius from the planet at any point. If a system survives for 1 Myr, we consider the system as stable; otherwise, the system is classified as unstable.

Hereafter we will refer to all systems by the initial semimajor axis and eccentricity of the secondary satellite.

3.3 Stability

In the following, we discuss our results regarding the stability of the systems when a secondary satellite is added. Also, we analyse the fate of the unstable systems.

In Fig. 2 we present our grid (semimajor axis versus eccentricity) of initial conditions. Green denotes stable initial conditions, and red denotes unstable ones. Later we will discuss the orbital evolution and the final configurations of the satellite systems, but for now it is important to note that even very eccentric initial conditions can provide long-term stable satellites owing to the effects of tides. As pointed out in the previous section, tides are a strong mechanism for damping the eccentricity of the orbiting bodies.

From Fig. 2 we can see that the systems with the secondary satellite initially placed inside 20 R_p are more likely to produce stable systems: this is the case because at these locations the gravitational effects of the primary satellite are weaker, and the evolution of the systems is dominated by the tidal interaction with the planet. Outside 20 R_p the effects of the tides are weaker, and the gravitational perturbations from the primary satellite are more pronounced. At these locations, we see a decrease in the number of stable systems, especially among those with orbits that are initially eccentric. We note that secondary satellites in eccentric orbits are more likely to suffer a close encounter with the primary satellite, resulting in collisions or ejection from the system. In this way, the action of the tides as a mechanism to dampen the eccentricity of the secondary satellites is very important to reduce the probability of these close encounters.

For systems with the secondary satellite placed at distances greater than 29 R_p we could not find stability. At these distances, the effects of the primary satellite are dominant, and close encounters that lead to the loss of the secondary satellites are common (the dash–dotted line in Fig. 2 shows the conditions for which the secondary satellites' apocentre crosses the orbit of the primary satellite and close encounters are more likely). In addition, we will show later that the overlapping of resonances could create a chaotic region close to the primary satellite.

Also in Fig. 2 we present the initial location of three mean-motion resonances (MMRs), the 3:1 near 19 R_p, the 2:1 near 25 R_p and the 3:2 near 31 R_p. These three MMRs play different roles in the stability of the systems. As can be seen, the 3:1 MMR is positioned inside a stable region, and thus the number of stable systems does not increase/decrease substantially because of the presence of the resonance. On the other hand, the 2:1 MMR is located in a transition region, where the number of stable systems decays. However, the system with secondary satellites starting near this region presents a increasing number of stable systems, which is directly correlated with the presence of the resonance. The outermost resonance we present is the 3:2 MMR slightly inside 31 R_p. This region is too close to the primary satellite to be stable, and the MMR resonance does not contribute to the stability of the systems: most of the systems with the secondary satellite starting at 31 R_p became unstable almost instantaneously. A more detailed study of the role the MMRs play in the systems will be presented in the next section.

To investigate the fate of the unstable systems, in Fig. 3 we show a diagram with only the unstable initial conditions, where the triangles represent a collision with the central planet, squares represent a collision with Kepler-1625 b-I, and circles represent ejection from the system. The colour bar on the right-hand side indicates the time it took for the system to become unstable, and the points marked in black are the conditions that become unstable instantaneously after the simulation starts.

From Fig. 3 it can be seen that, as expected, the satellites initially in inner orbits are more likely to collide with the central planet. In the same way, satellites initially in wider orbits are more likely to collide with the primary satellite or be ejected from the system. However, satellites in wider eccentric orbits also collide with the planet: this happens because close encounters with the primary satellite end with

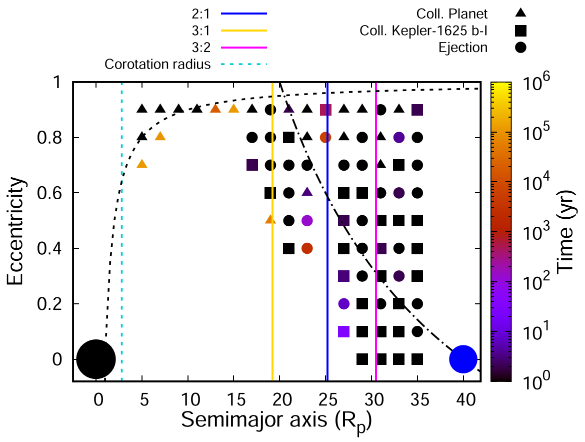

Figure 3. Grid with the unstable initial conditions of our models. The shape of the symbols indicates the fate of the satellite: triangles represent collision with the central planet, squares represent collision with the primary satellite (Kepler-1625 b-I), and circles represent ejection from the satellite system. The colour of the symbols indicates the time when the system became unstable according to the colour bar. The black dashed line shows where the secondary satellites' pericentres crosses the radius of the planet, and the black dash–dotted line shows where the secondary satellites' apocentres crosses the orbit of the primary satellite.

the secondary satellite being pushed inwards, towards the planet, and a collision eventually takes place. We found several cases of ejections of the secondary satellites – the ejections are caused mainly by close encounters with the primary satellite (especially for secondary satellites located in outer regions) or by a resonant break.

Statistically, of the 160 different systems shown here, we found that exactly half of the systems are stable and half are unstable. For all the 80 unstable systems, we found that the most common fate was ejection, with 30 occurrences (37.5 per cent), followed closely by collision with the primary satellite, 29 cases (36.25 per cent), and collision with the central planet, 21 cases (26.25 per cent). Because the most unstable systems are found closer to the primary satellite, the most common reasons for instability being ejection and collision with this satellite are to be expected.

4 DISCUSSION

In this section, we focus on stable systems and discuss their dynamical evolution, such as migration, eccentricity damping and resonant configurations. In addition, we analyse the influences of the initial semimajor axis and eccentricity on our findings.

4.1 Migration and eccentricity damping

In Fig. 4 we show the final distribution of the semimajor axis versus eccentricity for our stable cases. When comparing the initial and final semimajor axes of the satellites, it can be seen that in most cases the satellites migrated inwards or were pushed inwards owing to a close encounter with the primary satellite. Notably, we found several cases of stability inside 5 R_p, a region where the gravitational and tidal effects of the planet are stronger. These satellites present low eccentricities and will be long-term stable once they are outside their respective corotation radius, which means that there is no risk of these satellites colliding with the planet.

We found that the satellites migrating the most are those in initial eccentric orbits. Even though the secondary satellites are initially beyond the corotation radius of the system, because of their eccentric orbits the satellite tides prevail over the planetary tides, and in this case, as discussed above, the satellites migrate inwards until their eccentricity is damped to values below 0.1.

As an example, we show in Fig. 5 the evolution of the semimajor axis and eccentricity of the secondary (Earth-like) and primary (Kepler-1625 b-I) satellites for the case where the Earth-like satellite started at 13 R_p. The evolution of the semimajor axis and eccentricity of the secondary satellites are shown in the left-hand panels, while the same parameters for the primary satellites are presented in the right-hand panels. We differentiate each case by their initial eccentricity using a colour scheme: from $e_0 = 0.0$ to $e_0 = 0.8$ we have the colours light green, green, light blue, blue, magenta, red, orange, yellow, and pink, respectively. The evolution of the case with $e_0 = 0.9$ is not displayed because it results in an unstable system.

As expected, the secondary satellites with initially higher eccentricity migrate inwards faster and reach inner orbits. In this phase, the migration of the eccentric satellites is determined by the satellite tides regime. As the satellites migrate towards the planet, their eccentricity is damped by the tidal interactions with the central body. As soon as the eccentricity of the satellites reaches small values, lower than 0.1 (Bolmont et al. 2011), the inward migration halts, and at this point the strength of the planetary tides overcomes the satellite tides, and the evolution of the semimajor axis of these bodies is determined by the planet–satellite spin ratio, which in the cases shown here results in a slow outwards migration. While the migration regime changes, the eccentricity of the satellites continues to decrease faster because of the proximity to the planet. Eventually, this decrease in the eccentricity stops, and the eccentricity of the satellites reaches a non-zero equilibrium range of values.

It is worth mentioning the role of Kepler-1625 b-I in the evolution of the system. From the right-hand panel in Fig. 5 we see that the primary satellite's semimajor axis does not vary significantly. This is because these satellites are too far from the central planet to be tidally disturbed, and their interaction with the inner satellite did not affect their semimajor axis much. However, the eccentricities of the primary satellites are excited by the presence of the inner satellites. On the other hand, the presence of the outer satellites is the reason why the inner satellites never reach circular orbits, even with tidal damping acting on their eccentricities. Also, for the case where the secondary satellite started in a circular orbit (light green line in the bottom left-hand panel), we can see that the presence of Kepler-1625 b-I is crucial, as the secondary satellite's orbit is perturbed and its eccentricity increases to values near 0.001 almost instantaneously. Nevertheless, this non-zero eccentricity does not translate to a significant change in the semimajor axis of the Earth-like satellite in this specific case.

The pattern exemplified in Fig. 5 was found in most of our simulations, except for the cases where the satellites were trapped in a resonance or pushed out of a resonant configuration. That is, all the cases where the secondary satellite had an initial semimajor axis smaller than 17 R_p had a similar outcome to that described above. For systems with the secondary satellite initially in a wider orbit, a combination of weaker tidal forces and the presence of low-order MMR prevents the significant inward migration of the secondary satellite. In these cases, most of the satellites did not migrate much, and their final eccentricities are higher.

4.2 Resonances

In recent years, compact multiplanetary systems locked in resonances have been found (Mills et al. 2016; Luger et al. 2017; Leleu et al. 2021). According to Mills et al. (2016), the presence of MMRs in

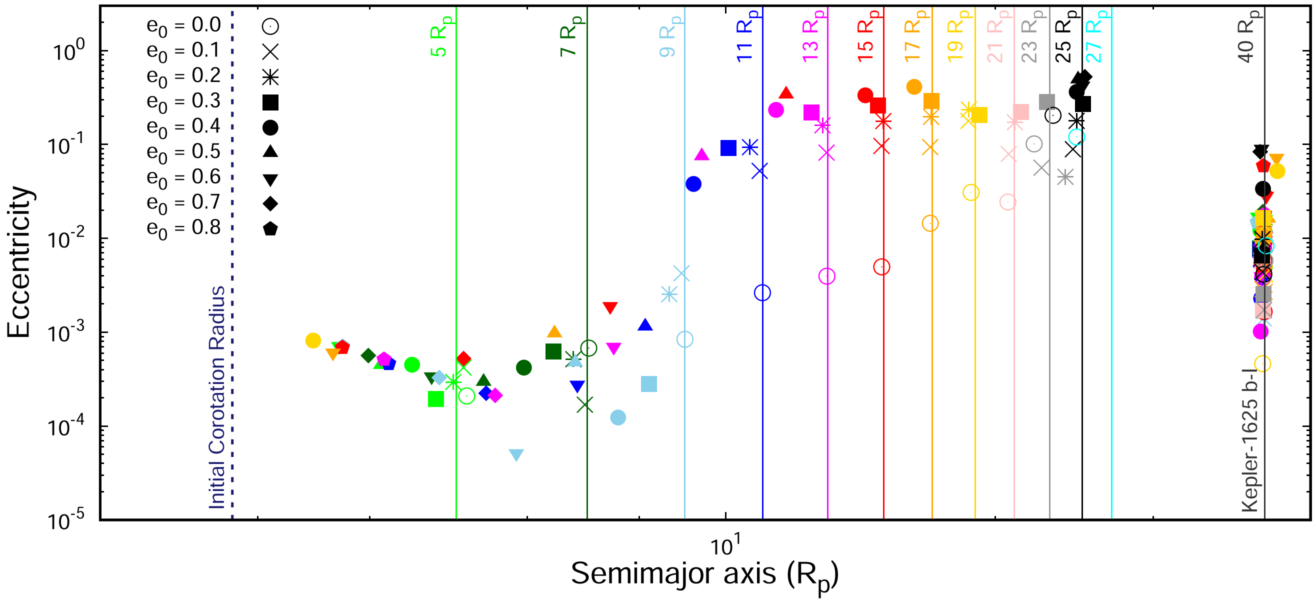

Figure 4. Final semimajor axis versus eccentricity distribution of the stable cases of our models. The models are separated by colour and shape. The colours identify the initial semimajor axis of the satellite (a_0) from 5 R_p to 35 R_p, with $\Delta a_0 = 2\ R_p$, as light-green (5 R_p), green (7 R_p), light-blue (9 R_p), blue (11 R_p), magenta (13 R_p), red (15 R_p), orange (17 R_p), yellow (19 R_p), pink (21 R_p), grey (23 R_p), black (25 R_p) and cyan (27 R_p). The vertical lines mark the initial semimajor axis by colour; the outermost vertical line marks 40 R_p, the initial position of Kepler-1625 b-I. The shapes represent the initial eccentricity of the satellite (e_0): 0.0 (open circle), 0.1 (cross), 0.2 (asterisk), 0.3 (square), 0.4 (filled circle), 0.5 (upward triangle), 0.6 (downward triangle), 0.7 (diamond) and 0.8 (pentagon). The bodies represented in the outermost vertical lines are the respective Kepler-1625 b-I for each case. The dashed dark-blue vertical line indicates the initial corotation radius of the system for the secondary satellite.

compact systems greatly helps the stability of the systems, exciting and stabilizing the eccentricity of the planets. In satellite systems, resonances also play a significant role, not only in the stability of the system but also in sculpting the final architecture of the system, the Laplace resonance presented by the Galilean system being the best-known example in our Solar system.

Here we will discuss the role that a few MMRs play in the stability of the systems.

4.2.1 Systems near the 3:1 MMR

We start our analysis with systems that are not in resonance but are very close. In Fig. 6 we show the evolution of the semimajor axis and eccentricity of the secondary and the primary satellites for the case where the Earth-like satellites start at 19 R_p. As before, on the left-hand side we have the evolution of the semimajor axis and eccentricity of the secondary satellites, while on the right-hand side we have the same parameters presented for the primary satellites.

At first, the evolution of the systems presented in Fig. 6 might resemble the evolution of systems locked in a MMR, where the motion of the secondary satellite is limited by the presence of the primary satellite while sustaining a non-zero eccentricity. In addition, in Fig. 7 we show the time evolution of the satellites' period ratio, P_1/P_2, where $P_1 = 2\pi/n_1$ is the orbital period of the primary satellite and $P_2 = 2\pi/n_2$ is the orbital period of the secondary satellite, with n_1 and n_2 being the respective mean motions. The satellites' period ratio is approximately three at the beginning of our simulations and, except for one case, most of the satellites preserve this period commensurability until the end of their evolution, with a small amplitude. In this way, one could argue that the satellites might be locked in a 3:1 MMR. However, to verify this we have to study the behaviour of the resonant angle of this hypothetical resonance.

From Murray & Dermott (1999) we have that the three resonant angles for a 3:1 MMR are

$$\begin{aligned} \phi_{3:1}^{(1)} &= 3\lambda_1 - \lambda_2 - 2\varpi_2, \\ \phi_{3:1}^{(2)} &= 3\lambda_1 - \lambda_2 - 2\varpi_1, \\ \phi_{3:1}^{(3)} &= 3\lambda_1 - \lambda_2 - \varpi_1 - \varpi_2, \end{aligned} \tag{9}$$

where λ_1 and ϖ_1 are the mean longitude and longitude of the pericentre for the primary satellite, respectively, and λ_2 and ϖ_2 are the same quantities for the secondary satellite.

For two bodies in resonance, one of the three angles described in equation (9) would be librating around one specific value. However, for all cases, the three angles were found to be circulating, which means that, despite the commensurability of the satellites' orbital periods , the satellites are not locked in resonance. As an example of the time evolution of the resonant angles for these cases, we show in Fig. 8 the behaviour of $\phi_{3:1}^{(1)}$ for the cases where the secondary satellites started with eccentricities from $e_0 = 0.0$ to $e_0 = 0.3$; the case with $e_0 = 0.4$ is not shown because the system is clearly out of a hypothetical MMR. The behaviours of $\phi_{3:1}^{(2)}$ and $\phi_{3:1}^{(3)}$ are similar to that of $\phi_{3:1}^{(1)}$.

In this case, instead of a MMR locking the motion of the satellites, the semimajor axes and eccentricities of the satellites are not damped because at 19 R_p the tidal effects coming from the planet are weak and the satellites preserve an orbital configuration similar to their initial conditions. Thus we cannot evaluate the role that the 3:1 MMR plays for the stability of the satellites, because the satellites near this resonance do not show any resonant behaviour.

Another important feature displayed in Fig. 6 is the behaviour of the secondary satellite that started with $e_0 = 0.4$ (magenta line). Different from the other cases, this satellite escaped the region near the 3:1 MMR thanks to multiple close encounters with the primary satellite, as can be seen by the erratic behaviour of its semimajor

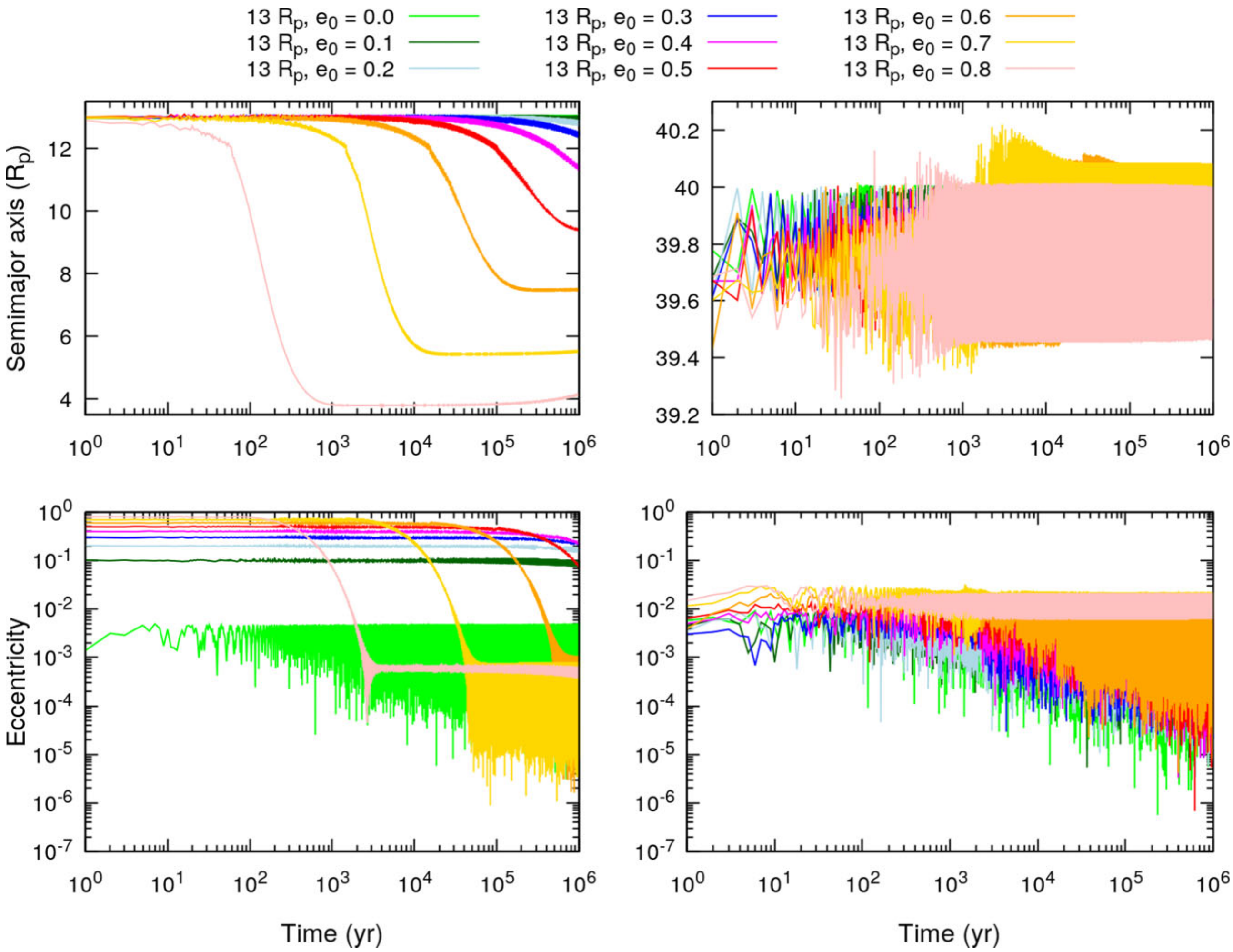

Figure 5. Time evolution of the semimajor axis and eccentricity of the primary and secondary satellites for the stable cases where the secondary satellites started at 13 R_{p}. In the left-hand panels, we have the evolution of the semimajor axis (upper panel) and eccentricity (lower panel) of the secondary satellites. In the right-hand panels, we have the evolution of the semimajor axis (upper panel) and eccentricity (lower panel) of the primary satellites. The cases are separated by the initial eccentricity of the secondary satellites using a colour scheme: from $e_0 = 0.0$ to $e_0 = 0.8$ we have the colours light green, green, light blue, blue, magenta, red, orange, yellow and pink, respectively. The evolution of the case with $e_0 = 0.9$ is not shown because it results in an unstable system.

axis, before a final encounter that resulted in the secondary satellite being pushed inwards. Because the damping effects of the tides on the satellite's eccentricity are stronger in the inner regions, the satellite's orbit is almost circularized before the satellite reaches the corotation radius. After this abrupt process of circularization, the satellite starts to experience an outward migration, resulting from the tides generated by the planet.

Because the secondary satellites around 19 R_{p} are not in MMR they are not free from a future close encounter with the primary satellite. As these satellites maintained high eccentricities during their evolution, a close encounter could take place at some point.

4.2.2 *Systems locked in 2:1 MMR*

As noted above, as we start the secondary satellites farther from the planet, the effects of the tides become weaker and the mutual gravitational interaction between the primary and secondary satellites is stronger. In this way, we found that when the secondary satellites start beyond 20 R_{p}, the percentage of stable systems decreases steeply. At these outer locations, the migration rate and eccentricity damping induced by the tides are smooth, and the secondary satellites are more likely to suffer a disruptive close encounter with the primary satellite, especially the satellites in eccentric orbits. However, for the cases where the secondary satellites start at 25 R_{p} a high number of systems are stable, which is due to the presence of a 2:1 MMR near this initial position.

In Fig. 9 we show the evolution of the semimajor axis and eccentricity of the primary and secondary satellites for a stable system when the secondary satellite starts at 25 R_{p}. The high number of stable systems presented might be explained by the location of a 2:1 MMR with the primary satellite near the orbital distance where the satellites are initialized. Also, from Fig. 9 it can be seen that, despite small amplitudes, after 100 yr the semimajor axis of the secondary satellites does not change significantly. The same is true for the eccentricities of the satellites, which remain high in some cases.

Similar to the cases with the secondary satellites starting at 19 R_{p} it seems that the systems presented in Fig. 9 display a resonant configuration between the satellites. To validate this hypothesis, we once again study the resonant angle for each system. In this case, the resonant angle refers to a 2:1 MMR and it is given by

$$\phi_{2:1} = 2\lambda_1 - \lambda_2 - \varpi_2. \tag{10}$$

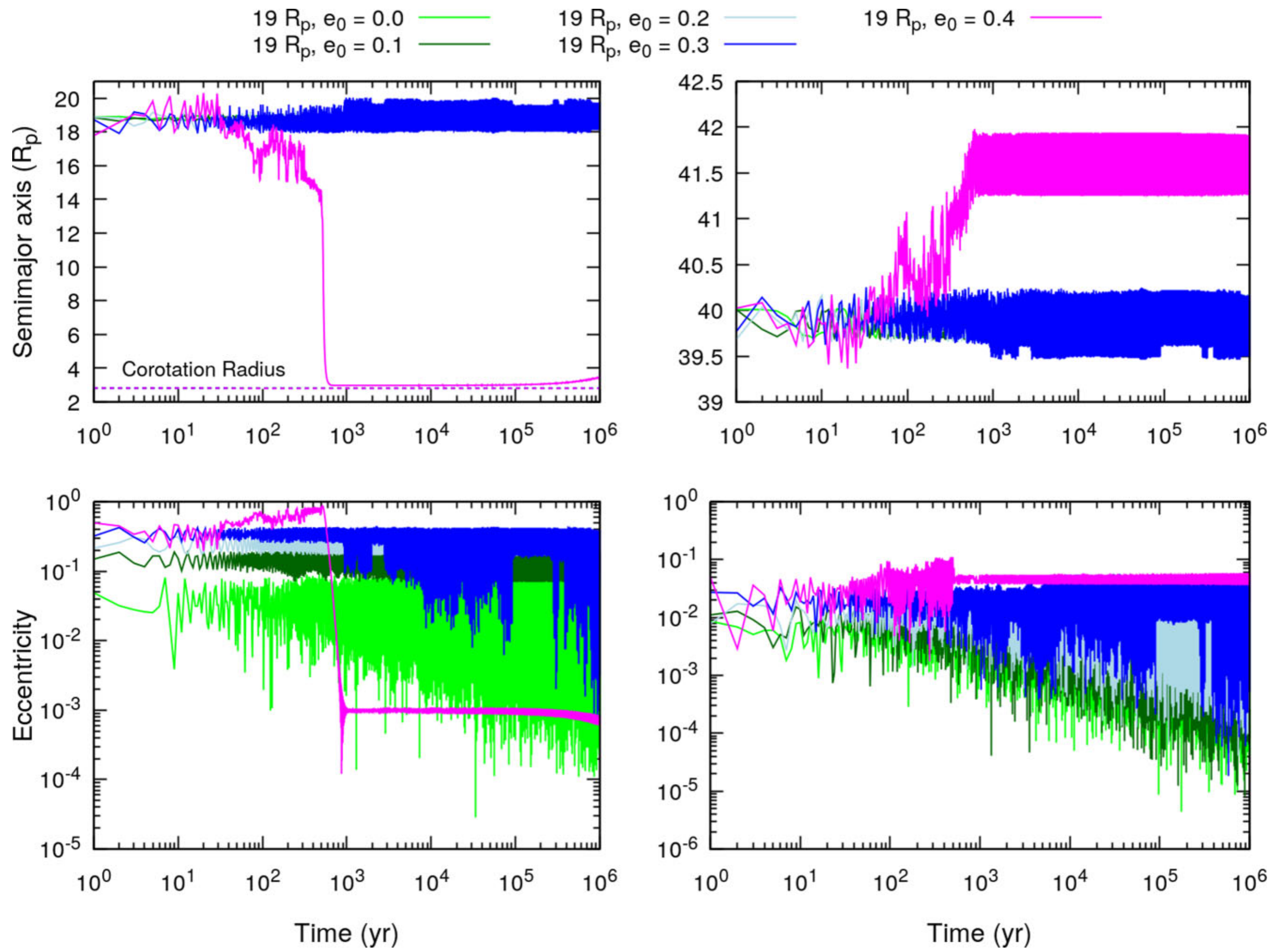

Figure 6. Time evolution of the semimajor axis and eccentricity of the primary and secondary satellites for the stable cases where the secondary satellites started at 19 R_p (near the 3:1 MMR). In the left-hand panels, we have the evolution of the semimajor axis (upper panel) and eccentricity (lower panel) of the secondary satellites. In the right-hand panels, we have the evolution of the semimajor axis (upper panel) and eccentricity (lower panel) of the primary satellites. The cases are separated by the initial eccentricity of the secondary satellites using a colour scheme: from $e_0 = 0.0$ to $e_0 = 0.4$, with $\Delta e_0 = 0.1$,we have the colours light green, green, light blue, blue, magenta, respectively. The evolution of the other cases is not shown because they result in unstable systems. The horizontal dashed line indicate the corotation radius.

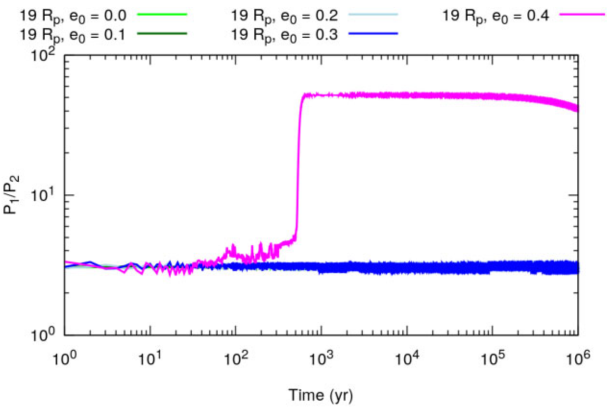

Figure 7. Time evolution of the satellites' period ratio for the stable systems presented in Fig. 6 (near the 3:1 MMR).

In Fig. 10 we show the resonant angle for all the stable systems with the secondary satellite starting at 25 R_p.

The analysis of Fig. 10 is straightforward. The case where the Earth-like satellite is initialized in a circular orbit presents a circulating resonant angle, which means that the satellites are not locked in a MMR. From Fig. 9 it can be seen that this case is the one where the semimajor axis deviates the most from its initial value. The secondary satellite started at 25 R_p has a close encounter with the primary satellite (which is clear given the increase in its eccentricity and sudden decrease in semimajor axis soon after 10 yr) and finds a stable, but not resonant, configuration around 23 R_p.

Except for the case where the Earth-like satellite is initialized in a circular orbit, all other cases present a resonant angle librating around 0° with a maximum amplitude of 50°. This behaviour supports the claim that the satellites have their motion locked in a 2:1 MMR. Because the secondary satellites placed initially farther from the planet tend to become unstable with time, we argue that the 2:1 MMR between the satellites can be the dynamical mechanism ensuring the stability of these systems. On the other hand, in some resonant systems the secondary satellite is in a very eccentric orbit, which

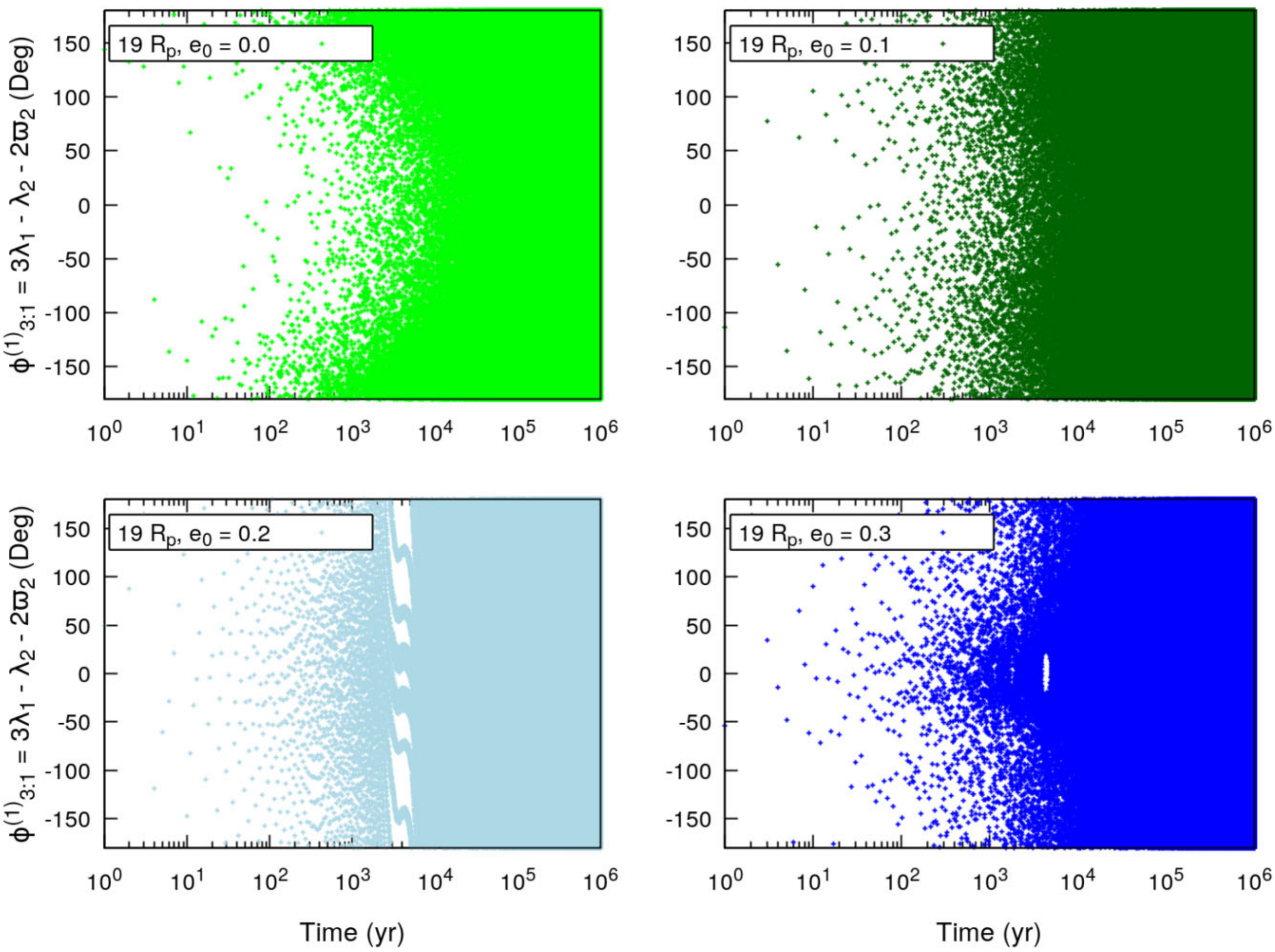

Figure 8. Time evolution of the resonant angle $\phi^{(1)}_{3:1} = 3\lambda_1 - \lambda_2 - 2\varpi_2$ (first line in equation 9) for the stable cases where the secondary satellites started at 19 R_p (near the 3:1 MMR). From top left to bottom right we have the cases separated by the initial eccentricity of the secondary satellites, from $e_0 = 0.0$ to $e_0 = 0.3$. The case with $e_0 = 0.4$ was omitted from the graph because the system is clearly not in a MMR.

might lead to a disruptive close encounter and the break of the resonant configuration between the satellites: such a dynamical event could jeopardize the stability of the systems.

4.2.3 Unstable systems near the 3:2 MMR

Beyond 25 R_p we have the presence of a 3:2 MMR resonance located near 31 R_p. However, this region was found to be empty of stable systems. The systems with the secondary satellite starting at 31 R_p became unstable almost instantaneously given the strong gravitational influence of the primary satellite. For these systems, the most common fate for the secondary satellite is a collision with the primary satellite (50 per cent of the systems), followed by ejection (30 per cent) and collision with the planet (20 per cent).

Another reason for the lack of stable systems in the 3:2 MMR location could be the overlapping of resonances. As the distances from the primary satellite are shortened, successive first-order resonances of the form $p + 1$: p will appear, each one independent of the other. As each resonance has a given width, at short distances from the exterior perturber these resonances will eventually start to overlap. As a consequence of this effect, chaotic motion could arise, leading to instability.

The location where resonance overlapping is present can be estimated analytically in some simpler cases, for example the planar circular-restricted three-body problem (Wisdom 1980). For a circular-restricted three-body problem where the particle has small eccentricity ($e \leq 0.15$), Murray & Dermott (1999) estimated the half-width from the perturber where the resonances will start to overlap as

$$\Delta a_{\rm overlap} \approx 1.24\mu^{2/7} a_{\rm out}, \tag{11}$$

where $\mu = M_{\rm out}/(M_{\rm in} + M_{\rm out})$ is the mass of the external perturber weighted by the sum of the masses of the central body and the perturber respectively, and $a_{\rm out}$ is the semimajor axis of the external perturber. Particles at $a_{\rm out} \pm \Delta_{\rm overlap}$ will present chaotic orbits. Extrapolating equation (11) for our systems, assuming $M_{\rm in} = M_p = 3\, M_{\rm Jup}$, $M_{\rm out} = M_1 = 1\, M_{\rm Nep}$ and $a_{\rm out} = a_1 = 40\, R_p$ we have $\Delta_{\rm overlap} \approx 15.6\, R_p$, which means that the whole region outside $\sim 24.4\, R_p$ would be chaotic. This is only a rough estimation for our cases because the secondary satellite is not a massless particle, and it is only valid for the satellites starting with $e_0 < 0.2$, because equation (11) is not applicable for cases where $e > 0.15$. However, this approximation somewhat fits our results, as we found that just a single initial condition starting beyond 25 R_p resulted in a stable system.

We point out that the regions of instability will change if the masses of the bodies considered and the initial radial separation of the primary satellite are different.

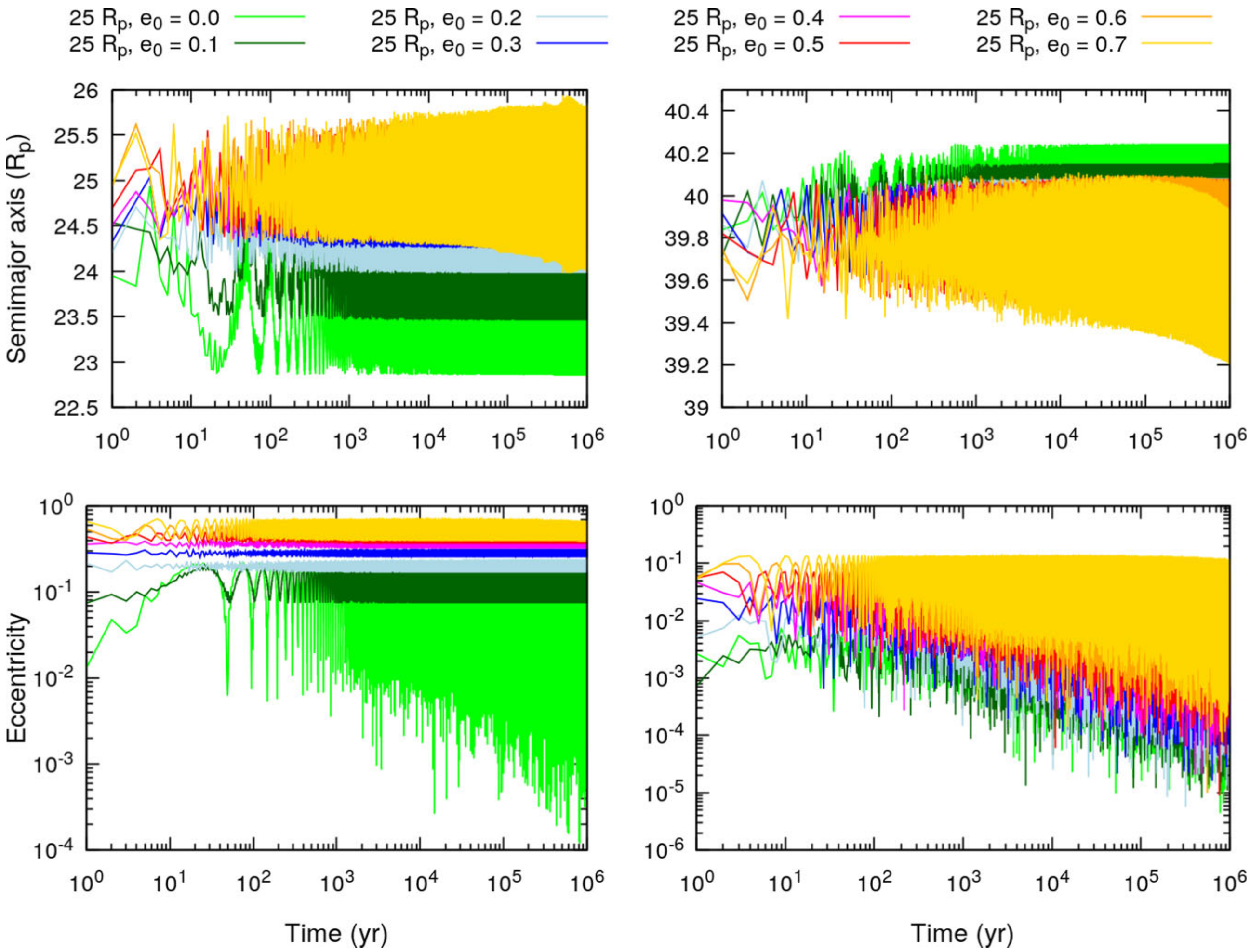

Figure 9. Time evolution of the semimajor axis and eccentricity of the primary and secondary satellites for the stable cases where the secondary satellites start at 25 $R_{\rm p}$ (near the 2:1 MMR). In the left-hand panels, we have the evolution of the semimajor axis (upper panel) and eccentricity (lower panel) of the secondary satellites. In the right-hand panels, we have the evolution of the semimajor axis (upper panel) and eccentricity (lower panel) of the primary satellites. The cases are separated by the initial eccentricity of the secondary satellites using a colour scheme – from $e_0 = 0.0$ to $e_0 = 0.7$ we have the following colours: light green, green, light blue, blue, magenta, red, orange and yellow, respectively. The evolution of the cases with $e_0 = 0.8$ and $e_0 = 0.9$ are not shown because they result in unstable systems.

5 CONCLUSIONS

In this work, we have explored the dynamical stability of an Earth-like satellite in the Kepler-1625 b system, considering that the system already has a massive satellite, the Neptunian-like candidate Kepler-1625 b-I.

In this study, we tried to answer the following questions.

(i) Given that Kepler-1625 b-I is stable, is it possible to have another massive moon in this system?

(ii) Are there preferred orbital configurations or locations for the extra satellite?

(iii) How will Kepler-1625 b-I dynamically affect this extra satellite?

To answer these questions, we performed *N*-body simulations considering a system formed by the central planet, Kepler-1625 b-I, and an extra Earth-sized satellite, using the *N*-body code POSIDONIUS. To accurately model the system, we took into account the tidal effects generated by the satellites on the planet and by the planet on the satellites, and the effects due to the rotational deformation of the simulated bodies.

We focused on the region between the planet and Kepler-1625 b-I (initially at 40 $R_{\rm p}$), such that we built a grid of initial conditions varying the semimajor axis and the eccentricity of the satellites. For the semimajor axis of the secondary satellites, we chose to place the innermost case at $a_0 = 5\,R_{\rm p}$, outside the corotation radius of the system, while $a_0 = 35\,R_{\rm p}$ was taken as the outermost initial semimajor axis, using $\Delta a_0 = 2\,R_{\rm p}$ as the width of our grid. For each initial semimajor axis we simulated 10 different cases, varying the eccentricity of the secondary satellite, from $e_0 = 0.0$ to $e_0 = 0.9$. We opted to include highly eccentric cases in our grid because we are considering the tidal effects on the satellites, which could dampen the eccentricity of such bodies to values close to zero. Thus, we have in total 160 different initial conditions.

Fig. 2 answers our first question. Yes, it is possible to have two massive satellites, an Earth-like and a Neptune-like satellite, around the planet Kepler-1625 b. We found that 50 per cent of our simulations ended with a system with two satellites stable for 1 Myr. As expected, the satellites with initial high eccentricity and orbits closer to the planet suffered a collision with the central body almost instantaneously. The same was true for the satellites initially

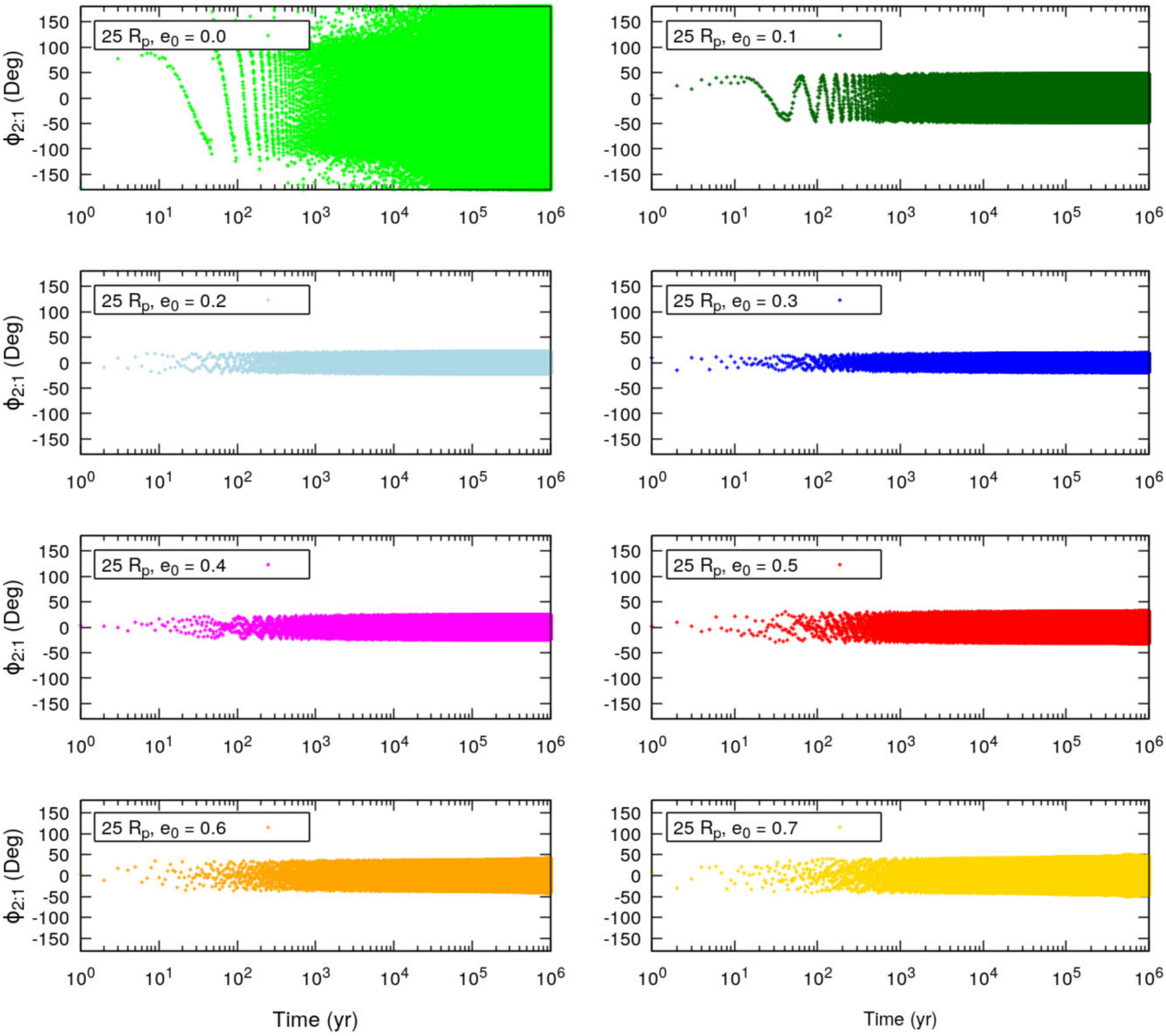

Figure 10. Time evolution of the resonant angle $\phi_{2:1} = 2\lambda_1 - \lambda_2 - \varpi_2$ for the stable cases where the secondary satellites start at 25 R_p (near the 2:1 MMR). From top left to bottom right we have the cases separated by the initial eccentricity of the secondary satellites, from $e_0 = 0.0$ to $e_0 = 0.7$.

in wider orbits, closer to Kepler-1625 b-I. Our results show that the cases where the secondary satellites were initially within 20 R_p have a higher chance of producing stable systems, even for initially eccentric configurations.

The second main question we try to answer is related to the final location of the surviving secondary satellites. We found that the primary satellite tends to remain at $\sim 40\,R_p$ for most of the cases, unless close encounters between the satellites take place. On the other hand, its orbit acquired some non-negligible eccentricity (between 0.001 and 0.1) due to the gravitational interactions with the inner satellites, even when close encounters are not found.

For the Earth-like satellites, our results showed that there is no preferred location for these satellites to be stable inside 25 R_p. Beyond this limit, the satellite will be mostly unstable due to gravitational effects from the primary satellite, generating chaotic motion produced by resonance overlapping. For the surviving systems, we found that most of the secondary satellites migrated inwards, especially the eccentric satellites (owing to the action of the satellite tides).

In addition to the satellites that experience inward migration, we have satellites that for one reason or another do not present a significant migration. These satellites are either in circular orbits, too far away to experience strong tidal interactions with the planet, or are trapped in MMRs with the primary satellite.

The third main question we answer is related to the dynamical effects of Kepler-1625 b-I on an inner massive satellite. As mentioned above, most of the satellites initially placed closer to the primary satellite ($a_0 > 25\,R_p$) become unstable.

Our results show that MMRs are responsible for most of the stable systems when the secondary satellite starts at wider orbits. We kept track of satellites starting close to the 2:1, 3:2 and 3:1 MMRs. Only the 2:1 MMR effectively influenced the stability of the satellites. The 3:2 resonance was located too close to the primary satellite, and thus the satellites near this MMR were unstable. On the other hand, the stable satellites near the 3:1 commensurability never became locked in resonance, and this resonance did not protect the most eccentric satellites from being unstable.

In summary, our work shows that the satellite system around Kepler-1625 b could be even more fascinating than is currently predicted. The system has the potential to harbour not just one but two planet-sized satellites. This theoretical secondary satellite does not show a preferable location inside 25 R_p and could be stable in almost-circular orbits close to the planet or in wider orbits locked in a MMR with Kepler-1625 b-I.

In this work, we have restricted ourselves to studying the stability of regions between the planet and the predicted location of Kepler-1625 b-I, leaving the study of regions beyond 40 R_p and co-orbital configurations for future analysis. These two studies will be complementary to that presented here, because a more extended region of the system will be explored.

Furthermore, we have only studied the coplanar case, assuming that all bodies involved have zero inclination. However, Kepler-1625 b-I, if confirmed, is predicted to have a high inclination. In this case, an additional study taking into account inclined bodies is needed. We expect that the addition of inclined bodies will not affect the stability of the innermost surviving satellites because their evolution will be still dictated by the tides from the planet. On the other hand, the outer satellites will be more likely to be affected by an inclined body and eventually become inclined or unstable. Moreover, the stability of the outermost satellites relies on the appearance of MMRs: this could be an issue when inclined bodies are considered.

ACKNOWLEDGEMENTS

We thank the anonymous referee for their valuable comments and suggestions that helped to improve the quality of this paper. This work was possible thanks to the scholarship granted from the Brazilian Federal Agency for Support and Evaluation of Graduate Education (CAPES), in the scope of the Program CAPES-PrInt, process number 88887.310463/2018-00, mobility number 88887.583324/2020-00 (RAM). JM is grateful for financial support from The São Paulo Research Foundation - FAPESP (grant: 2019/21857-3). RAM, OCW and JM are grateful for financial support from FAPESP (grant: 2016/24561-0) and The National Council for Scientific and Technological Development - CNPq (grant: 305210/2018-1). This research was supported by resources supplied by the Center for Scientific Computing (NCC/GridUNESP) of São Paulo State University (UNESP).

DATA AVAILABILITY

The data underlying this paper will be shared on reasonable request to the corresponding author.

REFERENCES

Agnor C. B., Hamilton D. P., 2006, Nature, 441, 192
Ávila P. J., Grassi T., Bovino S., Chiavassa A., Ercolano B., Danielache S. O., Simoncini E., 2021, Int. J. Astrobiology, 20, 300
Barr A. C., 2016, Astron. Rev., 12, 24
Ben-Jaffel L., Ballester G. E., 2014, ApJ, 785, L30
Bennett D. P. et al., 2014, ApJ, 785, 155
Blanco-Cuaresma S., Bolmont E., 2016, Proc. Internat. Astron. Union, 12, 341
Blanco-Cuaresma S., Bolmont E., 2017, in EWASS Special Session 4 (2017): Star-planet interactions (EWASS-SS4-2017)
Bolmont E., Raymond S. N., Leconte J., 2011, A&A, 535, A94
Bolmont E., Selsis F., Raymond S. N., Leconte J., Hersant F., Maurin A.-S., Pericaud J., 2013, A&A, 556, A17
Bolmont E., Raymond S. N., Leconte J., Hersant F., Correia A. C. M., 2015, A&A, 583, A116
Bolmont E., Oza A., Blanco-Cuaresma S., Mordasini C., Auclair-Desrotour P., Leleu A., 2019, in EPSC-DPS Joint Meeting 2019. p. 1590
Bolmont E., Demory B. O., Blanco-Cuaresma S., Agol E., Grimm S. L., Auclair-Desrotour P., Selsis F., Leleu A., 2020, A&A, 635, A117
Correia A. C. M., Rodríguez A., 2013, ApJ, 767, 128
Fox C., Wiegert P., 2021, MNRAS, 501, 2378
Hamers A. S., Portegies Zwart S. F., 2018, ApJ, 869, L27
Hansen B. M. S., 2010, ApJ, 723, 285
Hansen B. M. S., 2019, Science Advances, 5, eaaw8665
Heller R., 2018, A&A, 610, A39
Heller R., Pudritz R., 2015a, A&A, 578, A19
Heller R., Pudritz R., 2015b, ApJ, 806, 181
Heller R. et al., 2014, Astrobiology, 14, 798
Heller R., Hippke M., Placek B., Angerhausen D., Agol E., 2016, A&A, 591, A67
Heller R., Rodenbeck K., Bruno G., 2019, A&A, 624, A95
Hippke M., 2015, ApJ, 806, 51
Hussmann H., Rodríguez A., Callegari N., Shoji D., 2019, Icarus, 319, 407
Hut P., 1981, A&A, 99, 126
Kipping D., 2021, MNRAS, 500, 1851
Kollmeier J. A., Raymond S. N., 2019, MNRAS, 483, L80
Kreidberg L., Luger R., Bedell M., 2019, ApJ, 877, L15
Leconte J., Chabrier G., Baraffe I., Levrard B., 2010, A&A, 516, A64
Leleu A. et al., 2021, A&A, 649, A26
Lewis K. M., Ochiai H., Nagasawa M., Ida S., 2015, ApJ, 805, 27
Luger R. et al., 2017, Nat. Astron., 1, 1
Martin D. V., Fabrycky D. C., Montet B. T., 2019, ApJ, 875, L25
Mathur S. et al., 2017, ApJS, 229, 30
Mignard F., 1979, Moon Planets, 20, 301
Mills S. M., Fabrycky D. C., Migaszewski C., Ford E. B., Petigura E., Isaacson H., 2016, Nature, 533, 509
Moraes R. A., Vieira Neto E., 2020, MNRAS, 495, 3763
Morton T. D., Bryson S. T., Coughlin J. L., Rowe J. F., Ravichandran G., Petigura E. A., Haas M. R., Batalha N. M., 2016, ApJ, 822, 86
Murray C. D., Dermott S. F., 1999, Solar System Dynamics. Cambridge Univ. Press, Cambridge
Oza A. V. et al., 2019, ApJ, 885, 168
Quarles B., Li G., Rosario-Franco M., 2020, ApJ, 902, L20
Rein H., Spiegel D. S., 2015, MNRAS, 446, 1424
Rosario-Franco M., Quarles B., Musielak Z. E., Cuntz M., 2020, AJ, 159, 260
Sánchez M. B., de Elía G. C., Downes J. J., 2020, A&A, 637, A78
Teachey A., 2021, MNRAS, 506, 2104
Teachey A., Kipping D. M., 2018, Sci. Advances, 4, eaav1784
Teachey A., Kipping D. M., Schmitt A. R., 2018, AJ, 155, 36
Teachey A., Kipping D., Burke C. J., Angus R., Howard A. W., 2020, AJ, 159, 142
Tokadjian A., Piro A. L., 2020, AJ, 160, 194
Wisdom J., 1980, AJ, 85, 1122
Zollinger R. R., Armstrong J. C., Heller R., 2017, MNRAS, 472, 8

This paper has been typeset from a TEX/LATEX file prepared by the author.

4.2 Moraes et al., 2023 - aceito na MNRAS

Monthly Notices of the ROYAL ASTRONOMICAL SOCIETY

MNRAS **520,** 2163–2177 (2023)
Advance Access publication 2023 January 27

https://doi.org/10.1093/mnras/stad314

The dynamics of co-orbital giant exomoons – applications for the Kepler-1625 b and Kepler-1708 b satellite systems

R. A. Moraes ,[1★] G. Borderes-Motta ,[2,3] O. C. Winter[1] and D. C. Mourão[1]

[1]*UNESP, São Paulo State University – Grupo de Dinâmica Orbital & Planetologia, Guaratinguetá, CEP 12.516-410, São Paulo, Brazil*
[2]*UC3M, Univ. Carlos III de Madrid – Bioengineering and Aerospace Engineering Department, Leganés E-28911, Madrid, Spain*
[3]*IRF, Swedish Institute of Space Physics, Kiruna SE-98128, Norrbotten, Sweden*

Accepted 2023 January 24. Received 2023 January 24; in original form 2022 August 9

ABSTRACT

Exomoons are a missing piece of exoplanetary science. Recently, two promising candidates were proposed, Kepler-1625 b-I and Kepler-1708 b-I. While the latter still lacks a dynamical analysis of its stability, Kepler-1625 b-I has already been the subject of several studies regarding its stability and origin. Moreover, previous works have shown that this satellite system could harbour at least two stable massive moons. Motivated by these results, we explored the stability of co-orbital exomoons using the candidates Kepler-1625 b-I and Kepler-1708 b-I as case studies. To do so, we performed numerical simulations of systems composed of the star, planet, and the co-orbital pair formed by the proposed candidates and another massive body. For the additional satellite, we varied its mass and size from a Mars-like to the case where both satellites have the same physical characteristics. We investigated the co-orbital region around the Lagrangian equilibrium point L_4 of the system, setting the orbital separation between the satellites from $\theta_{\rm min} = 30^{\circ}$ to $\theta_{\rm max} = 90^{\circ}$. Our results show that stability islands are possible in the co-orbital region of Kepler-1708 b-I as a function of the co-orbital companion's mass and angular separation. Also, we identified that resonances of librational frequencies, especially the 2:1 resonance, can constrain the mass of the co-orbital companion. On the other hand, we found that the proximity between the host planet and the star makes the co-orbital region around Kepler-1625 b-I unstable for a massive companion. Finally, we provide TTV profiles for a planet orbited by co-orbital exomoons.

Key words: planets and satellites: dynamical evolution and stability – planets and satellites: individual (Kepler-1625 b-I, Kepler-1708 b-I).

1 INTRODUCTION

To date, more than 5000 extrasolar planets, exoplanets, have been discovered. This increasing population of bodies presents an outstanding diversity of sizes, masses, and orbital characteristics. Based on the planets of our Solar system, one would expect an abundant population of natural satellites around exoplanets, the exomoons.

Exomoons are yet to be confirmed, but several candidates are reported in the literature (Ben-Jaffel & Ballester 2014; Bennett et al. 2014; Hippke 2015; Lewis et al. 2015; Teachey, Kipping & Schmitt 2018; Heller, Rodenbeck & Bruno 2019; Oza et al. 2019; Fox & Wiegert 2021; Kipping et al. 2022). However, these candidates should be regarded with caution. Some of these satellites are either dynamically unlikely, as is the case for the satellites proposed by Ben-Jaffel & Ballester (2014), which would be orbiting outside the Hill sphere of their host planet, or simply false positives, for example, the six candidates proposed by Fox & Wiegert (2021) that were refuted from both an observational perspective (Kipping 2020) and a stability perspective (Quarles, Li & Rosario-Franco 2020a). In addition, there are satellites proposed based only on indirect effects detected on the host planet (Oza et al. 2019). Among these candidates, the two most promising are Kepler-1625 b-I (Teachey et al. 2018) and Kepler-1708 b-I (Kipping et al. 2022). Both bodies are predicted to be planet-like satellites and were proposed based on transit light curves from the *Kepler Space Telescope* (*Kepler*).

The signs of Kepler-1625 b-I were first seen in three transit light curves from *Kepler* (Teachey et al. 2018) and subsequently identified in data from the *Hubble Space Telescope* (*HST*; Teachey & Kipping 2018). However, the only transit from *HST* did not provide enough information to settle the discussion. Moreover, further analysis of the transits found evidence both in favour (Teachey et al. 2020) and against (Rodenbeck et al. 2018; Heller et al. 2019; Kreidberg, Luger & Bedell 2019) the moon hypothesis, leaving Kepler-1625 b-I as a candidate.

Kepler-1708 b-I was the only emerging exomoon candidate from a survey of 70 transiting cool giant exoplanets compiled by Kipping et al. (2022) using *Kepler*'s archive. Although there is only one transit exhibiting a faint signal supporting the newest candidate, this evidence checked all the criteria applied by the authors. Recently, Cassese & Kipping (2022) showed that Kepler-1708 b-I is unlikely to be detected by *HST*, which leaves its status unresolved. Further analysis of the transit presented by Kipping et al. (2022) and more data are needed to validate or refute the candidate.

The lack of confirmed exomoons is due to various reasons, mainly technology limitations. The space telescopes *Kepler* and *CoRot* carried expectations on the potential detection of exomoons (Szabó et al. 2006; Simon, Szatmáry & Szabó 2007; Kipping, Fossey &

★ E-mail: ricardo.moraes07@gmail.com

Campanella 2009), but only a few candidates could be proposed using data from these facilities. The *HST* also could give us hints about exomoons. However, only one transit light curve of *HST* presented signs of natural satellites (Teachey & Kipping 2018).

In the near future, a new generation of space telescopes is expected to expand the horizon of possibilities for exomoon detection. The recently deployed *JWST* could provide transit light curves to allow the confirmation of the exomoon candidates (Kipping et al. 2022) in addition to detect new ones (Limbach et al. 2021). The 2026 *PLATO* mission will search for exoplanets around stars brighter than the ones observed by *Kepler* (Rauer et al. 2014), thus also increasing the possibility of finding exomoons around close-in giant planets (Heller 2018a; Hippke & Heller 2022).

While waiting for the new telescopes, astronomers have focused on developing techniques to search for signs of exomoons on the available data. Most of the efforts are directed towards the analysis of planetary transits, such that the exomoon's transit or its indirect effects on the planet's transit can be identified (Sartoretti & Schneider 1999; Simon et al. 2007; Kipping 2009a, b; Heller 2014; Kipping 2021; Teachey 2021). In addition, Hippke & Heller (2022) released PANDORA, the first publicly available transit-fitting software to search for transits of exomoons, which aims to increase the number of scientists looking for exomoons.

Exomoons can also be addressed from a theoretical point of view. In this way, it is possible to study the stability of exomoons, thus constraining the number, mass, and location of satellites around exoplanets.

Due to observation bias, most of the detected exoplanets are giant planets orbiting close to their host star. Naturally, the first studies about the stability of exomoons were focused on satellites around these planets. Barnes & O' Brien (2002) applied tidal theory and numerical simulations to constrain the mass of satellites around close-in giant planets that would survive tidal migration and be long-term stable. Their results predicted that Earth-like moons could be stable around Jovian planets depending on the star's mass and the star–planet separation. However, Barnes & O' Brien (2002) considered the planet's inner properties and rotation to be stable for billions of years, which does not correspond to reality. Over long periods of time, planets might shrink (Fortney, Marley & Barnes 2007), while their interior cools and hardens (Guenel, Mathis & Remus 2014). Alvarado-Montes, Zuluaga & Sucerquia (2017), Sucerquia et al. (2019), and Sucerquia et al. (2020) described the tidal migration of exomoons using more robust models. Alvarado-Montes et al. (2017), for example, focused on the radius contraction and internal structure evolution of the planets to constrain the tidal migration of satellites around close-in giant planets. The authors proposed that exomoons exposed to tides would have three fates: (1) fall into the planet; (2) orbital detachment, being ejected from the planet's Hill sphere; (3) migration to a place of stability, in a quasi-stationary orbit. They found that the inward migration leading to fate (1) is suppressed, such as the exomoons will migrate towards an asymptotic maximum distance leading to fate (3) where the satellites will be stable for long periods of time. Later, Sucerquia et al. (2020) named this distance as *satellite tidal orbital parking*.

Domingos, Winter & Yokoyama (2006) numerically studied the stability of prograde and retrograde orbits of satellites around giant planets. The authors were able to derive analytical expressions for the critical semimajor axis for the stability of exomoons in both prograde and retrograde motion. The estimations presented by Domingos et al. (2006) were recently updated by Rosario-Franco et al. (2020). From an analytic perspective, Donnison (2010) applied the Hill stability criteria (Murray & Dermott 1999) to place limits on the critical separation between planets and stable satellites for various planet-satellite mass ratios. On the other hand, Namouni (2010) showed that Galilean-like satellites are unlikely to survive the inward migration of their host planet. During an inwards migration, the planet's Hill radius shrinks, such as the orbits of hypothetical satellites would become more unstable, leading to the ejection of the moons. The results of Namouni (2010) could be related to the lack of satellites detected so far around close-in giant planets.

After the announcement of Kepler-1625 b-I, new models for the stability and formation of exomoons were designed specifically for this candidate. Studies have shown that the origins of this candidate could be explained by both capture (Hamers & Portegies Zwart 2018; Heller 2018b; Hansen 2019) and *in situ* formation (Moraes & Vieira Neto 2020). However, as these models aimed to reproduce the characteristics of Kepler-1625 b-I as reported by Teachey et al. (2018) and Teachey & Kipping (2018), their applicability to other satellite systems cannot be assured (Kipping et al. 2022).

Given the size, mass, and orbital separation of Kepler-1625 b-I (Teachey et al. 2018; Teachey & Kipping 2018), it is expected that this satellite candidate underwent an intense phase of tidal migration after its formation or capture. Assuming that the host planet is a Jupiter-like body, several studies showed that a Neptune-like satellite would survive the tidal interactions with the host planet and be stable for long periods of time (Rosario-Franco et al. 2020; Tokadjian & Piro 2020; Quarles, Li & Rosario-Franco 2020b). In addition to the satellite candidate's stability, Kollmeier & Raymond (2019) and Rosario-Franco et al. (2020) showed that theoretical submoons could also be possible around Kepler-1625 b-I. Moreover, Moraes et al. (2022) showed that an extra Earth-like satellite could be stable in the Kepler-1625 b satellite system. The authors explored the regions inside the predicted orbit of Kepler-1625 b-I and found that planetary and satellite tides could stabilize inner satellites, such as these bodies will not fall into the planet or migrate outwards and collide with the satellite candidate. Also, the authors pointed out that the formation of mean motion resonances between the satellites is a dynamical mechanism that secures the stability of both satellites, even when one of the moons has an eccentric orbit.

As it was only recently announced, there are only a few theoretical studies assessing the origins and stability of the exomoon candidate Kepler-1708 b-I. Kipping et al. (2022) studied the post-formation tidal evolution of the candidate, assuming that the satellite was formed *in situ* at twice the Roche limit. The authors found that once the moon is initially beyond the corotation radius of the system with low eccentricity, the satellite migrates outwards to its proposed position. The authors pointed out that this result does not contribute to determining a possible formation scenario for the candidate, owing to the fact that any model that forms a massive satellite in a tight configuration with the planet could reproduce the tidal outwards migration they presented.

As shown by Moraes et al. (2022), more than one massive moon might be stable in the Kepler-1625 b satellite system. Here, we investigate the possibility of extra satellites being stable in a co-orbital configuration with Kepler-1625 b-I and Kepler-1708 b-I. In our Solar system, several satellites can be found exhibiting co-orbital motion, for example, the Saturnian satellite Tethys and its co-orbital companions Telesto and Calypso, and the classic example of satellites in co-orbital motion, Janus and Epimetheus also in the Saturn system.

Since Kepler-1625 b-I is predicted to be a Neptune-like satellite and Kepler-1708 b-I is expected to be a Super-Earth-like body, we aim to search for stable co-orbital companions that are also planet-like bodies. As shown by Gascheau (1843) and Routh (1874), for the general three-body problem the Lagrangian points L_4 and L_5 can be linearly stable depending on the mass of the bodies.

Before going any further describing our approach to the proposed problem, we must answer the following question: Is it possible to have co-orbital systems composed of planet-like bodies?

As mentioned before, we have co-orbital satellites in our Solar system. However, they are usually formed by two bodies with not comparable masses, with the Janus–Epimetheus system as a remarkable exception, around a planet that is significantly bigger. On the other hand, Kepler-1625 b-I and Kepler-1708 b-I are planet-like satellites, and we are proposing that these bodies have planet-like co-orbital companions. In this way, mechanisms that produce co-orbital planets could be applied to planet-like satellites.

Recently, Long et al. (2022) presented strong evidences that dust could be trapped around the Lagrangian points of a young planet candidate immersed on the LkCa 15 disc using data from the ALMA telescope. This potential discovery was already theoretically predicted in the literature. Montesinos et al. (2020) showed that up to cm-sized particles could be trapped around Lagrangian points in protoplanetary discs. The authors identified that the formation of local vortices at L_4 and L_5 in the early stages of planetary formation are responsible for this dust accumulation. If dust can agglomerate at the Lagrangian points of a giant planet, then the *in situ* formation of Earth-size co-orbital companions might be possible due to the coagulation of these particles into a single massive rocky object (Chiang & Lithwick 2005; Beaugé et al. 2007; Lyra et al. 2009; Giuppone, Benítez-Llambay & Beaugé 2012). In addition, Laughlin & Chambers (2002) used hydrodynamic simulations to show that a pair of Jupiter-like co-orbital planets could be formed by accretion in a protoplanetary disk, and this 1:1 resonance configuration would be sustainable even after the inwards migration of the planets. Other methods such as pull-down capture of a companion into co-orbital orbit, formation due to direct collision (Chiang & Lithwick 2005), convergent migration of multiple protoplanets (Thommes 2005; Cresswell & Nelson 2006) and gravitational scattering of planetesimals by a protoplanet (Kortenkamp 2005) have been proposed as alternative methods to the *in situ* formation for the origins of co-orbital planets.

For the formation of co-orbital massive satellites, Moraes & Vieira Neto (2020) showed that in-situ in a massive-solid-enhanced circumplanetary disc could explain the origins of Kepler-1625 b-I. Also, the authors showed that other satellites could form as well. This formation mechanism is compatible with the formation of co-orbital planets if dust could accumulate at the Lagrangian point of the satellite. On the other hand, if Kepler-1625 b-I was captured in a compact configuration, this object could capture pre-existing surviving satellites into co-orbital orbits during its outwards migration phase. Heller (2018b) proposed that Kepler-1625 b-I was part of a binary planetary system before being captured and that the other part of the binary was ejected during the capture phase. It is tempting to suppose that if the binary was captured intact, a co-orbital satellite system could survive. However, the author did not explore this hypothesis, and the successful capture of the complete binary seems unlikely. Another possibility is that the planet-like satellite has its own submoons that ended up being detached from the satellite and later captured into a co-orbital configuration. Even though this is a valid hypothesis, given that submoons are stable only to one-third of the satellite's Hill radius (Rosario-Franco et al. 2020), here we will be simulating co-orbital companions that are much more massive than the mass limit for submoons proposed by Kollmeier & Raymond (2019) and Rosario-Franco et al. (2020).

In order to study the stability of massive co-orbital satellites in the Kepler-1625 b and Kepler-1708 b systems, we will consider two scenarios. First, the simulated systems will be composed of the planet, the satellite candidate, and the co-orbital companion, neglecting the presence of the star. This assumption considers that Kepler-1625 b-I and Kepler-1708 b-I are both well inside the stability limit for exomoon's stability (Domingos et al. 2006; Rosario-Franco et al. 2020). In this case, we will be working with a general three-body problem. Subsequently, we will add the star of each system to the simulations. As we will see, co-orbital architectures are sensitive to perturbations, and initial conditions, such as even weaker gravitational effects, could break a once stable configuration, thus justifying the presence of the star. In addition, we want to explore the detectability of systems with co-orbital satellites. In this way, we study the influences of co-orbital satellites over the planet's transit timing variations (TTVs).

The stability of the co-orbital region of Kepler-1625 b-I and Kepler-1708 b-I will be studied considering co-orbital companions with different: masses, sizes, and initial angular positions. The radius of the bodies is taken into account only to allow collisions. Here, we do not consider any non-gravitational effect.

This paper is organized as follows. In Section 2, we present a review of the physical and orbital characteristics of the bodies forming the Kepler-1625 and Kepler-1708 systems, the initial conditions explored for the extra satellite in each case, and our numerical tools. Then, in Sections 3 and 4, we discuss our results regarding the stability and amplitude of libration of co-orbital satellites, the role of resonances on the surviving of the satellites, how the star of each system influences the stability of the co-orbital region, and an analysis of the planet's TTVs for the cases where co-orbital satellites are possible. In Section 5, we summarize our results and draw our conclusions.

2 MODEL

In this section, we describe some physical and orbital characteristics of the Kepler-1625 and Kepler-1708 systems, the different systems and initial conditions considered, and present the numerical methods used in this work.

2.1 The Kepler-1625 system

The Kepler-1625 system is composed of a G-type star with approximately 8.7 ± 2.1 Gyr (Teachey & Kipping 2018), which names the system. The star is located in the Cygnus constellation, and it is a solar-mass object ($M_\star \sim 1.079\,\mathrm{M}_\odot$) with radius $R_\star \sim 1.793\,\mathrm{R}_\odot$ (Mathur et al. 2017).

To date, only one planet has been detected in the system, Kepler-1625b. The planet was first detected via planetary transit in 2015 with data from *Kepler* (Mullally et al. 2015) and confirmed in 2016 (Morton et al. 2016). Kepler-1625 b has a predicted semimajor axis of $a_p \sim 0.87$ au (Morton et al. 2016; Heller 2018b) and its believed to have a coplanar and circular orbit (Teachey et al. 2018). The planet has a radius of $R_p = 1.18$ Jupiter's radius (R_J), however, its mass is still not well constrained. Recent photodynamical models showed a distribution of mass peaking at $M_p = 3$ Jupiter's masses (M_J) as the most likely value for the mass of Kepler-1625 b (fig. 10 from Teachey et al. 2020).

The exomoon candidate Kepler-1625 b-I was initially predicted to be a Neptune-like body, with a semimajor axis of $\sim 19.1\,R_p$ and a circular inclined orbit (Teachey et al. 2018). The inclination found for

Table 1. Canonical parameters adopted in this work for the systems Kepler-1625 and Kepler-1708. We consider the planets and satellites in circular and coplanar orbits, except when stated differently.

System	$M_\star$ $M_\odot$	$R_\star$ $R_\odot$	M_p M_J	R_p R_J	a_p ua	M_s $M_\oplus$	R_s $R_\oplus$	a_s R_p
Kepler-1625	1.079	1.793	3.0	1.18	0.87	17.15	3.865	40.0
Kepler-1708	1.1	1.1	0.81	0.89	1.64	5.0	2.61	11.7

the satellite depends on the detrending method used for transit reduction. Teachey & Kipping (2018) found that the candidate's inclination will be $42^{+15\circ}_{-18}$ for linear detrending, $49^{+21\circ}_{-22}$ for quadratic detrending, and $43^{+15\circ}_{-19}$ for exponential detrending. In the same work, the author refined the semimajor axis of the satellite, also varying from one data reduction to another, 45^{+10}_{-5}, 36^{+10}_{-13}, and 42^{+7}_{-4} R_p for linear, quadratic, and exponential detrending, respectively. Because of these uncertainties, many theoretical studies adopted the canonical value of 40 R_p for the semimajor axis of the satellite (Hamers & Portegies Zwart 2018; Moraes & Vieira Neto 2020; Moraes et al. 2022; Sucerquia et al. 2022), which agrees with the prediction given by Martin, Fabrycky & Montet (2019). However, other authors used different values for the planet-satellite separation (Tokadjian & Piro 2022).

2.2 The Kepler-1708 system

The Kepler-1708 system is formed by a star, a planet, and the recently proposed exomoon. The star is an F-type, Sun-like object located in the Cygnus constellation. The mass and radius of this body are $M_\star \sim 1.1\,\mathrm{M}_\odot$ and $R_\star \sim 1.1\,\mathrm{R}_\odot$, respectively (Kipping et al. 2022). The age of the system is estimated to be around 3.16 Gyr.

The planet Kepler-1708b was first detected in 2011 by the *Kepler* mission, but only recently validated by Kipping et al. (2022). The planet has an estimated semimajor axis of $1.64^{+0.10}_{-0.10}$ au and is classified as a cool-giant. The planet's eccentricity is not well determined, and only an upper limit can be found, $e_p < 0.4$. The same is true for the physical characteristics of the planet. Its mass has an upper bound of 4.6 M_J and a radius of $R_p \sim 0.89\,R_J$ (Kipping et al. 2022). Assuming that the planet has a density similar to Jupiter, Tokadjian & Piro (2022) set the mass of Kepler-1708 b to be $M_p = 0.81\,M_J$. The exomoon candidate is predicted to be a Super-Earth-like body with radius $R_s = 2.61^{+0.42}_{-0.43}\,R_\oplus$ and an upper limit for the mass of $M_s < 37\,\mathrm{M}_\oplus$ (Kipping et al. 2022). To find a better estimation for the satellite's mass, Tokadjian & Piro (2022) set the density of this body to be approximately equal to Neptune's. In this way, one can find $M_s = 5\,\mathrm{M}_\oplus$. Kipping et al. (2022) also found estimations for the orbital radius, $R_s = 11.7^{+3.8}_{-2.2}$ planetary radius, and inclination, $9^{+38\circ}_{-45}$, of the candidate. Despite the uncertainties, if confirmed, the satellite is expected to have low inclination. The motion of Kepler-1708 b-I is predicted to be circular around the host planet.

In Table 1, we present the canonical values for the systems Kepler-1625 and Kepler-1708 adopted in this work.

2.3 Initial conditions

2.3.1 *Models without the star – local system*

Domingos et al. (2006) and Rosario-Franco et al. (2020) calculated the stability region for exomoons around a planet. The most conservative limit proposed in the aforementioned analysis points to exomoons in circular and coplanar orbits being stable if they are located inside 0.40 Hill radius of the host planet. Neglecting the planet's eccentricity, the Hill radius of a planet can be written as

$$R_{H,p} = a_p \sqrt[3]{\frac{M_p}{3M_\star}}. \tag{1}$$

Using the canonical values for the systems Kepler-1625 and Kepler-1708 given in Table 1, from equation (1), one can see that exomoons Kepler-1625 b-I and Kepler-1708 b-I have, respectively, $a_s \sim 0.264\,R_{H,p}$ and $a_s \sim 0.047\,R_{H,p}$. In both cases, the proposed satellites are well inside the stability limit of 0.40 $R_{H,p}$. Thus, these bodies are gravitationally influenced mainly by their parent planet, such as the star of each system should not play a significant role in their orbital evolution and could be neglected.

To model our systems, we consider a planetocentric coordinate system, with the planet as the central body. The satellite candidate, Kepler-1625 b-I or Kepler-1708 b-I (hereafter 'primary satellite'), and the extra satellite (hereafter 'co-orbital companion') are initially in a co-orbital configuration, i.e. the satellites have the same semi-major axis and are only angularly separated.

Moraes et al. (2022) showed that the hypothetical Kepler-1625 b satellite system could be stable with two massive exomoons. The authors drew their conclusions after finding that an extra Earth-like satellite could survive in orbits internal to Kepler-1625 b-I. Here, we will extend this work investigating the possibility of co-orbital satellites in this system and in the Kepler-1708 system. To do so, we will explore a wide range of masses for the co-orbital companion since the stability in the three-body problem involving co-orbital bodies is very sensitive to the mass ratio between the co-orbital pair and the central body.

In our simulations, the mass and radius of the planets and the satellite candidates are taken from Table 1. In all cases, the satellites are in circular and coplanar orbits around the respective planet. The planet–satellite separation is also presented in Table 1.

For the Kepler-1625 system, we consider 18 different types of bodies as co-orbital companions, from Mars-sized to Neptune-sized. We varied the masses of these bodies from $M_2 = 0.107$ to $17.15\,\mathrm{M}_\oplus$, with the intermediate bodies having $M_2 = i\,\mathrm{M}_\oplus$, $i = 1, \cdots, 16$. The radius of the satellites was interpolated using cubic splines taking the values of Mars, Earth, and Neptune as inputs.

Similarly, for the Kepler-1708 system, we have 12 different types of co-orbital companions. The smaller and lighter body is a Mars-like companion, while for the other cases, we consider bodies with $M_2 =$ 0.5 to 5 $M_\oplus$, with $\Delta M_2 = 0.5\,M_\oplus$ and radius interpolated as before.

Once we set the characteristics of the co-orbital companion, we shall explore the initial angular position related to the primary satellite. Fig. 1 illustrates the initial set-up of our systems. We opted to vary the initial angular separation between the co-orbital satellites from $\theta_{\min} = 30^\circ$ to $\theta_{\max} = 90^\circ$, which means we will be exploring the surroundings of the Lagrangian equilibrium point L_4. In preliminary investigations, we found that for angular separations lesser than 30°, the co-orbital structure of the satellites is instantaneously destroyed.

Because of the symmetry of the problem, the results and discussions presented in the following sections are the same for the

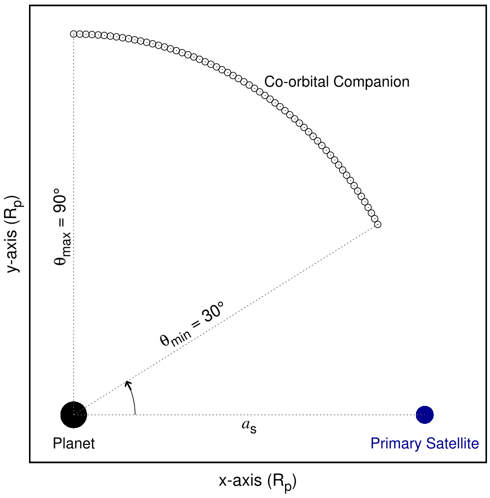

Figure 1. Illustration of our system's initial set-up. The planet (black circle) is at the origin of the coordinate system, the primary satellite (blue circle) is placed at a_s from the planet, and the co-orbital companion (open circles) is initially placed at a_s from the planet with an angular separation θ measure from the horizontal line that connects the planet and the primary satellite anticlockwise, from 30° to 90°.

respective regions around L_5. Thus, we will not analyse the case with the co-orbital companion near L_5.

We consider the satellites to be coplanar to the respective planet and initially in circular orbits. However, Kepler-1625 b-I is thought to be in an inclined configuration (Teachey et al. 2018), but since we are neglecting the presence of the star, we can assume that both satellites are in the same plane as the planet.

2.3.2 Models with the star – complete system

After our initial analysis, we will include the star of the systems and study its gravitation effects on the stability of the co-orbital architectures. For example, Kepler-1625 b has a semimajor axis smaller than 1 au, and it is a three Jupiter's masses planet. In this case, the gravitational interaction between the planet and the star could generate a non-negligible movement on the centre of mass of the system, which ultimately translates as a wobble on the star. This change in the centre of mass of the system will induce additional movement on the planet and thus jeopardize the fate of co-orbital satellites. Also, by adding the star to our simulations we can access the effects of co-orbital moons on the TTVs of the planets.

The set-ups of the simulations with the star are the same as described before without the star. The planets are considered in circular orbits with the semimajor axis taken from Table 1. Regarding the planet's inclination, Kepler-1708 b and its satellites are considered coplanar to the star. For the Kepler-1625 system, we study the case with the planet coplanar and with an inclination of 45° relative to the star (other inclinations could be chosen, given the uncertainties on this parameter (Teachey et al. 2018).

2.4 Numerical tools

For our study, we rely on numerical simulations to properly follow the time evolution of these systems since all the bodies involved gravitationally interact with each other.

Our numerical simulations were performed using the IAS15 integration scheme (Rein & Spiegel 2015) implemented in the package POSIDONIUS (Blanco-Cuaresma & Bolmont 2016). POSIDONIUS is often used in problems involving tides or other dissipative effects. However, because of familiarity with this numerical package, we found it convenient to make use of IAS15 written in RUST and opted simply to disable all the dissipative effects implemented in POSIDONIUS, computing only the gravitational interaction between the bodies. For comparison, we randomly chose some of our initial conditions and also simulated with the widely used REBOUND (Rein & Liu 2012) package. The results produced by both packages showed good agreement with compatible computational times.

3 RESULTS FOR THE LOCAL SYSTEM: PLANET-SATELLITE-CO-ORBITAL COMPANION

In this section, we present our results regarding the stability, shape, and amplitude of the co-orbital exomoons' orbits for the systems Kepler-1625 and Kepler-1708 considering a local system composed of the host planet, the satellite candidate, and the co-orbital companion.

3.1 Stability

First, we present our results for the stability of the systems. We consider a system stable if both satellites are still co-orbitals at the end of the simulations. If the co-orbital configuration is destroyed, we label the system as unstable, regardless of the fate of the satellites after they leave their co-orbital architecture.

As the literature about the dynamics of two massive co-orbital bodies is limited, we will also use results from the co-orbital restricted three-body problem as a first approximation of our findings, such that a comparison between these results can be established.

In Fig. 2, we present our grid of initial conditions (mass of the co-orbital companion versus angular separation) for the system Kepler-1625 (left-hand panel) and Kepler-1708 (right-hand panel), respectively. In green, we have the initial conditions that became stable systems, and in red the unstable conditions. The simulations were carried out for 1 Myr. As one can see, in both cases, the initial conditions for stable systems are around L_4 ($\theta = 60°$), which is an equilibrium point in the restricted three-body problem. The stability of L_4 for the general three-body problem was already predicted, but not shown, by Érdi & Sándor (2005); here, we find that to be true for some cases. Also, there is a pronounced asymmetry for conditions around L_4, especially when the co-orbital companion is less massive. These asymmetries are due to the shape of the co-orbital companion's orbit, which is more elongated in the opposite direction of the primary satellite. This feature will be explored in detail when we address the shape of the satellites' orbit.

For all the unstable systems, we found one of the following fates for the satellites: (i) collision between the satellites, (ii) collision between one satellite and the planet, and (iii) ejection of one satellite. Thus, for the local systems, we did not find in our simulations systems where both satellites survived after leaving their co-orbital configuration.

For the Kepler-1625 system, we can see a correlation between the stability and mass of the co-orbital companion (the left-hand panel of Fig. 2). The entire co-orbital region is unstable when the extra satellite has $M_2 = 5$–$8\,M_\oplus$ and $M_2 = 11$–$12\,M_\oplus$, and not even the equilibrium point at $\theta = 60°$ gave birth to stable systems. For $M_2 = 9$–$10\,M_\oplus$, only a small region close to L_4 is stable. On the other hand, for $M_2 \geq 13\,M_\oplus$ the number of stable systems increases,

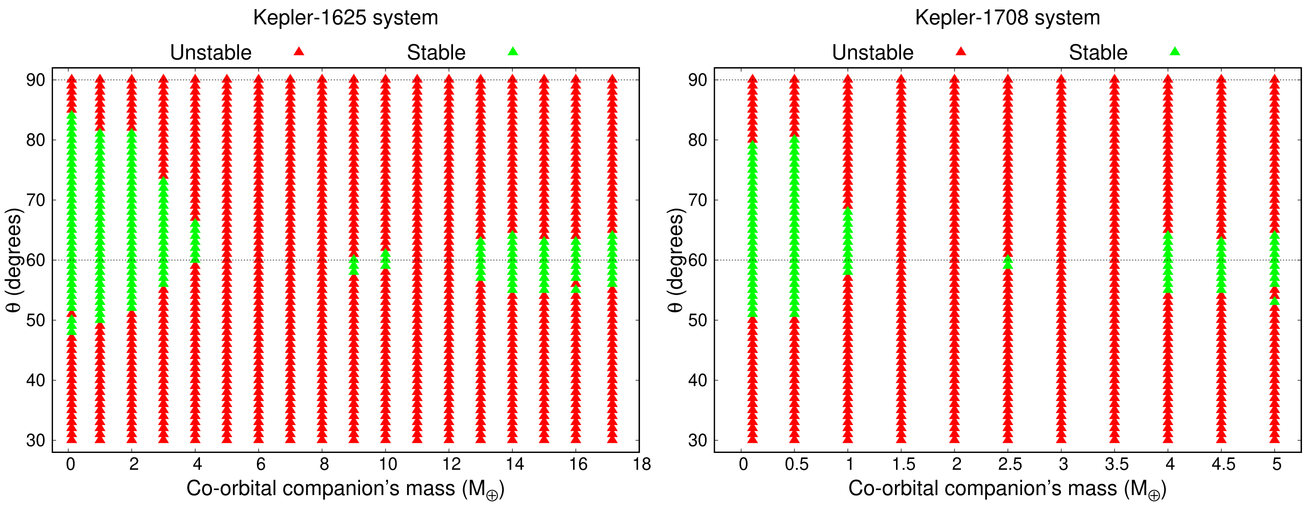

Figure 2. Grid with the initial conditions for the Kepler-1625 system (left-hand panel) and Kepler-1708 system (right-hand panel). In green, we have the conditions that end up being stable after 1 Myr, and in red the unstable cases. The horizontal dotted lines mark initial conditions at 60° and 90°.

which is counterintuitive. As the mass of the co-orbital companion increases, gravitational interactions between the satellites become stronger. In this way, one would expect the systems' stability to be compromised. However, we found the opposite. As we increased the mass of the co-orbital companions, more stable systems were found.

The same behaviour is seen for the system Kepler-1708 (the right-hand panel of Fig. 2). The unstable region as a function of the secondary satellite's mass extends from $M_2 = 1.5$ to $2.0\,\mathrm{M}_\oplus$ and from $M_2 = 3.0$ to $3.5\,\mathrm{M}_\oplus$. Same as before, in between these two unstable islands, there is a local stability close to L_4 for the systems with $M_2 = 2.5\,\mathrm{M}_\oplus$. Similar to the results for the system Kepler-1625, after the unstable valley, we found more stable conditions as the masses of the secondary satellites are increased.

The above-mentioned results suggest that the instability found for certain values of M_2 is caused by some dynamic effect that depends on the mass of the co-orbital companion. This effect will be explored in the following.

3.2 Resonances of libration frequency

In the restricted three-body problem, the motion of a co-orbital particle about the L_4 of the system is composed by the superposition of two motions (Murray & Dermott 1999). The first motion is a long-period motion of an epicentre librating about the L_4 of the system. Around this epicentre, the co-orbital satellite executes a short-period epicyclic motion, such as the final motion will be the summation of these two movements (figs 3.14 and 3.15 from Murray & Dermott 1999).

Although some similarities between the restricted and general three-body problems are expected, as the co-orbital satellites we are simulating are not particles, they will gravitationally affect the primary satellite, in which both bodies will librate with a particular frequency. To illustrate this behaviour, we show in Fig. 3 the motion of the co-orbital (left-hand panel) and the primary satellite (righ-hand panel) in the frame rotating with the initial circular frequency for 142 yr. For this example, we are considering the Kepler-1625 system, where the co-orbital companion is a Mars-size body and the satellites are initially 48° apart from each other. The same pattern of motion was found for the satellites in the Kepler-1708 system.

As one can see, the motions of both satellites depicted in Fig. 3 are similar to the motion of a particle about L_4 in the restricted three-body problem. The epicentre of the co-orbital companion is librating around L_4, while a short-period epicyclic pattern is observed in the loops of the satellite's trajectory. The same is true for the primary satellite, but in this case, the motion is performed near its initial position. The trajectory of both satellites in the rotating frame is tadpole-like, where the amplitude of the orbits is proportional to the perturbations felt by each satellite.

Similar to the restricted case, here the tadpole-like orbits are more elongated in the opposite direction of the primary satellite. In this way, a greater number of stable systems are expected when we place the co-orbital satellites with $\theta > 60^\circ$ than otherwise. This feature explains the asymmetries in the distribution of stable conditions around $\theta = 60^\circ$ shown in Fig. 1.

The numbered points in both panels of Fig. 3 represent the position of each satellite at the same time. If we follow these points, we notice that the satellites' motions are synchronized, such as both satellites crossed their initial semimajor axis at the same time (points of closest and farthest approach). Also, while one satellite is in the inner portion of its orbit (closer to the planet) the other is in the outer portion (farther from the planet) (Fig. 4). At their closest approach, the satellites exchange angular momentum, such as the orbit of the smaller satellite shrinks while the orbit of the bigger satellite expands. The ballet performed by the satellites resembles the motion of Janus and Epimetheus in the Saturn system, but with both satellites having tadpole-like orbits (Epimetheus is in a horseshoe orbit).

The two motions that shaped the orbits of the satellites have an associated frequency since the epicentric and epicyclic motions have long and short periods, respectively. In the restricted three-body problem, the commensurability of these frequencies can give birth to resonances of libration, which may cause instabilities in the system (Érdi & Sándor 2005). For the restricted three-body problem, we can define the mass parameter $\mu = M_1/(M_p + M_1)$, where M_p and M_1 are the masses of the central planet and the orbiting massive body, respectively. The frequencies of motion of a particle around L_4 are given by Murray & Dermott (1999),

$$\lambda_{1,2} = \pm \frac{\sqrt{-1 - \sqrt{1 - 27(1-\mu)\mu}}}{\sqrt{2}} \tag{2}$$

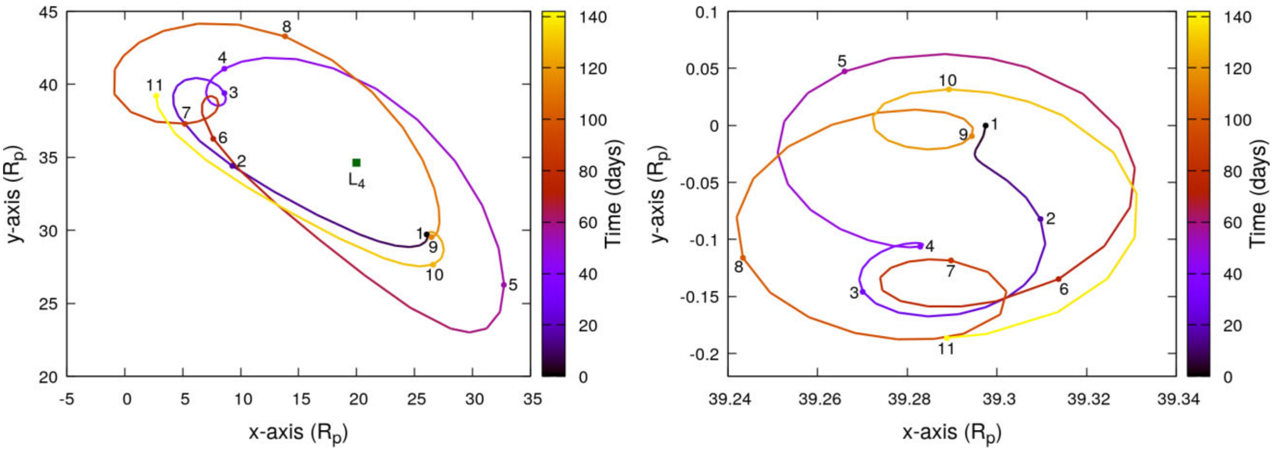

Figure 3. Motion of the co-orbital (left-hand panel) and the primary satellite (right-hand panel) in the Kepler-1625 system. The orbits of the satellites are depicted in the rotating frame for 142 yr. The co-orbital companion has 0.107 $M_\oplus$ (Mars-size) and the satellites were initially $\theta = 48^\circ$ apart from each other. The colour bar indicates the time. The numbered points show the trajectory sequence of both satellites, such as corresponding positions have the same number.

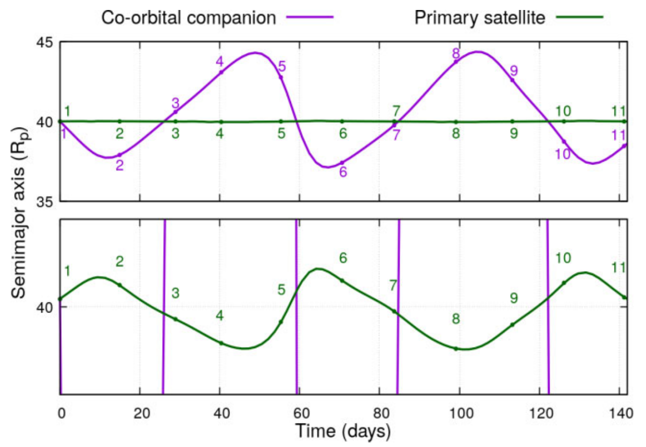

Figure 4. Evolution of the semimajor axis versus time of the satellites for the system Kepler-1625, where the co-orbital companion has 0.107 $M_\oplus$ (Mars-size) and the satellites were initially 48° apart from each other. The bottom panel is a zoom on the region with a semimajor axis between 39.95 and 40.05 R_p. The numbered points correspond to the same points presented in Fig. 3.

and

$$\lambda_{3,4} = \pm \frac{\sqrt{-1 + \sqrt{1 - 27(1-\mu)\mu}}}{\sqrt{2}}, \quad (3)$$

where $\lambda_{1,2}$ is the frequency of the short-period epicyclic motion and $\lambda_{3,4}$ is the frequency of the long-period motion of the epicentre about L_4.

Taking the ratio $\lambda_{1,2}/\lambda_{3,4}$, if we can find commensurabilities between the frequencies that can be written as the ratio of two integers, we will have resonances of librational frequencies.

One should notice that these frequencies (equations 2 and 3) depend on the mass parameter of the system, such as different resonances will appear only for systems with specific values of μ.

As shown by Érdi & Sándor (2005) (their fig. 6), some librational frequencies, in their study the 2:1 and 3:1, can cause instabilities in co-orbital systems. They showed that around the 2:1 resonance, stable systems are not found for any value of eccentricity of the secondary body, thus creating an instability island for certain values of μ. Also, the authors found that the 3:1 resonance causes the number of stable systems to decrease abruptly. However, they still found stability for cases with lower eccentricities of the secondary body. Other librational frequency resonances can be spotted in their work, for example, the 3:2, but similar to the 3:1 resonance, this commensurability only leads to a decrease in the number of stable systems, implying that stability in this case only can be found if the secondary body does not have an eccentric orbit ($e < 0.1$).

Some results from the restricted three-body problem are expected to hold in the non-restricted case. In Fig. 2, we have unstable regions for certain masses of the co-orbital companion. These results are similar to the ones found by Érdi & Sándor (2005), thus the nature of the instability could be the same.

To compare our results with the restricted case we define the mass parameter in our systems as

$$\bar{\mu} = \frac{M_1 + M_2}{M_p + M_1 + M_2}, \quad (4)$$

which is a generalization of the mass parameter considered in the restricted case.

Gascheau (1843) and Routh (1874) found that, if the co-orbital bodies were in circular and coplanar motion, the Lagrangian points L_4 and L_5 will be linearly stable if

$$\frac{M_p M_1 + M_p M_2 + M_1 M_2}{\left(M_p + M_1 + M_2\right)^2} < \frac{1}{27}. \quad (5)$$

Neglecting terms of second order and more in equation (5), we have (Leleu, Robutel & Correia 2015)

$$\frac{M_1 + M_2}{M_p + M_1 + M_2} \leq \frac{1}{27}. \quad (6)$$

One can see that the left-hand side of equation (6) is equal to the definition of $\bar{\mu}$ (equation 4). Thus, we have that $\bar{\mu} \leq 1/27 \sim 0.037$ (Gascheau's criterion). In our case, the motions of the two satellites are coplanar to the planet but only initially circular, i.e. the satellites can acquire non-negligible eccentricities during their evolution. In this way, Gascheau's criterion may not always apply, and the stability at L_4 is not guaranteed. In fact, Deprit & Deprit-Bartholome (1967) showed that for small values of eccentricity, the Gascheau's criterion applied to the restricted three-body problem (equation 5 with $M_2 = 0$), $\mu < 0.0385$ (also known as Routh's critical mass ratio), makes the co-orbital region around the Lagrangian points unstable.

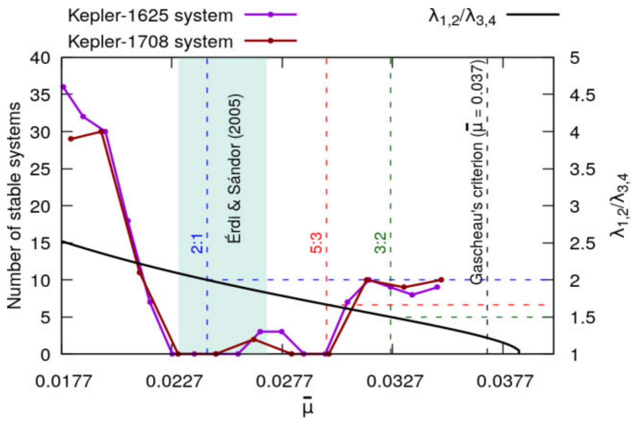

Figure 5. Number of stable systems as a function of the mass parameter $\bar{\mu}$ for the system Kepler-1625 (purple dotted line) and Kepler-1708 (dark-red dotted line). The dots mark the value of $\bar{\mu}$ as we vary the mass of the co-orbital companion. The black curve is the ratio $\lambda_{1,2}/\lambda_{3,4}$ as a function of $\bar{\mu}$, the vertical black dashed line marks the Gascheau's criterion limit ($\bar{\mu} = 0.037$), the blue, red and green dashed lines denote the location of the 2:1, 5:3 and 3:2 librational frequency resonances for the restricted three-body problem and the region in cyan is an approximation of the region of instability found by Érdi & Sándor (2005) (their fig. 6).

To estimate the locations of the librational frequency resonances in our systems, we calculate the ratio of the frequencies of motion, $\lambda_{1,2}/\lambda_{3,4}$ (equations 2 and 3), using the mass parameter $\bar{\mu}$ defined in equation (4) for all our systems. We expect that this ratio will give us an approximation for the location of the resonances once the frequencies of motion are valid only for the restricted three-body problem.

In Fig. 5, we show the number of stable systems as a function of the mass parameter $\bar{\mu}$ for the system Kepler-1625 (purple dotted line) and Kepler-1708 (dark-red dotted line), and the ratio $\lambda_{1,2}/\lambda_{3,4}$ as a function of $\bar{\mu}$ (represented by the black curve) which we used to find the libration frequency resonances 2:1 (blue dashed line), 5:3 (red dashed line) and 3:2 (green dashed line). To directly compare our results with Érdi & Sándor (2005), we draw the region in cyan, representing an approximation of the instability region they found.

From Fig. 5 one can see that the island of instability found by Érdi & Sándor (2005) was recovered in our simulations. This instability is driven by the 2:1 libration frequency resonance. As we increase the mass of the co-orbital companions, and consequently the value of $\bar{\mu}$, we found stable satellites only near L_4. In these cases, the 2:1 resonance is still affecting the co-orbital satellites, but close to L_4, the perturbations are weaker.

Near the 5:3 resonance, we also found only unstable systems. This result agrees with the prediction of Érdi & Sándor (2005), where the authors found only a few stable orbits for satellites in nearly circular motion. We also located the 3:2 libration frequency resonance. For this value of $\bar{\mu}$, equivalent to $M_2 = 16\,M_\oplus$ (system Kepler-1625) and $M_2 \sim 4.5\,M_\oplus$ (system Kepler-1708), we found eight and nine initial conditions that returned stable systems for the Kepler-1625 and the Kepler-1708 system, respectively. In all cases, both satellites sustained an almost circular orbit around the planet. These results are in good agreement with the findings of Érdi & Sándor (2005) as well.

3.3 Angular instabilities

In addition to the instabilities that appeared because of the variation in the mass of the co-orbital companion, we detected some smaller islands of instability inside larger islands of stability for certain angular separations. In the Kepler-1625 system, there are two cases of angular instabilities. These two cases appear when we set the co-orbital companion to (i) a Mars-sized body initially with $\theta = 51^\circ$ and (ii) a 16-Earth masses body initially with $\theta = 56^\circ$. For case (i), the system becomes unstable after ∼1362 yr when a collision between the satellites takes place. In case (ii), the two satellites also collided, but after only ∼62 yr. For the Kepler-1708 system, when the co-orbital satellites have the same masses ($5\,M_\oplus$) we found instability for two specific angles inside a stability island, $\theta = 54^\circ$ and 55°. In both cases, the satellites collided with each other before 2 yr.

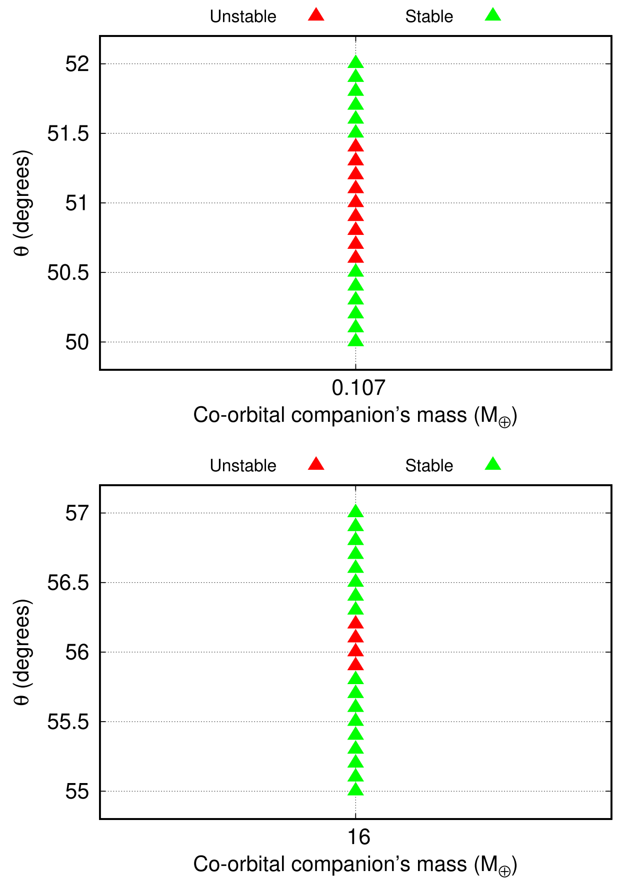

Figure 6. Zoom on the angular separation of the isolated instabilities found in the Kepler-1625 system for a Mars-sized co-orbital companion initially at $\theta = 51^\circ$ (top panel) and for a 16-Earth masses co-orbital companion initially at $\theta = 56^\circ$ (bottom panel).

Even though the nature of the above-mentioned instabilities is the same, to make the manuscript clearer we will separate the analysis of the Kepler-1625 and Kepler-1708 systems.

3.3.1 *Kepler-1625 system*

Fig. 6 shows a zoom on the angular separation of the co-orbital satellites around the angles we found peculiar instabilities. For these cases, we performed more simulations using $\Delta\theta = 0.1^\circ$ to identify the extension of the instability islands. As one can see the instabilities are local, with small amplitudes (less than 1°). The structure of these instabilities suggests that initially, we had large stable islands, but due to resonant effects, these islands fragmented into smaller ones.

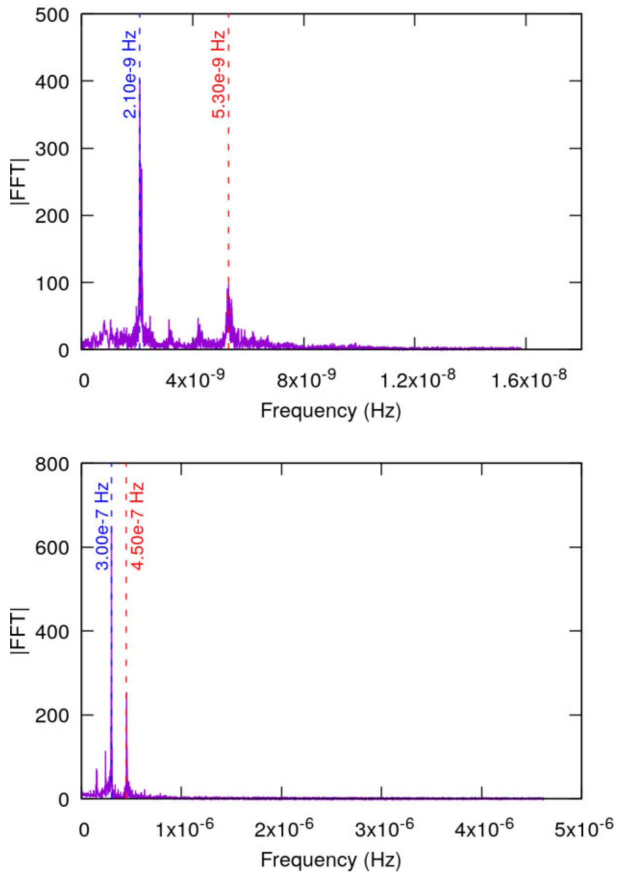

Figure 7. Magnitude of the Fast Fourier Transform associated with the frequencies present in the evolution of the angular separation of the satellites in the Kepler-1625 system. Top panel: The co-orbital satellite is a Mars-sized body with an initial angular separation of 51°. Bottom panel: The co-orbital satellite is a 16-Earth masses body with an initial angular separation of 56°.

In these cases, the unstable regions are dominated by chaotic motion (see fig. 3 in Liberato & Winter 2020).

One should notice that the librational frequency resonances we studied before cannot be responsible for these local instabilities since the frequencies given by equations (2) and (3) are functions of the mass parameter of the system, while these new features are related to the angular separation of the satellites.

To find the potential resonances acting on θ, we will study the time evolution of the angular separation between the co-orbital satellites. In this way, we can apply a Fast Fourier Transform (FFT) to isolate the dominant frequencies in the time series and investigate if resonances are causing the instabilities we observed.

Fig. 7 shows the magnitude of the FFT associated with the frequencies present in the evolution of the angular separation between the co-orbital satellites.

On the top panel of Fig. 7, we have the FFT analysis of the frequencies of θ for the co-orbital pair formed by the primary satellite and the Mars-sized companion. As one can see, there are two peaks of magnitude around $2.10 \times 10^{-9}\ Hz$ and $5.30 \times 10^{-9}\ Hz$, representing the two dominant frequencies in θ. Taking the ratio of these two frequencies, we find approximately a 5/2 commensurability, which can be understood as a 5:2 resonance between the libration of the co-orbital satellite about L_4 and the angular motion period of the satellites. This third-order resonance was responsible for increasing the eccentricity of the co-orbital companion. In this way, the orbits of the satellites crossed and led to a collision between the bodies.

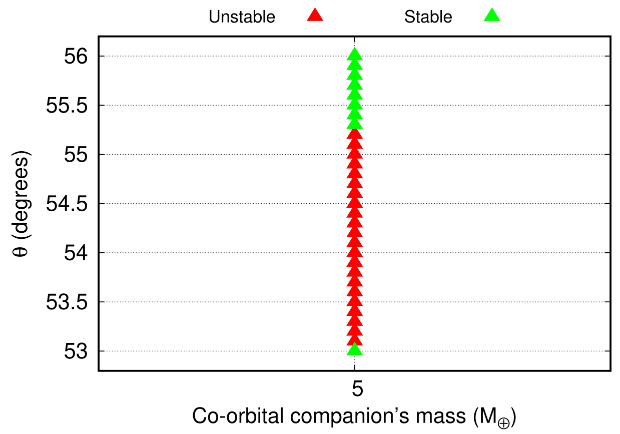

Figure 8. Zoom on the angular separation of the isolated instabilities found in the Kepler-1708 system for a 5-Earth masses co-orbital companion initially located at $\theta = 54°$ and 55°.

The same discussion applies to the co-orbital pair of the primary satellite and the 16-Earth masses companion with initial angular separation $\theta = 56°$. The FFT analysis revealed the frequencies $3.00 \times 10^{-7}\ Hz$ and $4.50 \times 10^{-7}\ Hz$ as the dominant ones on the evolution of θ. Once again, comparing these frequencies, we find a 3:2 commensurability. This particular resonance suddenly increased the eccentricity of both satellites resulting in a collision.

3.3.2 Kepler-1708 system

For the Kepler-1708 system, we found an island of instability inside a greater island of stable initial conditions only for the systems where the satellites have the same masses, 5 $M_\oplus$. In this case, the satellites are stable when their initial angular separation is $\theta = 53°$ and for $\theta = 56°-64°$, leaving a gap of unstable conditions for $\theta = 54°$ and 55°.

To precisely locate the border of this instability, we follow the approach used for the Kepler-1625 system, first refining the initial conditions between $\theta = 53°$ and 55° using $\Delta\theta = 0.1°$ and then applying an FFT analysis for the frequencies of θ. Differently from the previous cases, for the Kepler-1708 system, the amplitude of the angular instability is wider than 1° (Fig. 8) extending from 53.1° to 55.2°. In most cases, the satellites collided with each other within one year, which could point toward the presence of strong resonances acting over the satellites' angular separation.

Fig. 9 shows the FFT analysis of the frequencies in the evolution of θ for the initial separations of 54° (top panel) and 55° (bottom panel), respectively. In both cases, taking the ratio between the dominant frequencies, we find approximately 2, which indicates the proximity of the 2:1 resonance. This first-order resonance abruptly increases the eccentricity of the satellite leading to an almost instantaneous collision.

3.4 Amplitude of motion

As shown before, the orbits of the primary satellite and its co-orbital companion have a tadpole-like shape. However, we did not address the amplitude of these motions since we only showed one example (a system with a Mars-like co-orbital companion with an initial angular separation of $\theta = 48°$ in the Kepler-1625 system).

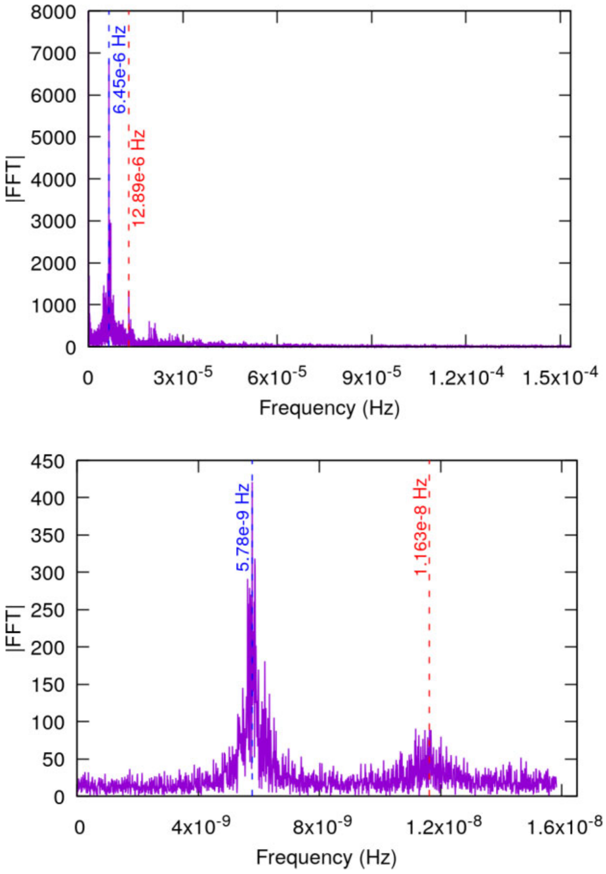

Figure 9. Magnitude of the Fast Fourier Transform associated with the frequencies present in the evolution of the angular separation of the satellites in the Kepler-1708 system. Top panel: Initial angular separation of 54°. Bottom panel: Initial angular separation of 56°. In both cases the satellites have the same masses, 5 $M_\oplus$.

The amplitude of the satellites' orbits depends on the magnitude of the perturbations they will receive from the other satellite and the planet. On the other hand, these perturbations are proportional to the mass and initial angular separation of the co-orbital pair. For example, less massive co-orbital companions will be more affected by perturbations from the primary satellite than more massive companions. Also, as the L_4 is an equilibrium point, such as the net force at this point is minimum, at this location, the amplitude of the satellites' motion is expected to be small.

In Fig. 10, we show the amplitude of motion of the co-orbital companion satellites ($\Delta\theta_2$) for each initial angular separation for the Kepler-1625 (left-hand panel) and Kepler-1708 (right-hand panel) system, respectively. For better visualization, we only present the cases for $\theta \leq 60°$, but for greater separations, the behaviour follows the same pattern. The primary satellite always starts at $\theta = 0°$. Thus, its angular displacement is not significant compared to the motion of the co-orbital companion. In this way, we will neglect the analysis of this motion.

As expected, the motions of the co-orbital companions are around L_4 ($\theta = 60°$), although not necessarily symmetrical. Also, as the mass parameter $\bar{\mu}$ decreases, stable orbits with larger amplitudes of libration are possible (Leleu, Robutel & Correia 2018). In our simulations, we did not find satellites in horseshoe orbits. Roberts (2002) showed throughout analytic calculations that horseshoe configurations in the general three-body problem are stable only for $\bar{\mu} \leq 3 \times 10^{-4}$, which is not the case for our systems. For the restricted three-body problem, numerical simulations found this limit to be $\mu \leq 9.5 \times 10^{-4}$ (Liberato & Winter 2020).

Stable co-orbital companions initially farther from L_4 presented a larger amplitude of motion because of the perturbations they received from the primary satellite at the moment of their closest approach. If the satellites are too close to each other, this close encounter may result in collisions or ejections of the less massive body. On the other hand, for satellites with initial $\theta > 60°$, the amplitude of libration is similar to the ones presented here.

4 RESULTS FOR THE COMPLETE SYSTEM: STAR-PLANET-SATELLITE-CO-ORBITAL COMPANION

In this section, we study the stability of co-orbital exomoons taking into account the star of the systems. The initial conditions for the planet-satellites systems will be the same as in Section 3, only adding the star as the central body and considering the respective planet with the semimajor axis given in Table 1. The planets will be considered in circular and coplanar orbits. For the system Kepler-1625, the planet is predicted to have a non-neglectable inclination Teachey et al. (2018), in this case, we will also simulate the case with $I_p = 45°$.

In adding the star, we will study the influence of the satellites on the planet's motion. In this way, we can find the planet's TTVs characterized by the presence of co-orbital exomoons.

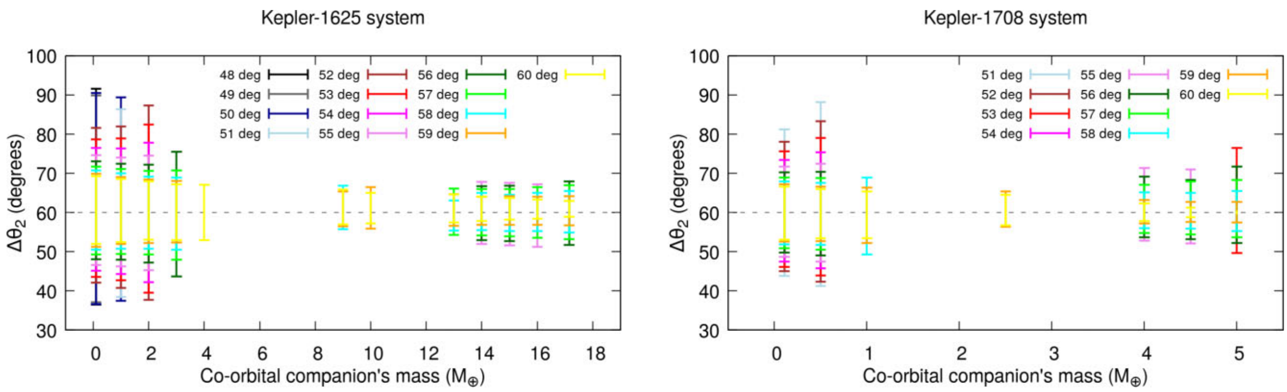

Figure 10. Amplitude of libration of the co-orbital companions ($\Delta\theta_2$) versus their masses for the systems Kepler-1625 (top panel) and Kepler-1708 (bottom panel). The colour scheme represents the initial θ of each satellite.

Table 2. Results of our simulations for the system Kepler-1625 considering the star. For each column, we have the systems separated by the mass of the co-orbital companion (M_2), and the number and percentage of systems with collisions between the planet and the co-orbital companion (Coll. $M_p - M_2$), collisions between the satellites (Coll. $M_1 - M_2$), collisions between the planet and Kepler-1625 b-I (Coll. $M_p - M_2$), ejections of the co-orbital companion (M_2 Ejected), ejections of Kepler-1625 b-I (M_1 Ejected), and ploonets. In the last row, we have the summation of all simulated cases and their respective percentages.

M_2 $\mathrm{M}_\oplus$	Coll. $M_p - M_2$	Coll. $M_1 - M_2$	Coll. $M_p - M_1$	M_2 Ejected	M_1 Ejected	Ploonet
0.107	26 (∼ 42.6 per cent)	28 (∼ 45.9 per cent)	7 (∼ 11.5 per cent)	–	–	–
1.0	24 (∼ 39.3 per cent)	31 (∼ 50.8 per cent)	6 (∼ 9.8 per cent)	–	–	–
2.0	24 (∼ 39.3 per cent)	33 (∼ 54.1 per cent)	4 (∼ 6.6 per cent)	–	–	–
3.0	22 (∼ 36.1 per cent)	33 (∼ 54.1 per cent)	5 (∼ 8.2 per cent)	–	–	1 (∼ 1.6 per cent)
4.0	20 (∼ 32.8 per cent)	32 (∼ 52.5 per cent)	9 (∼ 14.8 per cent)	–	–	–
5.0	24 (∼ 39.3 per cent)	29 (∼ 47.5 per cent)	7 (∼ 11.5 per cent)	1 (∼ 1.6 per cent)	–	–
6.0	23 (∼ 37.7 per cent)	28 (∼ 45.9 per cent)	8 (∼ 13.1 per cent)	2 (∼ 3.3 per cent)	–	–
7.0	16 (∼ 26.2 per cent)	35 (∼ 57.4 per cent)	7 (∼ 11.5 per cent)	3 (∼ 4.9 per cent)	–	–
8.0	16 (∼ 26.2 per cent)	32 (∼ 52.4 per cent)	3 (∼ 4.9 per cent)	9 (∼ 14.8 per cent)	1 (∼ 1.6 per cent)	–
9.0	16 (∼ 26.2 per cent)	36 (∼ 59.0 per cent)	4 (∼ 6.6 per cent)	4 (∼ 6.6 per cent)	1 (∼ 1.6 per cent)	–
10.0	10 (∼ 16.4 per cent)	42 (∼ 68.9 per cent)	2 (∼ 3.3 per cent)	6 (∼ 9.8 per cent)	1 (∼ 1.6 per cent)	–
11.0	14 (∼ 22.9 per cent)	36 (∼ 59.0 per cent)	5 (∼ 8.2 per cent)	5 (∼ 8.2 per cent)	1 (∼ 1.6 per cent)	–
12.0	12 (∼ 19.7 per cent)	43 (∼ 70.5 per cent)	2 (∼ 3.3 per cent)	1 (∼ 1.6 per cent)	1 (∼ 4.9 per cent)	–
13.0	10 (∼ 16.4 per cent)	39 (∼ 63.9 per cent)	–	7 (∼ 11.5 per cent)	5 (∼ 8.2 per cent)	–
14.0	13 (∼ 21.3 per cent)	36 (∼ 59.0 per cent)	2 (∼ 3.3 per cent)	7 (∼ 11.5 per cent)	3 (∼ 4.9 per cent)	–
15.0	17 (∼ 27.9 per cent)	29 (∼ 47.5 per cent)	1 (∼ 1.6 per cent)	8 (∼ 13.1 per cent)	6 (∼ 9.8 per cent)	–
16.0	10 (∼ 16.4 per cent)	37 (∼ 60.7 per cent)	2 (∼ 3.3 per cent)	9 (∼ 14.8 per cent)	3 (∼ 4.9 per cent)	–
17.15	3 (∼ 4.9 per cent)	45 (∼ 73.8 per cent)	1 (∼ 1.6 per cent)	10 (∼ 16.4 per cent)	2 (∼ 3.3 per cent)	–
Total	**300** (∼ **27.3** per cent)	**624** (∼ **56.8** per cent)	**75** (∼ **6.8** per cent)	**72** (∼ **6.6** per cent)	**26** (∼ **2.4** per cent)	**1** (∼ **0.09** per cent)

In the following, we analyse the results for the Kepler-1625 and Kepler-1708 systems, separately.

4.1 Kepler-1625 system

For the Kepler-1625 system considering the star, all the simulated cases ended with unstable systems regardless of the mass of the co-orbital companion, its initial angular position, or the inclination of the planet. In Table 2, we present a summary of the outcomes of the simulations separated by the co-orbital companions' masses.

Even though the satellites are well inside the Hill radius, $a_s \sim 0.264\, R_{\mathrm{H},p}$, the gravitational perturbations of the star are strong enough to disrupt the initial co-orbital architecture of the satellites. The systems fall apart usually within a few centuries, resulting in collisions between the planet and the satellites, collisions between the satellites, ejections of one of the moons, or the exomoon leaving its planetocentric orbit and assuming an orbit around the star, thus becoming a planet or a *ploonet* (Sucerquia et al. 2019).

From Table 2, one can see that the most common outcome of our simulations was the collision between the satellites, especially for more massive co-orbital companions. This result is expected in the case of unstable systems since the satellites share the same orbit. Also, we point out the high number of systems ending with the collision between the co-orbital companion and the planet. In this case, the satellite is stripped from its co-orbital orbit, suffers an eccentricity excitation, and collides with the parent body.

To consider the possibility of satellites being ejected from the system, we set the distance of 300 au from the star as the maximum distance a body could reach. Former satellites whose orbits extend beyond this limit are considered ejected from the system. Satellites were ejected only for systems with 5-Earth masses satellites as co-orbital companions. For these systems, the close encounters between satellites are very energetic, resulting in the ejection of one of the satellites, usually the smaller one. Although, we also found cases in which the most massive satellite was the first body ejected from the system.

For the system formed with a 3-Earth masses co-orbital companion initially at $\theta = 65°$, we found that the secondary satellite was ejected from its planetocentric orbit in an inner heliocentric orbit. However, the satellite did not collide with the star and survived as a detached moon, or *ploonet* as named by Sucerquia et al. (2019). We follow the evolution of this body for 45 thousand years, and the *ploonet* remained in a stable configuration with the rest of the system. It is out of the scope of this work to investigate in detail the long-term evolution of this body, especially because it represented only 0.09 per cent of the total sample. However, as shown in Hansen (2022), unbound moons detached from their planet through tidally driven outward migration are likely to collide with the parental body within millions of years. In this way, the *ploonet* we found could have the same fate long-term.

4.2 Kepler-1708 system

4.2.1 Stability

Different from the Kepler-1625 system, adding the star of the system Kepler-1708 did not significantly change our results regarding the stability of the co-orbital satellites.

In Table 3, we present a summary of the stable system for the cases with and without the star. As one can see, small differences between the results appear only on the border of the stability regions for some systems, while most of the results from Section 3 are recovered. In this case, we argue that the gravitational influences of the star are minor or even negligible for the Kepler-1708 system.

There are mainly two reasons for the star not being relevant for the stability of co-orbital satellites on the Kepler-1708 system: (i) the star–planet separation; (ii) the position of the satellites related to the planetary Hill radius.

Kepler-1708 b is a cool-giant with a semimajor axis of $a_p = 1.64$ au. As the gravitational force of a body into another is inversely

Table 3. Stable initial conditions for the system Kepler-1708 for the cases with and without the star. The results are presented as a function of the mass of the co-orbital companion (M_2).

M_2 $M_\oplus$	θ without the star (deg)	θ with the star (deg)
0.107	51–79	50–79
0.5	51–80	51–80
1.0	58–68	59–68
1.5	–	–
2.0	–	–
2.5	59–60	59–60
3.0	–	–
3.5	–	–
4.0	55–64	56–64
4.5	55–63	55–63
5.0	53, 56–64	53, 56–64

proportional to the distance between them, the influence of the star over the orbit of the planet, and consequently over its satellites, is less significant than what is expected for a close-in planet. For example, in the Kepler-1625 system, the star–planet distance is 0.87 au and we found that co-orbital satellites are unstable if the star is considered.

The exomoon candidate Kepler-1708 b-I is predicted to have a semimajor axis of $a_s \sim 0.047\ R_{\mathrm{H},p}$. At this distance, the gravitational force of the star is supplanted by the presence of the planet. Thus, the satellites will not feel the presence of the star. For the Kepler-1625 system, the satellites are farther from the planet ($0.264\ R_{H,p}$), while the planet is closer to the star. The combination of these two features jeopardized the presence of massive co-orbital satellites to Kepler-1625 b-I.

4.2.2 *TTVs considering co-orbital exomoons*

Several authors proposed that TTVs could be used to indirectly detect the presence of more bodies in an exoplanetary system, planets (Holman & Murray 2005; Agol et al. 2005; Nesvorný & Vokrouhlický 2014; Agol & Fabrycky 2018), or exomoons (Sartoretti & Schneider 1999; Szabó et al. 2006; Simon et al. 2007; Kipping 2021). This indirect effect manifests itself as fluctuations in the timing of planetary transits and can be used to infer the presence of planets and moons in systems where at least one planet is known to be transiting.

In this section, we present a TTV analysis for the stable systems with co-orbital exomoons for the Kepler-1708 system.

Our synthetic TTVs will be constructed as follows: (i) we set-up a coplanar system, (x, y), with the star in the origin of the system. The planet is positioned at (a_p, 0), and the satellites are placed around the planet; (ii) we define that the observer is located along the positive direction of the x-axis; (iii) the system will be integrated forward in time, with the planet motion being restricted to the (x, y) plane and anticlockwise; (iv) at each half day interval we will verify if the planet crossed the x-axis from negative y to positive y. If this is the case, we take the time before and after the passage through x and apply a bisection method to precisely find the time of crossing, which we define as a transit time; (v) we stop the simulation when 200 transits are obtained; (vi) at last, we remove the linear trend from our transit times applying a linear least square fit to our data. This process is done for systems considering only Kepler-1708 b-I and systems with the exomoon candidate and its co-orbital companion, such as we can measure the contribution of the co-orbital companion

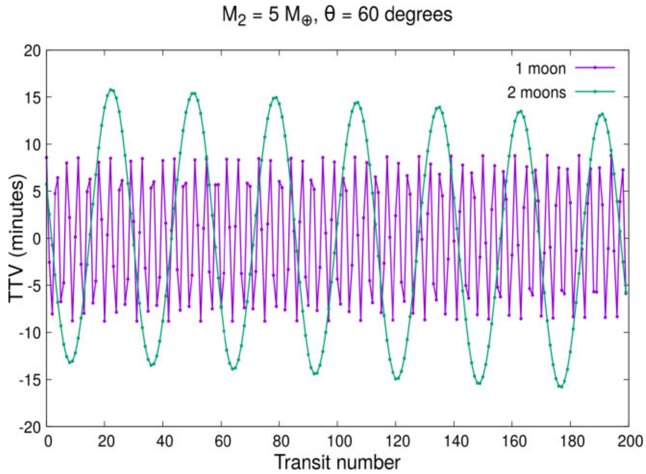

Figure 11. TTVs for a planet with only one moon (purple) and for a planet with a co-orbital pair of satellites (green). The satellites have the same masses, 5 $M_\oplus$, and they are initially 60° apart from each other.

to the planet's TTV. The simulations are performed using the IAS15 integrator from the REBOUND.[1]

In Fig. 11, we compare the TTVs generated by a system with only one moon and a system with a 5 $M_\oplus$ co-orbital companion. As one can see, the amplitude of the TTV increased by more than 5 min with the addition of a co-orbital satellite with the same mass as the primary satellite. This variation is significant since the original amplitude of the TTV, considering only one moon, is smaller than 9 min, which is an expected outcome. As shown by Kipping (2009a), the amplitude of the TTV is proportional to the mass of the exomoons. Also, we found that the presence of a co-orbital moon increased the periodicity of the TTVs, allowing us to draw a smoother fit for our data.

For less massive co-orbital companions, the effects on the planet's TTV are minor. For example, for a Mars-like companion, the amplitude of the TTV only increased about 0.1 min.

We also investigated the influences of the initial angular separation of the satellites on the planet's TTVs, but no significant changes were found.

5 CONCLUSIONS

In this work, we studied the stability of co-orbital exomoons using the candidates Kepler-1625 b-I and Kepler-1708 b-I as case studies. The proposed exomoons are predicted to be Super-Earth-like satellites. Thus, we opted to work with massive planet-sized satellites as co-orbital companions. We considered bodies with mass and size varying from Mars-like to a body with the same physical attributes of the respective proposed satellite. The latter being chosen so we will have co-orbital satellites with the same mass and size.

We considered two scenarios, with and without the star as the central body. In the first case, the planet is the central object and the system's dynamics are modelled by the general three-body problem. Adding the star, we increase the complexity and reality of the problem. The gravitational effects of the star will be of great relevance for the Kepler-1625 system since the host planet, in this case, have a semimajor axis smaller than 1 au. Also, considering the

[1] We opted to use REBOUND instead of POSIDONIUS here because REBOUND allows us to control the integration time and time-step more easily than POSIDONIUS.

star, we can predict the effects of co-orbital satellites on the planet's TTV, which is not found in the literature yet.

This work aimed to

(i) verify the conditions for stability of co-orbital massive exomoons on the Kepler-1625 b and the Kepler-1708 b systems;
(ii) study the role of libration resonances on the stability of the systems;
(iii) understand the correlation between the amplitude of libration of the co-orbital companion satellite and the perturbations from the primary satellite;
(iv) measure the effects of the system's star over co-orbital exomoons;
(v) provide planetary TTV profiles for systems with co-orbital exomoons.

In the following, we discuss our results for the systems with and without the star separately.

5.1 Local system: planet–satellite–co-orbital companion

As predicted by Gascheau (1843) and stated later by Érdi & Sándor (2005), the vicinity of L_4 was indeed stable for most of the different co-orbital companions we tested. However, we find that for less massive satellites (Mars-like bodies), this region can extend for initial angular separations between 48° and 84° for the Kepler-1625 system and from 51° to 79° for the Kepler-1708 system. The extension of the stable region slowly decreases as we increased the mass and size of the co-orbital companion until we found stable configurations only near L_4, as initially expected. Also, we found instability islands for specific values of co-orbital satellites' mass, $M_2 = 5$–$8\,\mathrm{M}_\oplus$ and $M_2 = 11$–$12\,\mathrm{M}_\oplus$ for the Kepler-1625 system, and $M_2 = 1.5$–$2.0\,\mathrm{M}_\oplus$ and $M_2 = 3$–$3.5\,\mathrm{M}_\oplus$ for the Kepler-1708 system. For these systems, not even the initial conditions placed at L_4 survived.

To understand the causes of the instabilities as a function of the mass of the co-orbital companion, we went back to the results of the restricted three-body problem and drew comparisons between our results and the classical ones.

In Érdi & Sándor (2005), the authors mapped the stability of co-orbital systems with different mass parameters under the assumptions of the restricted-three body problem, considering two massive bodies and a particle. They found that librational resonances play a decisive role in raising instabilities depending on the mass parameter of the system. Also, some of these resonances, the 2:1 for example, are so strong that the co-orbital region is unstable for particles, even if the secondary body is in initially circular motion around the primary body.

First of all, we showed that similarly to the restricted case, in our systems, the motion of the co-orbital satellites is described by the superposition of two different motions: a short-period epicyclic motion about the epicentre; and a long-period motion of the epicentre about L_4. Thus, we calculate an approximation for the frequencies of these two motions using equations (2) and (3), derived for the restricted-three body problem, with the mass parameter $\bar{\mu}$ given by equation (4).

From our analysis, we found that the 2:1 and 5:3 libration resonances may be responsible for the islands of instabilities we detected as we increased the mass of the co-orbital satellites to some specific values. Our results corroborate the findings of Érdi & Sándor (2005) and show that some characteristics of the restricted three-body problem may be valid for the general case. Also, we searched for the location of the 3:2 librational resonance and found that the stable systems at this location have satellites with low eccentricity. The same behaviour was spotted in the restricted case.

In addition to the librational resonances driven by the mass parameter of the system, we found isolated unstable initial conditions located inside islands of stability ($M_2 = 0.107\,\mathrm{M}_\oplus$ and $\theta = 51°$, and $M_2 = 15\,\mathrm{M}_\oplus$ and $\theta = 56°$ for the Kepler-1625 system, and $M_2 = 5\,\mathrm{M}_\oplus$ and $\theta = 54°$–$55°$ for the Kepler-1708 system). These instabilities appeared as a function of the initial angular separation of the co-orbital pair.

To find the nature of these two unstable conditions, we generated a time series of the evolution of the angular separation of the satellites and applied an FFT analysis to this series to search for the dominant frequencies of the problem for each case.

For all systems, we found two dominant frequencies. Taking the ratio of the respective frequencies for each system we found some resonances between the motion of the satellites. For the Kepler-1625 system, we found that the instability for the case with $M_2 = 0.107\,\mathrm{M}_\oplus$ and $\theta = 51°$ was generated by a 5:2 resonance between the motion of the satellites, while for the system with $M_2 = 15\,\mathrm{M}_\oplus$ and $\theta = 56°$ we found that a 3:2 resonance was the cause of the instability. In these two situations, the resonances increased the eccentricity of the satellites, which ultimately led to a collision between the co-orbital bodies. The same pattern appeared for the Kepler-1708 system, in this case, a 2:1 resonance was responsible for the instabilities when the co-orbital companion was a $M_2 = 5\,\mathrm{M}_\oplus$ body initially at $\theta = 54°$ and 55°.

Also, we investigated the amplitude of libration of the stable satellites. Here, we gave special attention to the motion of the co-orbital companion, once the movement of the primary satellite in the rotating frame is almost negligible.

The amplitude of libration of the co-orbital satellites is proportional to the mass of the satellite and its initial angular separation. As $\bar{\mu}$ decreases, stable orbits with larger amplitudes of libration become possible (Leleu et al. 2018). This result was confirmed in our simulations. We found that Mars-like satellites have orbits with larger amplitudes when compared with more massive satellites for the Kepler-1625 system. The surviving co-orbital companions in the Kepler-1708 system presented wider motion amplitude when their masses were $M_2 = 0.5\,M_\oplus$ instead of $M_2 = 0.107\,M_\oplus$, but given the proximity of these values, our conclusions remain unaffected. Horseshoe orbits are not stable for the values of $\bar{\mu}$ considered here. Thus, we did not find this configuration in our results.

On the other hand, we found that co-orbital companions initially farther from L_4 are likely to present larger amplitude in their motions. For these cases, the perturbations from the primary satellite and the planet are more pronounced and the amplitude of the tadpole orbit described by the co-orbital companions on the rotating frame increases. If the satellites are angularly closer and suffer a close encounter then the system might become unstable. After reaching instability, the co-orbital satellite may collide with the primary satellite or the planet or even be ejected from the system.

5.2 Complete system: star–planet–satellite–co-orbital companion

The addition of the star proved to be catastrophic for the survival of co-orbital satellites in the Kepler-1625 system. We found that despite the satellites being deep within the Hill radius of the planet, the gravitational influence of the star is still enough to break the co-orbital architectures of the satellites. We found that the most common outcome for the satellites is the collision between them. This is expected given that the satellites initially share the same orbit and experiment close encounters when the initial architecture breaks. In conclusion, massive co-orbital satellites are unlikely on the Kepler-1625 system given the initial conditions we assumed for the planet and satellites.

Our results do not affect previous findings regarding the stability of multiple satellites in the Kepler-1625 system. Here, the initial co-orbital configuration is a major constraint of the problem.

On the other hand, the co-orbital satellites in the Kepler-1708 systems are only marginally disturbed by the addition of the star. This is mainly due to planet–star separation and mass ratio and the initial position of the satellites, inside 5 per cent of the planet's Hill radius.

Once we found stable co-orbital satellites for the Kepler-1708 system, we analysed the influences of this type of configuration on the planet's TTVs. As expected, the amplitude of the TTV increased as the mass of the co-orbital companion increased. For $M_2 = 5\,\mathrm{M}_\oplus$, we found an increase of about 5 min on the amplitude of the TTV compared with the case with only one moon. For smaller co-orbital companions, these effects are more subtle. The initial angular position of the co-orbital satellites is not relevant for the TTV produced by the planet.

Finally, the results presented here are dependent on the initial conditions adopted. For the Kepler-1625 system, there are papers showing that the planet–satellite separation can be smaller than the adopted 40 R_p. This consideration alone will place the satellite in a position where the effects of the star will be less relevant, consequently increasing the possibility of finding stable co-orbital satellites. Moreover, for the local systems, we considered that the planet and the satellites are in the same orbital plane, even though the planet is thought to be inclined regarding its star. When adding the star, we simulated the cases with the planet coplanar and inclined ($I_p = 45°$), which did not change the scenario of instability for co-orbital satellites. The Kepler-1708 system has even more uncertainties than the previous system. We opted to consider the system's properties presented in the paper that proposed the exomoon candidate (Kipping et al. 2022) and in the study that explored the tidal evolution of the satellite (Tokadjian & Piro 2022). All in all, more details about these systems are needed to build more accurate models.

ACKNOWLEDGEMENTS

RAM dedicates this paper to his late mentor and friend Willy Kley. The authors thank the anonymous referee for the valuable comments and suggestions that significantly improved this manuscript and Muller Lopes for the help with the TTV analysis. This work was possible thanks to the scholarship granted from the Brazilian Federal Agency for Support and Evaluation of Graduate Education (CAPES), in the scope of the Program CAPES-PrInt, process number 88887.310463/2018-00, Mobility number 88887.583324/2020-00 (RAM). RAM, OCW, and DCM thank the financial support from FAPESP (Grant: 2016/24561-0) and CNPq (Grant: 305210/2018-1). This research was supported by resources supplied by the Center for Scientific Computing (NCC/GridUNESP) of the São Paulo State University (UNESP).

DATA AVAILABILITY

The data underlying this paper will be shared on reasonable request to the corresponding author.

REFERENCES

Agol E., Fabrycky D. C., 2018, in Deeg H. J., Belmonte J. A., eds, Handbook of Exoplanets. Springer International Publishing, Switzerland, p. 7
Agol E., Steffen J., Sari R., Clarkson W., 2005, MNRAS, 359, 567
Alvarado-Montes J. A., Zuluaga J. I., Sucerquia M., 2017, MNRAS, 471, 3019
Barnes J. W., O' Brien D. P., 2002, ApJ, 575, 1087
Beaugé C., Sándor Z., Érdi B., Süli Á., 2007, A&A, 463, 359
Ben-Jaffel L., Ballester G. E., 2014, ApJL, 785, L30
Bennett D. P. et al., 2014, ApJ, 785, 155
Blanco-Cuaresma S., Bolmont E., 2016, Proceedings of the International Astronomical Union. Cambridge Univ. Press, Cambridge, p. 341
Cassese B., Kipping D., 2022, MNRAS, 516, 3701
Chiang E. I., Lithwick Y., 2005, ApJ, 628, 520
Cresswell P., Nelson R. P., 2006, A&A, 450, 833
Deprit A., Deprit-Bartholome A., 1967, AJ, 72, 173
Domingos R. C., Winter O. C., Yokoyama T., 2006, MNRAS, 373, 1227
Donnison J. R., 2010, MNRAS, 406, 1918
Érdi B., Sándor Z., 2005, Celest. Mech. Dyn. Astron., 92, 113
Fortney J. J., Marley M. S., Barnes J. W., 2007, ApJ, 659, 1661
Fox C., Wiegert P., 2021, MNRAS, 501, 2378
Gascheau G., 1843, C. R. Acad. Sci. Paris, 16, 393
Giuppone C. A., Benítez-Llambay P., Beaugé C., 2012, MNRAS, 421, 356
Guenel M., Mathis S., Remus F., 2014, A&A, 566, L9
Hamers A. S., Portegies Zwart S. F., 2018, ApJL, 869, L27
Hansen B. M. S., 2019, Sci. Adv., 5, eaaw8665
Hansen B. M. S., 2022, MNRAS, 520, 761
Heller R., 2014, ApJ, 787, 14
Heller R., 2018a, in Deeg H. J., Belmonte J. A., eds, Handbook of Exoplanets. Springer International Publishing, Switzerland, p. 35
Heller R., 2018b, A & A, 610, A39
Heller R., Rodenbeck K., Bruno G., 2019, A & A, 624, A95
Hippke M., 2015, ApJ, 806, 51
Hippke M., Heller R., 2022, A&A, 662, A37
Holman M. J., Murray N. W., 2005, Science, 307, 1288
Kipping D. et al., 2022, Nature Astron., 6, 367
Kipping D. M., 2009a, MNRAS, 392, 181
Kipping D. M., 2009b, MNRAS, 396, 1797
Kipping D. M., Fossey S. J., Campanella G., 2009, MNRAS, 400, 398
Kipping D., 2020, ApJ, 900, L44
Kipping D., 2021, MNRAS, 500, 1851
Kollmeier J. A., Raymond S. N., 2019, MNRAS, 483, L80
Kortenkamp S. J., 2005, Icarus, 175, 409
Kreidberg L., Luger R., Bedell M., 2019, ApJ, 877, L15
Laughlin G., Chambers J. E., 2002, AJ, 124, 592
Leleu A., Robutel P., Correia A. C. M., 2015, A&A, 581, A128
Leleu A., Robutel P., Correia A. C. M., 2018, Celest. Mech. Dyn. Astron., 130, 24
Lewis K. M., Ochiai H., Nagasawa M., Ida S., 2015, ApJ, 805, 27
Liberato L., Winter O. C., 2020, MNRAS, 496, 3700
Limbach M. A., Vos J. M., Winn J. N., Heller R., Mason J. C., Schneider A. C., Dai F., 2021, ApJ, 918, L25
Long F. et al., 2022, ApJ, 937, L1
Lyra W., Johansen A., Klahr H., Piskunov N., 2009, A&A, 493, 1125
Martin D. V., Fabrycky D. C., Montet B. T., 2019, ApJ, 875, L25
Mathur S. et al., 2017, ApJS, 229, 30
Montesinos M., Garrido-Deutelmoser J., Olofsson J., Giuppone C. A., Cuadra J., Bayo A., Sucerquia M., Cuello N., 2020, A&A, 642, A224
Moraes R. A., Borderes-Motta G., Winter O. C., Monteiro J., 2022, MNRAS, 510, 2583
Moraes R. A., Vieira Neto E., 2020, MNRAS, 495, 3763
Morton T. D., Bryson S. T., Coughlin J. L., Rowe J. F., Ravichandran G., Petigura E. A., Haas M. R., Batalha N. M., 2016, ApJ, 822, 86
Mullally F. et al., 2015, ApJS, 217, 31
Murray C. D., Dermott S. F., 1999. Solar System Dynamics, Cambridge University Press, Cambridge, p. 93
Namouni F., 2010, ApJ, 719, L145

Nesvorný D., Vokrouhlický D., 2014, ApJ, 790, 58
Oza A. V. et al., 2019, ApJ, 885, 168
Quarles B., Li G., Rosario-Franco M., 2020a, ApJ, 902, L20
Quarles B., Li G., Rosario-Franco M., 2020b, ApJ, 902, L20
Rauer H. et al., 2014, Exp. Astron., 38, 249
Rein H., Liu S. F., 2012, A&A, 537, A128
Rein H., Spiegel D. S., 2015, MNRAS, 446, 1424
Roberts G. E., 2002, J. Differ. Equ., 182, 191
Rodenbeck K., Heller R., Hippke M., Gizon L.,2018, A&A, 617,A69
Rosario-Franco M., Quarles B., Musielak Z. E., Cuntz M., 2020, AJ, 159, 260
Routh E. J., 1874, Proc. London Math. Soc., s1-6, 86
Sartoretti P., Schneider J., 1999, A&AS, 134, 553
Simon A., Szatmáry K., Szabó G. M., 2007, A&A, 470, 727
Sucerquia M. et al., 2022, MNRAS, 512, 1032
Sucerquia M., Alvarado-Montes J. A., Zuluaga J. I., Cuello N., Giuppone C., 2019, MNRAS, 489, 2313
Sucerquia M., Ramírez V., Alvarado-Montes J. A., Zuluaga J. I., 2020, MNRAS, 492, 3499
Szabó G. M., Szatmáry K., Divéki Z., Simon A., 2006, A&A, 450, 395
Teachey A., 2021, MNRAS, 506, 2104
Teachey A., Kipping D. M., 2018, Sci. Adv., 4, eaav1784
Teachey A., Kipping D. M., Schmitt A. R., 2018, AJ, 155, 36
Teachey A., Kipping D., Burke C. J., Angus R., Howard A. W., 2020, AJ, 159, 142
Thommes E. W., 2005, ApJ, 626, 1033
Tokadjian A., Piro A. L., 2020, AJ, 160, 194
Tokadjian A., Piro A. L., 2022, ApJ, 929, L2

This paper has been typeset from a TEX/LATEX file prepared by the author.

4.3 Sfair et al., 2025 - submetido

Version June 13, 2025
Preprint typeset using LaTeX style openjournal v. 09/06/15

THE MOON AS A POSSIBLE SOURCE FOR EARTH'S CO-ORBITAL BODIES

R. Sfair
UNESP - São Paulo State University, Grupo de Dinâmica Orbital e Planetologia, Av. Ariberto Pereira da Cunha, 333, Guaratinguetá, 12516-410, SP, Brazil
LIRA, Observatoire de Paris, Université PSL, Sorbonne Université, Université Paris Cité, CY Cergy Paris Université, CNRS, 92190 Meudon, France and
Institute for Astronomy and Astrophysics, Department of Computational Physics, Eberhard Karls Universität Tübingen, Auf der Morgenstelle 10, 72076 Tübingen, Germany

L. C. Gomes
UNESP - São Paulo State University, Grupo de Dinâmica Orbital e Planetologia, Av. Ariberto Pereira da Cunha, 333, Guaratinguetá, 12516-410, SP, Brazil

O. C. Winter
UNESP - São Paulo State University, Grupo de Dinâmica Orbital e Planetologia, Av. Ariberto Pereira da Cunha, 333, Guaratinguetá, 12516-410, SP, Brazil

R. A. Moraes
UNESP - São Paulo State University, Grupo de Dinâmica Orbital e Planetologia, Av. Ariberto Pereira da Cunha, 333, Guaratinguetá, 12516-410, SP, Brazil and
IFES - Federal Institute of Education, Science and Technology of Espirito Santo, Rodovia Miguel Curry Carneiro, 799, Nova Venécia, 29830-000, Espirito Santo, Brazil

G. Borderes-Motta
Astronomical Institute of the Czech Academy of Sciences, ASU-CAS, Fričova 298, 25165 Ondřejov, Czech Republic and
Swedish Institute of Space Physics, IRF, Bengt Hultqvists väg 1, 981 92 Kiruna, Sweden

C. M. Schäfer
Institute for Astronomy and Astrophysics, Department of Computational Physics, Eberhard Karls Universität Tübingen, Auf der Morgenstelle 10, 72076 Tübingen, Germany

Version June 13, 2025

Abstract

There is a growing number of Earth's co-orbital bodies being discovered. At least five of them are known to be temporarily in quasi-satellite orbits. One of those, 469219 Kamo'oalewa, was identified as possibly having the same composition as the Moon. We explore the conditions necessary for lunar ejecta to evolve into Earth's co-orbital bodies, with particular attention to the formation of quasi-satellite orbits. We systematically investigate the parameter space of ejection velocity and geographic launch location across the entire lunar surface. The study employs numerical simulations of the four-body problem (Sun-Earth-Moon-particle) with automated classification methodology for identifying all co-orbital states. Particles are ejected from randomly distributed points covering the entire lunar surface with velocities ranging from 1.0 to 2.6 times the Moon's escape velocity. Trajectories co-orbital to Earth are found to be a common outcome, with approximately 6.68% of all simulated particles evolving into Earth co-orbital motion and 1.92% specifically exhibiting quasi-satellite behavior. We identify an optimal ejection velocity ($1.2v_{esc}$) for quasi-satellite production, yielding over 6% conversion efficiency at this specific velocity. The spatial distribution of successful ejections shows a strong preference for the equatorial regions of the trailing hemisphere. Collisions with Earth or the Moon occur for only 4% of the sample. Our extended integrations reveal exceptionally long-lived configurations, including tadpole orbits persisting for 10,000 years and horseshoe co-orbitals maintaining stability for 5,000 years. Our results strengthen the plausibility of lunar origin for Earth's co-orbital bodies, including quasi-satellites like Kamo'oalewa and 2024PT5. We identify both "prompt" and "delayed" co-orbital formation mechanisms, with a steady-state production regime that could explain the presence of lunar-derived objects in Earth's co-orbital regions despite the infrequent occurrence of major lunar impacts capable of launching meter-scale fragments.

Subject headings: Moon, co-orbital, quasi-satellite

1. INTRODUCTION

In the context of the planar circular restricted 3-body problem there are the well known Lagrangian equilibrium points (L_i, $i = 1, \ldots, 5$). The triangular points, L_4 and L_5 can be stable depending on the mass ratio of the two massive bodies (Gascheau 1843). When stable, the system can show libration

rafael.sfair@unesp.br
claudio.gomes@unesp.br
othon.winter@unesp.br
ricardo.moraes@unesp.br
gborderes@example.com
ch.schaefer@uni-tuebingen.de

regions along the orbit of the secondary body, whose trajectories will be under the 1:1 mean motion resonant effect.

There are several distinct solutions for this co-orbital motion, including the tadpole and the horseshoe orbits (Murray and Dermott 1999; Namouni *et al.* 1999). Within the class of co-orbital motions there are also the retrograde or quasi-satellite orbits. These trajectories are similar to that of satellites, but lie far out of the Hill sphere of the secondary body, and they are unstable in the inner Solar System. Compound co-orbital trajectories, including one or more of these classes of motion, with transitions between classes along the time are also possible (Wiegert *et al.* 1997). In general, the quasi-satellite behaviour occurs as a compound class of motion with the horseshoe motion.

The number of discovered bodies in co-orbital motion with respect to the Earth has significantly increased in the last decades. At the moment, five bodies are known to be in quasi-satellite motion (Chodas 2016; de la Fuente Marcos and de la Fuente Marcos 2016), two in tadpole motion (Connors *et al.* 2011; Santana-Ros *et al.* 2022) and eight in horseshoe or compound horseshoe/quasi-satellite motion (Connors *et al.* 2002; Brasser *et al.* 2004; Christou and Asher 2011), as listed in Table 1.

TABLE 1
Bodies in co-orbital motion with the Earth.

Body	Trajectory	Diameter[a] (m)
2004 GU9	Quasi-satellite	160-360
2006 FV35	Quasi-satellite	140-320
2013 LX28	Quasi-satellite	130-300
2014 OL339	Quasi-satellite	70-160
Kamo'oalewa	Quasi-satellite	30-45
2010 TK7	Tadpole	250-500
2020 XL5	Tadpole	1,100-1,260
2010 SO16	Horseshoe	230-480
2002 AA29	Horseshoe	20-30
54509 YORP	Horseshoe	150×128×93
3753 Cruithne	Horseshoe	5,000
2001 GO2	Horseshoe-Quasi-satellite	40-80
1998 UP1	Horseshoe-Quasi-satellite	210-470
2009 BD	Horseshoe-Quasi-satellite	7-15
2003 YN107	Horseshoe-Quasi-satellite	10-30

[a] Estimated size based on the magnitude.

With the expressive number of known Near-Earth objects (NEO), almost 37 thousand bodies as of Feb. 2025[1], it is expected that NEOs constitute the main source of Earth's co-orbital bodies. Yet, the ~40 meters wide object (469219) Kamo'oalewa, currently in the most stable known quasi-satellite motion with the Earth (de la Fuente Marcos and de la Fuente Marcos 2016), shows an L-type reflectance spectrum that matches lunar silicate material. This points towards a possible origin of the object as a fragment ejected from the Moon (Sharkey *et al.* 2021). More recently, the ~10 meters diameter object 2024PT5 has also been identified as potentially having lunar origin based on its spectral properties (Kareta *et al.* 2025). This object had a close approach with Earth in September/November 2024 with a remarkably low velocity relative to Earth (de la Fuente Marcos *et al.* 2024).

The dynamical evolution of lunar ejecta has been investigated extensively by Gladman *et al.* (1995), who performed numerical simulations to determine the fate of material launched from the lunar surface. Their study used a two-stage approach, first modeling particles in the Earth-Moon system (geocentric phase) and then following their heliocentric evolution after escape. They found that approximately 20-25% of lunar ejecta would collide with Earth over timescales of $\sim 10^5$ years, with most impacts occurring within the first 10,000 years following a steep initial decline. While their work focused on determining whether lunar ejecta impact Earth or Moon or escape into heliocentric orbits, they did not specifically investigate the formation of co-orbital configurations.

Several recent studies have investigated the lunar origin hypothesis for Earth's co-orbitals. Castro-Cisneros *et al.* (2023) performed numerical simulations to investigate the possibility of Kamo'oalewa being ejected from the Moon, focusing primarily on particles launched from the lunar equatorial region. Their results supported a lunar origin for objects like Kamo'oalewa, finding that approximately 6% of particles launched from the lunar equator became co-orbital with Earth within 5,000 years.

In a follow-up study, Castro-Cisneros *et al.* (2025) maintained the focus on equatorial launch sites while examining the influence of Earth's eccentricity on the formation of quasi-satellite orbits, concluding that Earth's eccentricity had minimal effect on co-orbital outcomes.

Jiao *et al.* (2024) took a different approach, combining SPH simulations with N-body integrations to determine the specific ejection site of Kamo'oalewa from the lunar surface. Their analysis suggested that Kamo'oalewa likely originated from the Giordano Bruno crater approximately 1-10 million years ago, finding that within 10 million years after ejection, the percentage of particles residing in Earth co-orbital states reached at most 1%.

The Chinese space agency's Tianwen-2 mission (Zhang *et al.* 2021) is scheduled to launch in May 2025. One of its goals is to land on the asteroid Kamo'oalewa and collect a 100 g sample that will be returned to Earth by a capsule. In addition to collecting material, remote sensing observations will take place in orbit around Kamo'oalewa. The mission results will provide critical data to test the lunar origin hypothesis and enhance our understanding of these unique objects (Venigalla *et al.* 2019).

In this work, we present a comprehensive study of the conditions required for lunar ejecta to become Earth co-orbitals, expanding previous research in some aspects. Unlike prior studies that focused primarily on quasi-satellite orbits (Castro-Cisneros *et al.* 2023) or limited launch sites (Castro-Cisneros *et al.* 2025; Jiao *et al.* 2024), we systematically investigate co-orbital states using particles ejected from the entire lunar surface with varying velocities. Our approach employs automated classification methodology for identifying all co-orbital states, eliminating the subjective visual inspection methods used in some of the previous works. This comprehensive sampling across the complete lunar surface allows us to identify not only the optimal ejection velocity for generating Earth co-orbitals, particularly quasi-satellites, but also the geographical distribution of favorable launch sites on the lunar surface.

The dynamical evolution is explored in the context of the restricted four-body problem, Moon-Earth-Sun-Particle. The numerical simulations are presented in section 2. In section 3 the main results are presented. Then, in section 4, we discuss the kind of asteroidal impact on the surface of the Moon that

[1] https://cneos.jpl.nasa.gov/stats/ totals.html

would generate a fragment the size of the known Earth's co-orbitals. Lastly, our final comments are presented in section 5.

2. NUMERICAL SIMULATIONS

We integrate a system composed of the Sun, Earth, Moon, and massless particles. The orbital elements, as well as the masses and radii of the Earth and the Moon, were gathered from JPL Horizons ephemeris (Giorgini *et al.* 1996)[2] referred to epoch 2000 January 01 12:00 (JD 2451545.0).

Unlike previous studies that focused primarily on equatorial regions or limited launch sites, our test particles were ejected from randomly distributed points covering the entire lunar surface. The velocity vectors were primarily normal to the surface and outward-pointing. We also tested a control sample with non-normal velocity vectors varying randomly in azimuth while maintaining the outward direction, confirming that launch azimuth does not significantly affect outcome statistics.

Our simulations systematically explored the velocity parameter space from 1.0 up to 2.6 times the lunar escape velocity (2.4 km/s), with an ensemble of 6,000 particles for each chosen velocity, totalizing 54,000 particles. This range of velocities was selected based on preliminary results showing a significant drop in co-orbital production at higher ejection speeds, as shown in Figure 1. To assess the independence of results from the launch epoch, we conducted four separate simulation sets with different initial positions of the Moon in its orbit around Earth (at quarter-period intervals).

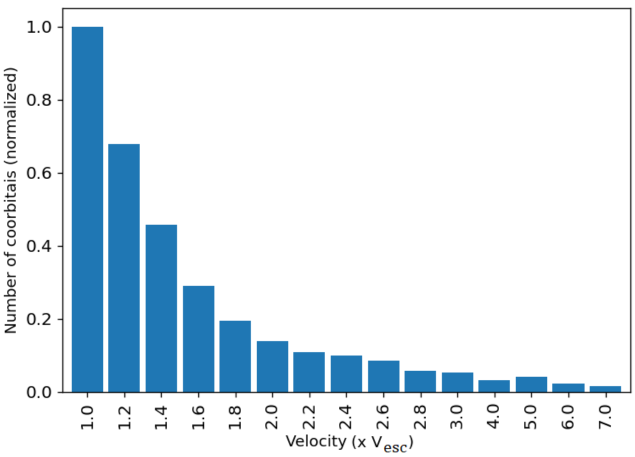

FIG. 1.— Number of co-orbitals normalized for each simulated ejection velocity, which ranges from 1.0 to 7.0 times the lunar escape velocity.

The system was integrated for 1,000 years with the high order integrator IAS15 available in the REBOUND package (Rein and Spiegel 2015). For selected cases, we extended the integration time to 50,000 years with the addition of Venus, Mars, and Jupiter to capture long-term stability characteristics.

We implemented automated, quantitative criteria for classifying orbital states, eliminating the subjective visual inspection methods. Specifically, we consider a particle as co-orbital when its semi-major axis remains between 0.99 and 1.01 au for at least 8 consecutive years. Quasi-satellite classification is applied when the difference between the mean longitude of the particle and the mean longitude of Earth ($\Delta\lambda = \lambda_{\text{particle}} - \lambda_{\text{Earth}}$) oscillates around zero with an amplitude less than 7.5° for at least 10 years. Horseshoe orbits are identified when $\Delta\lambda$ oscillates around 180° with amplitude sufficient to encompass the L_4 and L_5 points, while tadpole orbits librate around either L_4 (60°) or L_5 (300°).

Our threshold-based classification approach provides a consistent, reproducible methodology for identifying all co-orbital states (tadpole, horseshoe, and quasi-satellite) while capturing transitions between these states, allowing for comprehensive population statistics. Collisions are recorded when the distance between a particle and any massive body becomes smaller than that body's radius, at which point the particle is removed from the simulation.

[2] http://ssd.jpl.nasa.gov/sbdb.cgi

3. RESULTS

Our numerical simulations revealed that lunar ejecta can naturally evolve into various co-orbital configurations with Earth. From the complete set of 54,000 simulated particles, approximately 6.68% evolved into Earth co-orbital motion, with 1.92% specifically exhibiting quasi-satellite behavior. The fraction of particles that collided with either Earth or the Moon was 4.01% (3.46% with Earth and 0.55% with the Moon). Ejection velocity is a critical parameter influencing both the likelihood and stability characteristics of resulting co-orbital states.

Fig. 2 shows a representative example of the orbital evolution of a particle that becomes co-orbital with the Earth. Along this trajectory, the horseshoe motion appears in two opportunities (~ 200 yr and ~ 600 yr). Between the two stages in horseshoe motion, the particle experiences a quasi-satellite motion for a period of about one hundred years. The temporal evolution of the orbital elements (semi-major axis, eccentricity and inclination) clearly shows a chaotic behaviour. However, during co-orbital phases, the orbital elements exhibit significantly more regular behavior, with notably reduced variations in semi-major axis and more constrained eccentricity excursions. This regularity is particularly evident during the stages of horseshoe (orange plots) and quasi-satellite (green plots) motions.

The main results of the full set of simulations are presented in Fig. 3. Each color represents one of the four simulation sets with different initial positions of the Moon on its orbit around Earth (at quarter-period intervals). In general, the results show that there is no significant difference between them, confirming that the launch epoch with respect to the Sun-Earth-Moon configuration does not appreciably affect co-orbital production rates, neither the collisions with the Earth or the Moon.

The outcomes in Fig. 3 are presented as a function of the ejection velocity. From top to bottom, the plots show the number of bodies that became co-orbital, quasi-satellite, collided with the Earth and collided with the Moon, respectively. Collision frequencies with both the Moon and Earth decline rapidly for ejection velocities exceeding $1.4v_{esc}$. The quasi-satellite formation exhibits a distinct non-monotonic trend, beginning at moderate levels for $1.0v_{esc}$, reaching maximum production at $1.2v_{esc}$ (exceeding 6% of all particles at this velocity), before gradually decreasing at higher velocities. This velocity-dependent pattern suggests an optimal ejection window for quasi-satellite formation. The overall co-orbital count shows minimum production at the lowest ejection velocity, then stabilizes across the intermediate velocity range before gradually declining at the highest velocities tested.

Our findings both complement and extend recent studies on the lunar origin of Earth co-orbitals. While Castro-

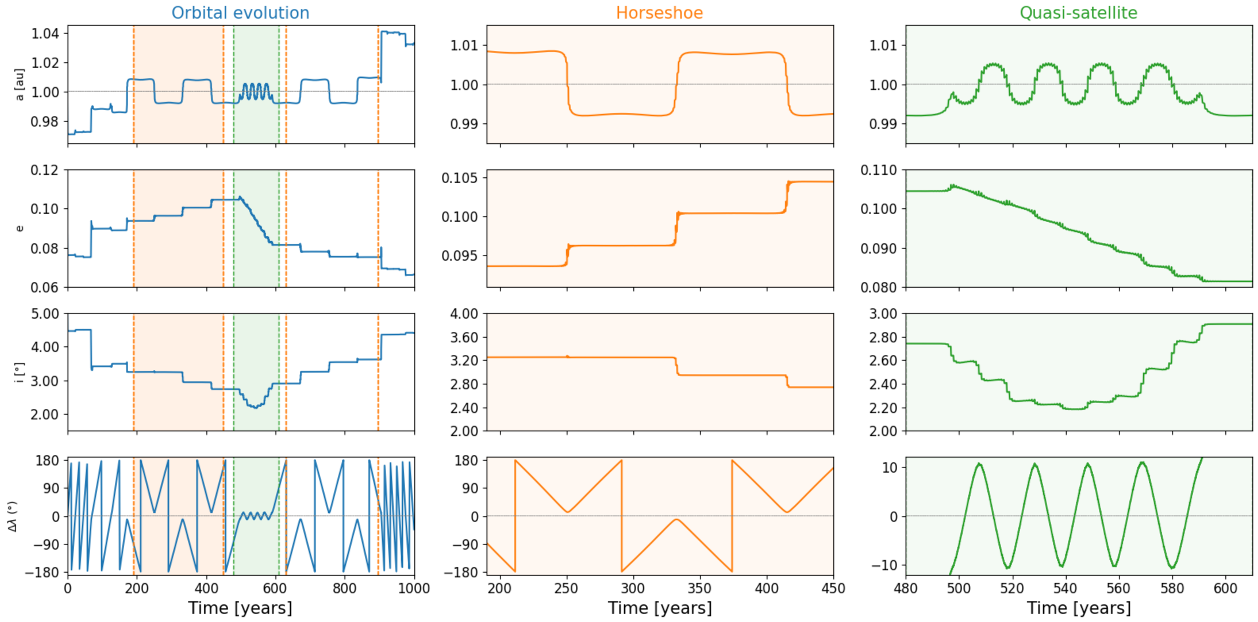

FIG. 2.— Example of the orbital evolution of a particle ejected from the Moon with velocity 2.0 v_{esc}. Plots of the temporal evolution of the semi-major axis, eccentricity, inclination and mean longitude with respect to the mean longitude of the Earth, from top to bottom respectively. In the middle column is shown a zoom of the orange region indicated in the plots of the left column. In the right column is shown a zoom of the green region indicated in the plots of the left column.

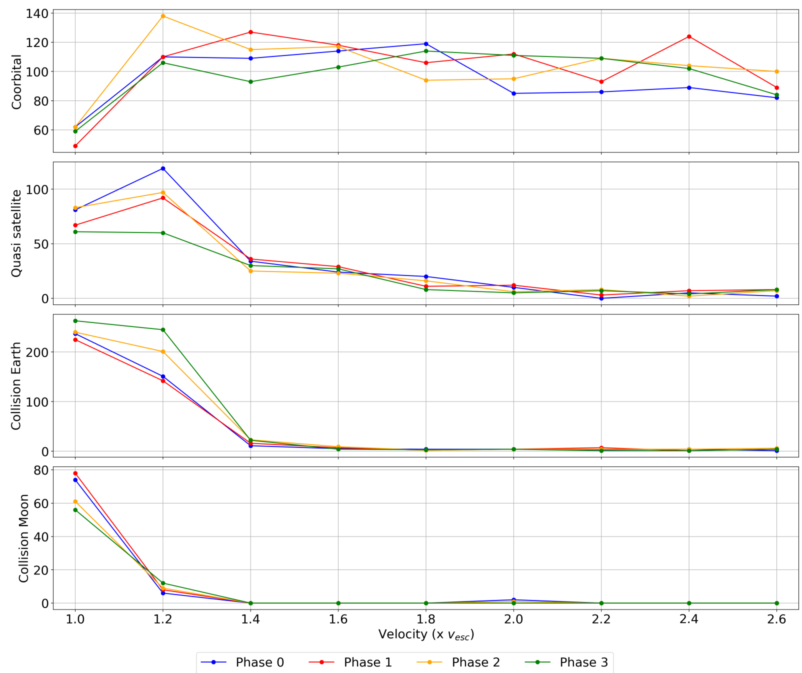

FIG. 3.— Simulation outcomes as a function of ejection velocity normalized to the lunar escape velocity (v_{esc}). Plots show the number of particles that became co-orbital, quasi-satellite, collided with Earth, and collided with the Moon (from top to bottom). Colors represent four sets of simulations with different initial positions of the Moon in its orbit around Earth, at quarter-period intervals.

Cisneros *et al.* (2023) observed that approximately 6% of particles launched from the lunar equator became co-orbital with Earth within 5,000 years, our comprehensive survey covering the entire lunar surface yields a comparable 6.68% co-orbital production rate, validating their results while providing a more complete spatial distribution. However, our finding that 1.92% of all particles exhibit quasi-satellite behavior is significantly higher than previously reported values. Jiao *et al.* (2024) found that within 10 million years after ejection from Giordano Bruno crater, the percentage of particles in Earth co-orbital states reached at most 1%, with only rare cases becoming long-lived quasi-satellites. This discrepancy likely stems from our finding of an optimal ejection velocity ($1.2v_{esc}$) for quasi-satellite production, which yields over 6% conversion efficiency at this specific velocity.

Unlike Castro-Cisneros *et al.* (2025), who focused on the influence of Earth's eccentricity on co-orbital formation while maintaining equatorial launch sites, our work systematically explores the parameter space of ejection velocity and geographic location. While they concluded that Earth's eccentricity had minimal effect on co-orbital outcomes, our results demonstrate that both velocity and launch location significantly impact co-orbital production and stability. Additionally, our automated classification methodology captures the full range of co-orbital states (tadpole, horseshoe, and quasi-satellite), whereas previous studies primarily focused on horseshoe-quasi-satellite transitions. This broader classification approach enabled our discovery of exceptionally long-lived cases with stability timeframes an order of magnitude longer than previously identified.

To further understand how ejection velocity influences co-orbital stability, we analyzed the residence time distribution of objects in these dynamical states. Fig. 4 shows the distribution of co-orbital objects as a function of initial ejection velocity, grouped by their residence time in co-orbital states. We classify objects into two categories: short-lived (<100 years) and long-lived (>100 years). Importantly, we count each particle only once in this analysis, regardless of how many times it may enter a co-orbital configuration during the simulation, to focus on the possibility of particles to achieve co-orbital states.

The distribution reveals a strong velocity dependence in co-orbital formation. For long-lived objects (orange bars), a clear peak occurs at $1.2v_{\rm esc}$, followed by a gradual decrease at higher velocities. In contrast, short-lived co-orbitals (blue bars) exhibit their maximum at $1.6v_{\rm esc}$. A particularly interesting feature appears at the minimum velocity of $1.0v_{\rm esc}$, where we observe an inversion in the typical pattern - long-lived co-orbitals exceed short-lived ones, suggesting that particles barely escaping lunar gravity preferentially establish stable configurations when they achieve co-orbital states.

This velocity-dependent behavior provides insight into conditions for generating Earth's co-orbital bodies. The pronounced peak at $1.2v_{\rm esc}$ for long-lived co-orbitals coincides with our observation that this velocity also produces the highest proportion of quasi-satellite trajectories (exceeding 6% of all outcomes at this velocity). The correlation between ejection velocity and orbital longevity demonstrates how initial conditions strongly influence the dynamical character of resulting co-orbital states.

Fig. 5 presents the temporal distribution of co-orbital entries throughout our 1,000-year simulation. Unlike Fig. 4, which counts each particle only once, this analysis records every individual entry event into a co-orbital state, allowing multiple counts per object. The histogram reveals two distinct phases in co-orbital formation from lunar ejecta: an initial peak during the first 100 years followed by a relatively uniform production rate that persists for the remainder of the simulation.

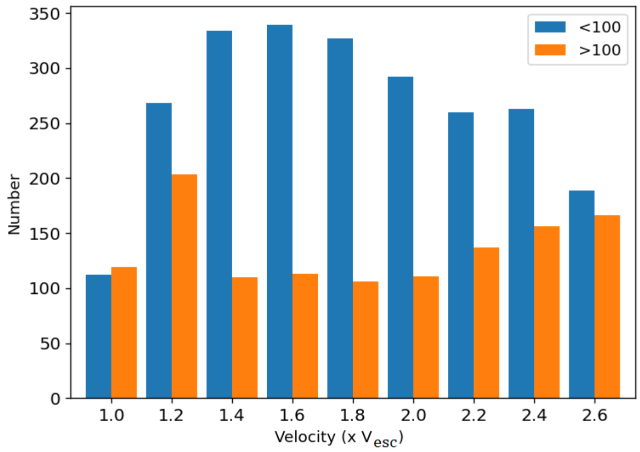

FIG. 4.— Distribution of co-orbital objects as a function of initial ejection velocity, categorized by by residence time. Blue bars represent objects with co-orbital durations less than 100 years, while orange bars indicate those exceeding 100 years. Each object is counted only once, regardless of multiple co-orbital entries.

The pronounced peak in the first time bin (0–100 years) contains approximately 1,000 short-lived entry events and 170 long-lived ones, significantly exceeding the subsequent time intervals. This initial surge represents particles that quickly transition into co-orbital states following ejection from the lunar surface. After this early phase, entry rates stabilize at approximately 500 events per 100-year interval for short-lived states and about 75 events per interval for long-lived configurations.

This transition to a steady-state production regime suggests a fundamental separation between "prompt" and "delayed" co-orbital formation mechanisms. The prompt mechanism captures particles that directly enter co-orbital configurations through relatively straightforward dynamical pathways. In contrast, the delayed mechanism involves more complex orbital evolution, where particles undergo sufficient perturbations in the Earth-Moon-Sun system before eventually achieving co-orbital states.

The near-constant rate of co-orbital entries following the initial surge suggests the establishment of a kind of steady-state in co-orbital production. This implies that lunar material can continuously replenish Earth's co-orbital population through stochastic processes, even centuries after the initial impact event. This persistent production mechanism could explain the presence of lunar-derived objects like Kamo'oalewa and 2024 PT5 in Earth's co-orbital regions despite their inherently temporary orbital configurations. Considering that major lunar impacts capable of launching meter-scale fragments occur infrequently, the steady-state mechanism provides a pathway for lunar material to enter co-orbital states across geological timescales.

The full statistical analysis of our 54,000 simulated particles yielded 6.68% of trajectories evolving into Earth co-orbital motion, with 1.92% specifically exhibiting quasi-satellite behavior. Collisions occurred in only 4.01% of cases (3.46% with Earth and 0.55% with the Moon). We found that ejection velocity strongly influences co-orbital outcomes,

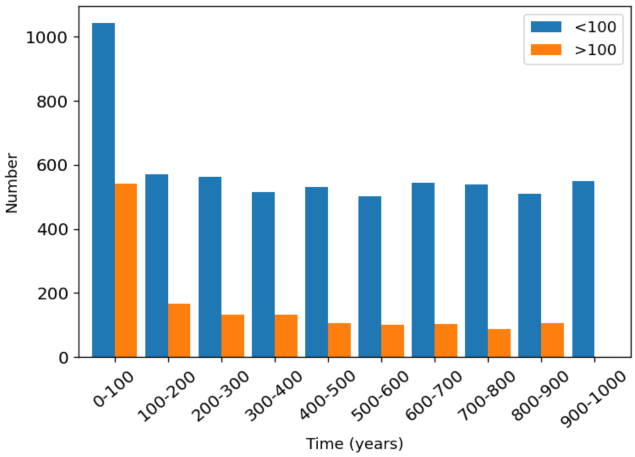

FIG. 5.— Temporal distribution of co-orbital entries throughout the 1,000-year simulation, binned in 100-year intervals. Blue bars represent entries into short-lived (<100 years) co-orbital states, while orange bars indicate entries into long-lived (>100 years) states. Unlike Fig. 4, this histogram counts each entry event separately, allowing multiple counts per particle.

with particles ejected at $1.2v_{\rm esc}$ produced the highest proportion of quasi-satellites, exceeding 6% at this specific velocity. This optimal ejection window represents a significant refinement compared to earlier studies that reported lower co-orbital conversion efficiencies (Jiao *et al.* 2024).

Our Earth collision rate differs from the 20-25% reported by Gladman *et al.* (1995) over 10^5 years due to our focus on velocities optimized for co-orbital formation. Their finding that most collisions occur within the first 10,000 years aligns with our observed temporal distribution. The differences in outcome statistics primarily reflect our exploration of higher velocity regimes and focus on co-orbital formation rather than direct Earth impact.

Our integration timeframes revealed exceptional orbital stability in certain cases, far exceeding previous estimates. The 1,000-year simulations identified quasi-satellites and horseshoe co-orbitals maintaining their respective states throughout the entire integration period. More significantly, our extended 50,000-year integrations discovered extremely long-lived configurations: tadpole orbits persisting for 10,000 years and horseshoe co-orbitals maintaining stability for 5,000 years. These longevity values substantially exceed the stability timeframes reported by Castro-Cisneros *et al.* (2023), who primarily observed persistence on timescales of hundreds of years. The significantly longer orbital stability we observed might be attributed to our approach of sampling the complete lunar surface rather than equatorial regions alone and systematically exploring ejection velocities, which revealed the critical 1.2 $v_{\rm esc}$ threshold for generating stable co-orbital configurations.

4. LUNAR ORIGIN OF CO-ORBITALS

We have evidence for ejected materials from the Moon based on both empirical meteorite data (Marvin 1983) and numerical simulations (Head *et al.* 2002). Images taken by the Lunar Orbiter III and V suggested that 40-100 m boulders ejected from lunar craters are not unusual. However, the ejection speeds of these boulders are typically very low (Bart and Melosh 2010). Using the classic Melosh theory for spallation (Melosh 1985), a 13.5 km diameter impactor is necessary to generate escaping ejecta blocks with 50 m in size.

By mapping and statistical analysis of six lunar secondary crater fields, Singer *et al.* (2020) find an estimation for the largest fragment size of the ejecta at escape velocity. They find for Copernicus and Kepler, with crater diameters of 93 km and 31 km, respectively, largest fragment sizes of 50 m and 30 m, which fit the size range of Kamo'oalewa.

In Jiao *et al.* (2024) they attempt to determine the location of the Kamo'oalewa ejection from the lunar surface with numerical simulations and SPH (smoothed particle hydrodynamics). Jiao *et al.* (2024) suggest that the ejection occurred in the impact that generated the Giordano Bruno crater due to the age of the crater. The Giordano Bruno crater is 22 km in diameter and is located approximately 36° North and 103° East (Morota *et al.* 2009). The results of our simulations agree with the possibility of the ejection from this location.

Fig. 6 shows the geographical distribution of initial conditions on the lunar surface that lead to Earth co-orbital objects. The map uses a lunar coordinate system where longitude 0° points toward Earth, longitude −90° represents the leading side (the direction of lunar orbital motion), and longitude 90° corresponds to the trailing side. The density distribution reveals a latitudinal dependence, with a higher concentration of ejections that resulted in co-orbital motion occurring near the equatorial regions (latitude $\approx 0°$). The map was generated using particle data at all simulated velocities and was aligned to match the four different Earth-Moon-Sun geometries. This equatorial preference is observed in the trailing side of the Moon (longitude $\approx 90°$), where the normalized density reaches its maximum values. A secondary concentration appears in the leading hemisphere (longitude $\approx -90°$), although with lower density values. This indicates that equatorial ejections, especially those from the trailing side, tend to be more efficient at producing Earth co-orbital objects.

When comparing the middle and bottom panels, we observe differences in the spatial distribution between short-lived (< 100 years) and long-lived (> 100 years) co-orbital objects. Long-term co-orbitals show a more concentrated distribution, primarily originating from the trailing hemisphere with an equatorial preference. In contrast, short-term co-orbitals exhibit a broader distribution across the lunar surface, including contributions from mid-latitude regions. These differences suggest that the longevity of co-orbital states may depend on the ejection location. This concentration pattern is consistent with the distribution of quasi-satellites and collisions, in agreement with Castro-Cisneros *et al.* (2023).

The lunar craters in Table 2 are taken from Mazrouei *et al.* (2019), which analyzes and quantifies the age of lunar craters with diameter ≥ 10 km and less than 1 Gyr. For this study, a cut was made in the named lunar craters with less than 150 Myr and diameter ≥ 15 km.

Examining the numbered craters in the top panel, we find that several coincide with regions of higher density in the co-orbital distribution. Craters located near the equatorial zone of the trailing hemisphere (particularly craters 3 and 9) align with areas showing enhanced production of co-orbital objects. Similarly, crater 8 in the leading hemisphere corresponds to the secondary density peak observed at longitude $\approx -135°$. The geographical correlation between these specific craters and regions favorable for generating co-orbital objects suggests that ejection events from these locations could have contributed to the population of Earth co-orbitals. We can observe that the equatorial band opposite to the lunar movement is favorable for generating co-orbitals, contrariwise the polar regions.

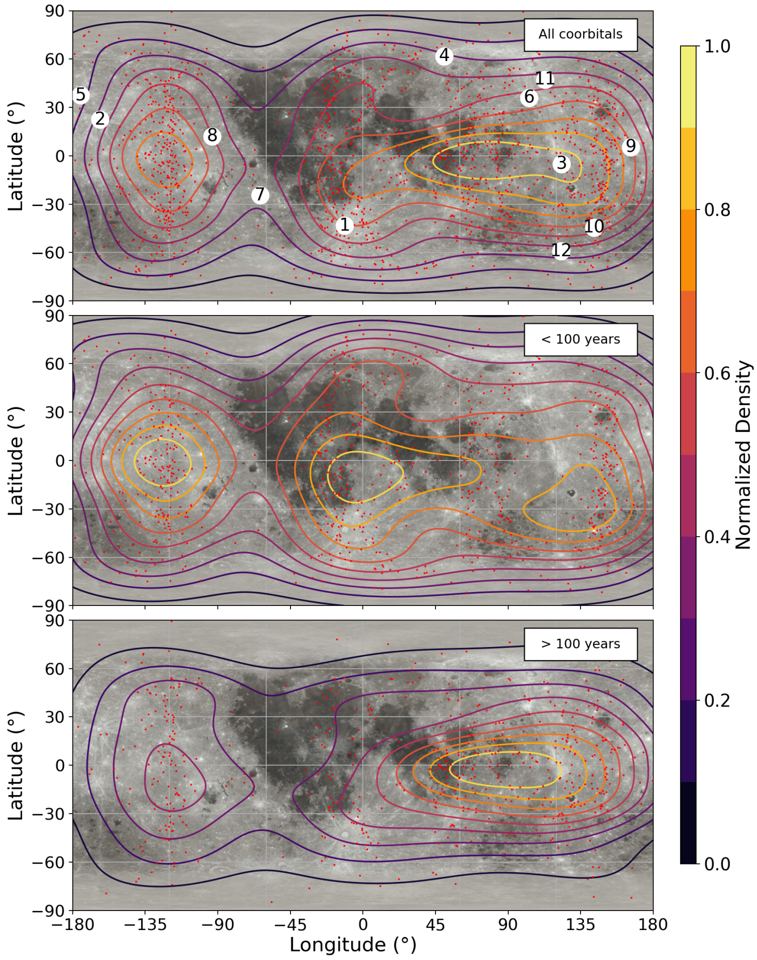

FIG. 6.— Distribution of initial conditions on the lunar surface that result in Earth co-orbital objects. The background grayscale image represents the lunar surface, with contour lines showing the normalized density of successful co-orbital objects. Red dots indicate specific launch locations. Top panel: All co-orbital objects. Numbered labels (1-12) indicate craters from Table 2. Middle panel: Short-term co-orbital objects with durations less than 100 years. Bottom panel: Long-term co-orbital objects with durations exceeding 100 years. Co-orbital objects with lifetimes shorter than 8 years were not considered.

TABLE 2
LIST OF NAMED CRATERS YOUNGER THAN 150 MYR AND LARGER THAN 15 KM IN DIAMETER, ORDER BY DIAMETER. ADAPTED FROM MAZROUEI *et al.* (2019).

n	Name	Lat (deg)	Long (deg)	D(km)
1	Tycho	43.3 S	11.22 W	85
2	Jackson	22.4 N	163.1 W	71
3	Necho	5.25 S	123.24 E	37
4	Thales	61.8 N	50.3 E	32
5	Moore F	37.4 N	175.0 W	24
6	Giordano Bruno	35.9 N	102.89 E	22
7	Byrgius A	24.5 S	63.7 W	19
8	Sundman V	11.9 N	93.5 W	18
9	Mandel'stam F	5.2 N	166.2 E	16
10	Ryder	44.5 S	143.2 E	16
11	Rayet Y	47.2 N	113.0 E	15
12	Fechner T	59.1 S	122.9 E	15

5. FINAL REMARKS

This work explored the conditions under which lunar ejecta can evolve into Earth's co-orbital bodies through comprehensive numerical simulations of the four-body problem (Sun-Earth-Moon-particle). By systematically sampling the entire lunar surface and a range of ejection velocities, we identified key factors governing the production of Earth co-orbitals, with special attention to quasi-satellite configurations.

Our numerical simulations demonstrate that lunar ejecta can naturally evolve into Earth co-orbital configurations, though with limited frequency. From our comprehensive sample of 54,000 simulated particles, approximately 6.68% evolved into Earth co-orbital motion, with only 1.92% specifically exhibiting quasi-satellite behavior. This finding extends previous work by Castro-Cisneros *et al.* (2023), who reported similar overall co-orbital production rates (6%) but focused primarily on equatorial launch sites. Our study systematically explores the entire lunar surface and reveals a non-monotonic relationship between ejection velocity and co-orbital formation, with particles ejected at $1.2v_{esc}$ showing a marked increase in quasi-satellite production efficiency (reaching 6% at this specific velocity). The spatial distribution of successful ejection sites shows a strong preference for the equatorial regions of the trailing hemisphere, consistent with theoretical expectations and previous studies. This preferential region appears particularly important for generating long-lived co-orbital configurations, as evidenced by our geographic density analysis. Our extended integrations revealed orbital stability timeframes may significantly exceed previous estimates, with tadpole orbits persisting for up to 10,000 years and horseshoe co-orbitals maintaining stability for up to 5,000 years—an order of magnitude longer than the stability periods reported by Castro-Cisneros *et al.* (2023), who primarily observed persistence on timescales of hundreds of years.

Our results strengthen the plausibility of lunar origin for Earth's co-orbital bodies, including quasi-satellites like Kamo'oalewa and 2024 PT5. While the production efficiency of such bodies remains low, our identification of an optimal ejection velocity window ($1.2v_{esc}$) and the extended orbital stability of certain configurations provide a viable pathway for lunar material to populate Earth's co-orbital zones. Unlike Jiao *et al.* (2024), who focused on ejecta specifically from the Giordano Bruno crater and reported co-orbital percentages of at most 1%, our broader survey reveals higher production rates (6.68% overall and up to 6% for quasi-satellites at optimal velocity) and identifies critical parameters governing co-orbital formation. Our approach also differs from Castro-Cisneros *et al.* (2025), who examined the influence of Earth's eccentricity on co-orbital outcomes while maintaining equatorial launch sites, as we systematically explore the entire parameter space of ejection velocity and geographic location.

We also identified a distinct of "prompt" and "delayed" co-orbital formation mechanisms through our temporal analysis. After an initial peak in the first 100 years, we observe a transition to a relatively constant rate of co-orbital entries (approximately 500 events per 100-year interval for short-lived states and about 75 events per interval for long-lived configurations). This steady-state production regime has not been previously reported and suggests a fundamental mechanism by which lunar material can continuously replenish Earth's co-orbital population even centuries after the initial impact event. This mechanism could explain the presence of lunar-derived objects like Kamo'oalewa and 2024 PT5 in Earth's co-orbital regions despite their inherently temporary orbital configurations and the infrequent occurrence of major lunar impacts. Our automated classification methodology also represents an advancement over the subjective visual inspection methods. By establishing quantitative criteria for identifying all co-orbital states (tadpole, horseshoe, and quasi-satellite), we provide a consistent, reproducible framework for population statistics that captures the full spectrum of dynamical behaviors, including transitions between states.

Future work will extend these simulations to include additional planetary perturbations and longer integration times, potentially revealing even more long-lived co-orbital configurations. Further investigation of the relationship between ejection conditions and orbital stability characteristics may provide additional constraints on the origin of specific Earth co-orbital objects and enhance our understanding of material exchange within the Earth-Moon system.

ACKNOWLEDGMENTS

This study was financed in part by the Brazilian Federal Agency for Support and Evaluation of Graduate Education (CAPES), in the scope of the Program CAPES-PrInt, process number 88887.310463/2018-00, International Cooperation Project number 3266, Fundação de Amparo à Pesquisa do Estado de São Paulo (FAPESP) - Proc. 2016/24561-0, Conselho Nacional de Desenvolvimento Científico e Tecnológico (CNPq) - Proc. 316991/2023-6. RS and CS acknowledge support by the DFG German Research Foundation (project 446102036).

REFERENCES

G. Gascheau, C. R. Acad. Sci. Paris **16**, 393 (1843).
C. D. Murray and S. F. Dermott, *Solar system dynamics* (1999).
F. Namouni, A. A. Christou, and C. D. Murray, Phys. Rev. Lett. **83**, 2506 (1999).
P. A. Wiegert, K. A. Innanen, and S. Mikkola, Nature **387**, 685 (1997).
P. Chodas, in *AAS/Division for Planetary Sciences Meeting Abstracts #48*, AAS/Division for Planetary Sciences Meeting Abstracts, Vol. 48 (2016) p. 311.04.
C. de la Fuente Marcos and R. de la Fuente Marcos, MNRAS **462**, 3441 (2016), arXiv:1608.01518 [astro-ph.EP].
M. Connors, P. Wiegert, and C. Veillet, Nature **475**, 481 (2011).
T. Santana-Ros, M. Micheli, L. Faggioli, R. Cennamo, M. Devogèle, A. Alvarez-Candal, D. Oszkiewicz, O. Ramírez, P. Y. Liu, P. G. Benavidez, A. Campo Bagatin, E. J. Christensen, R. J. Wainscoat, R. Weryk, L. Fraga, C. Briceño, and L. Conversi, Nature Communications **13**, 447 (2022).
M. Connors, P. Chodas, S. Mikkola, P. Wiegert, C. Veillet, and K. Innanen, Meteoritics & Planetary Science **37**, 1435 (2002).
R. Brasser, K. A. Innanen, M. Connors, C. Veillet, P. Wiegert, S. Mikkola, and P. W. Chodas, Icarus **171**, 102 (2004).
A. A. Christou and D. J. Asher, MNRAS **414**, 2965 (2011), arXiv:1104.0036 [astro-ph.EP].
B. N. L. Sharkey, V. Reddy, R. Malhotra, A. Thirouin, O. Kuhn, A. Conrad, B. Rothberg, J. A. Sanchez, D. Thompson, and C. Veillet, Communications Earth and Environment **2**, 231 (2021).
T. Kareta, O. Fuentes-Muñoz, N. Moskovitz, D. Farnocchia, and B. N. L. Sharkey, The Astrophysical Journal Letters **979**, L8 (2025).
R. de la Fuente Marcos, J. de León, C. de la Fuente Marcos, J. Licandro, M. Serra-Ricart, S. Geier, P. Gallinar, and M. Reyes-Ruiz, Astronomy & Astrophysics **670**, L10 (2024), arXiv:2411.08029 [astro-ph.EP].
B. J. Gladman, J. A. Burns, M. J. Duncan, and H. F. Levison, Icarus **118**, 302 (1995).
J. D. Castro-Cisneros, R. Malhotra, and A. J. Rosengren, "Lunar ejecta origin of near-earth asteroid kamo'oalewa is compatible with rare orbital pathways," (2023), arXiv:2304.14136 [astro-ph.EP].
J. D. Castro-Cisneros, R. Malhotra, and A. J. Rosengren, Icarus **429**, 116379 (2025), arXiv:2410.05428 [astro-ph.EP].
Y. Jiao, B. Cheng, Y. Huang, E. Asphaug, B. Gladman, R. Malhotra, P. Michel, Y. Yu, and H. Baoyin, Nature Astronomy **8**, 819–826 (2024).
T. Zhang, X. Kun, and D. Xilun, Nature Astronomy **5**, 730–731 (2021).
C. Venigalla, N. Baresi, J. D. Aziz, B. Bercovici, D. N. Brack, A. Dahir, S. De Smet, J. Fulton, M. M. Pellegrino, and S. Van wal, Journal of Spacecraft and Rockets **56**, 1121 (2019).
J. D. Giorgini, D. K. Yeomans, A. B. Chamberlin, P. W. Chodas, R. A. Jacobson, M. S. Keesey, J. H. Lieske, S. J. Ostro, E. M. Standish, and R. N. Wimberly, in *AAS/Division for Planetary Sciences Meeting Abstracts #28*, AAS/Division for Planetary Sciences Meeting Abstracts, Vol. 28 (1996) p. 25.04.
H. Rein and D. S. Spiegel, MNRAS **446**, 1424 (2015), arXiv:1409.4779 [astro-ph.EP].
U. B. Marvin, Geophysical Research Letters **10**, 775 (1983).
J. N. Head, H. J. Melosh, and B. A. Ivanov, Science **298**, 1752 (2002), https://www.science.org/doi/pdf/10.1126/science.1077483.
G. D. Bart and H. Melosh, Icarus **209**, 337 (2010).
H. J. Melosh, Geology **13**, 144 (1985), https://pubs.geoscienceworld.org/gsa/geology/article-pdf/13/2/144/3507836/i0091-7613-13-2-144.pdf.
K. N. Singer, B. L. Jolliff, and W. B. McKinnon, Journal of Geophysical Research: Planets **125**, e2019JE006313 (2020), https://agupubs.onlinelibrary.wiley.com/doi/pdf/10.1029/2019JE006313.
T. Morota, J. Haruyama, H. Miyamoto, C. Honda, M. Ohtake, Y. Yokota, T. Matsunaga, N. Hirata, H. Demura, H. Takeda, Y. Ogawa, and J. Kimura, Meteoritics & Planetary Science **44** (2009).
S. Mazrouei, R. R. Ghent, W. F. Bottke, A. H. Parker, and T. M. Gernon, Science **363**, 253 (2019), https://www.science.org/doi/pdf/10.1126/science.aar4058

This paper was built using the Open Journal of Astrophysics LaTeX template. The OJA is a journal which provides fast and easy peer review for new papers in the astro-ph section of the arXiv, making the reviewing process simpler for authors and referees alike. Learn more at http://astro.theoj.org.

4.4 Certificado XXV Escola de Verão em Dinâmica Orbital e Planetologia

25ª ESCOLA DE VERÃO
EM DINÂMICA ORBITAL E PLANETOLOGIA
22 a 26 de fevereiro de 2021
UNESP/FEG - Guaratinguetá-SP

Certifico que

RICARDO MORAES

participou da XXV ESCOLA DE VERÃO EM DINÂMICA ORBITAL E PLANETOLOGIA, realizada de maneira remota no período de 22 a 26 de fevereiro de 2021 na UNESP - Campus de Guaratinguetá e apresentou a palestra intitulada

EXOPLANETAS.

Prof. Dr. Valerio Carruba
Coordenador da XXV Escola de Verão
em Dinâmica Orbital e Planetologia

unesp

4.5 Certificado XX Colóquio Brasileiro de Dinâmica Orbital

XX Colóquio Brasileiro de Dinâmica Orbital, CBD0 2020/2021
Universidade Federal do ABC, UFABC, de 6 a 10 de dezembro de 2021
São Bernardo do Campo, SP, Brasil

CERTIFICADO

Certificamos que Ricardo A. Moraes (UNESP, Guaratinguetá, SP, Brasil) participou do CBDO 2020 / 2021 e apresentou o trabalho Stable Orbits In the Kepler 1625b Satellite System na categoria Pôster (sessão 7).

São Bernardo do Campo, 31 de janeiro de 2022

P/Comissão Organizadora
Prof. Cristiano Fiorilo de Melo
UFMG - Brasil

4.6 Certificado XXVI Escola de Verão em Dinâmica Orbital e Planetologia

UNIVERSIDADE ESTADUAL PAULISTA
"JÚLIO DE MESQUITA FILHO"

Campus de Guaratinguetá

Guaratinguetá, 25 de Fevereiro de 2022.

CERTIFICADO

O Grupo de Dinâmica Orbital e Planetologia certifica que **Ricardo Aparecido Moraes** apresentou a palestra:

Exoplanetas

na **26ª Escola de Verão em Dinâmica Orbital e Planetologia**, ocorrida na UNESP - Campus de Guaratinguetá, de 21 a 25 de fevereiro de 2022.

Profª Drª Daniela Cardozo Mourão
Organizadora da Escola

4.7 Livro de resumos dos pôsteres XI Taller de Ciencias Planetarias

XI TALLER DE CIENCIAS PLANETARIAS
XI REUNIÃO DE TRABALHO SOBRE CIÊNCIAS PLANETÁRIAS

14 al 18 de Febrero de 2022

Resúmenes de Presentaciones en Poster

Sesión de Posters I

RESUMEN 1

Astrometria das luas galileanas a partir de ocultações estelares.

Bruno Eduardo Morgado[1,2,3], Altair R. Gomes Júnior[4,2], Felipe Braga Ribas[5,3,2], Roberto Vieira Martins[3,2], Josselin Desmars[6,7], Valery Lainey[6], Emiliano D'Aversa[8], Marcelo Assafin[9], Bruno Sicardy[3], Desenvolvedores SORA[1,2,3,4], Observadores[10]

[1] Observatório Nacional, Brasil
[2] LIneA e INCT do e-Universo, Brasil
[3] LESIA, Observatoire de Paris-Meudon, França
[4] Grupo de Dinâmica Orbital e Planetologia - UNESP, Brasil
[5] Universidade Tecnológica Federal do Paraná, Brasil
[6] IMCCE, Observatoire de Paris, França
[7] Polytechnique des Sciences Avancées IPSA, França
[8] IAPS-INAF, Italia
[9] UFRJ/Observatório do Valongo, Brasil
[10] IOTA

afecta la eficiencia del transporte de agua. En este trabajo, se estudian sistemas binarios amplios donde la primaria está rodeada por una nube de cometas. En este escenario, para estimar la tasa de transporte de agua hacia los planetas en la zona más interna del sistema se calcula la probabilidad intrínseca de colisión de estos con los cometas dispersados por las perturbaciones de la binaria. Dado que la probabilidad de recibir una colisión con un cometa es uno de los parámetros que intervienen en el calculo del transporte de agua, es posible calcular la cantidad de agua transportada en diferentes configuraciones.

RESUMEN 34

ÓRBITAS ESTÁVEIS NO SISTEMA DE SATÉLITES DE KEPLER 1625b

Ricardo A. Moraes[1], Gabriel Borderes-Motta[2], Othon C. Winter[1], Julio Monteiro[1]

[1] UNESP, Univ. Estadual Paulista - Grupo de Dinâmica Orbital & Planetologia, Guaratinguetá
[2] Bioengineering and Aerospace Engineering Department, Universidad Carlos III de Madrid, Leganés, 28911, Madrid, Spain

Resumo

Desde que foi proposto o candidato à exolua Kepler 1625b-I mudou a forma com que os sistemas de satélites eram vistos. Por causa de suais características físicas e orbitais não usuais, muitas questões sobre sua origem e estabilidade surgiram. Atualmente já existem estudos dinâmicos suficientes que mostram que se o candidato a satélite for de fato confirmado, ele seria estável. A origem desse candidato também já foi explorada, trabalhos anteriores mostram que a origem mais provável para esse corpo seria a captura gravitacional, apesar de condições para a sua formação *in-situ* também terem sido investigadas. Neste trabalho nós damos um passo além, assumimos que Kepler 1625b-I é de fato uma exolua e estudamos a possibilidade de mais exoluas massivas serem estáveis nesse sistema. Para modelar este cenário nós realizamos simulações numéricas de N-corpos de um sistema que inclui o planeta, Kepler 1625b-I e um satélite extra com as características da Terra. Levando em conta estudos anteriores, os satélites simulados são expostos as forças de maré geradas a partir da interação entre satélites e planeta e as forças gravitacionais que surgem a partir da rotação do planeta. Nossos resultados mostram que esse satélite extra pode ser estável em diferentes regiões do sistema, tal que nenhuma preferência por uma região específica foi encontrada. Ainda, mostramos que a forte atuação da maré planetária sobre os

satélites é um mecanismo importante para se assegurar a estabilidade dos satélites em órbitas quase circulares próximos do planeta, enquanto que ressonâncias de movimento médio entre os satélites garantiram a estabilidade de satélites em órbitas mais distantes do planeta.

RESUMEN 35

Posible resonancia spin-orbita 1:2 en el sistema WASP-167/KELT-13 a partir del análisis de la serie de tiempos fotométrica de TESS

Mario Melita[1,2], Andrea Buccino[1], Luis Mammana[2,3]

[1] Insituto de Astronomía y Física del Espacio, CONICET-UBA, Argentina
[2] Facultad de Ciencias Astronómicas y Geofísicas, UNLP, Argentina
[3] Complejo Astronómico El Leoncito, CONICET-UNLP-UNC-UNSJ, Argentina

Resumen

WASP-167b/KELT-13b es un planeta transitante de tipo Júpiter caliente de radio 1.58 R_J y periodo orbital 2,02d, confirmado por mediciones de velocidad radial, orbitando una estrella de tipo F1V (Temple et al. 2017). Este es un sistema muy peculiar dado que el periodo de rotación intrínseco de la estrella es menor que el del planeta. Nosotros analizamos la serie fotométrica realizada por la misión espacial TESS y encontramos que el periodo de la estrella sería de un valor muy cercano a 1.01d. El periodograma de Lomb-Scargle muestra un pico doble alrededor de ese valor. Para entender la naturaleza de ese doble pico, hemos calculado el periodograma en una ventana que corre sobre la serie de tiempos (running-window”) y encontramos que el periodo de rotación, a su vez, tambien varía periódicamente. En conclusión, hemos encontrado que el sistema se encuentra en una resonancia spin-orbita 1:2, probablemente causada por la interaccion de mareas entre la estrella y el planeta. Pero el comportamiento del periodo intrínseco de rotación de la estrella es complejo, similar al que se evidencia en estudios de la interacción de mareas que consideran la disipación en ambos componentes del sistema (Luna et al. 2020).

Dynamical evolution of close-in binary systems by a super-Earth and its host star. 2020. Luna, S., Navone, H. y Melita M.D. A & A. 641, 109.

WASP-167b/KELT-13b: Joint discovery of a hot Jupiter transiting a rapidly-rotating F1V star. 2017. L.Y. Temple et al. MNRAS, 471, 3, 2743-2752.

4.8 Certificado 2nd International Stardust Conference - STARCON 2

DEPARTMENT OF MECHANICAL & AEROSPACE ENGINEERING

STARDUST

PUSHING THE BOUNDARIES OF SPACE RESEARCH TO SAVE OUR FUTURE

University of Strathclyde Engineering

14th November 2022.

Dr. Ricardo Moraes attended the STARCON 2, the final conference of Stardust Reloaded ITN project organized by the University of Strathclyde (UK) and held at ESA ESTEC (Netherlands) on 7-11 November 2022.

Dr. Moraes presented the regular talk on "*On the Possibility that 2016 HO3 Kamo'oalewa was a Piece of the Moon*".

The conference covered in detail the topics of "Space Traffic Management and Sustainability" and "Exploration of Asteroids" via organising two symposia run in parallel. The activities undertaken by the conference participant correspond to 5 ECTS credits.

____

Prof Massimiliano Vasile
Chair of STARCON 2 conference
Stardust-R Coordinator
University of Strathclyde

European Commission

Horizon 2020
European Union funding
for Research & Innovation

MARIE CURIE ALUMNI

4.9 Certificado XXI Colóquio Brasileiro de Dinâmica Orbital

MINISTÉRIO DA CIÊNCIA, TECNOLOGIA, INOVAÇÕES E COMUNICAÇÕES
INSTITUTO NACIONAL DE PESQUISAS ESPACIAIS

XXI Colóquio Brasileiro de Dinâmica Orbital

Instituto Nacional de Pesquisas Espaciais
São José dos Campos/SP
12 a 16 de dezembro de 2022

CERTIFICADO

*Certifico que **Ricardo A. Moraes**, participou do XXI CBDO, apresentando trabalho na forma de comunicação oral, intitulado "The Dynamics of Co-orbital Giant Exomoons - Applications for the Kepler-1625 b and Kepler-1708 b Satellite Systems".*

São José dos Campos/SP, 16 de dezembro de 2022

Antônio F. Bertachini de A. Prado

Antônio F. Bertachini de A. Prado
Presidente da Comissão Organizadora

INPE - 454

4.10 Comprovante de atividade didática

UNIVERSIDADE ESTADUAL PAULISTA

Câmpus de Guaratinguetá

ATESTADO

ATESTAMOS que o Prof. Dr. Ricardo Aparecido de Moraes, RG 46.803.031-1 - SP, ministrou/ministra aulas aos discentes do Programa de Pós-graduação desta Unidade Universitária, conforme abaixo descrito:

Programa: Física

Disciplina	Ano	Dt.Início	Dt.Término	Curso	Discentes	Hr/Aula
Tópicos Especiais "Formação de Satélites Regulares"	2021	22/03/2021	16/07/2021	MD	2	180
Dinâmica Orbital	2022	16/05/2022	02/09/2022	MD	3	90

Guaratinguetá, 13 de janeiro de 2023

4.11 Comprovante de orientação de Mestrado - Julio Cesar Monteiro dos Santos

UNIVERSIDADE ESTADUAL PAULISTA

Câmpus de Guaratinguetá

ATESTADO

Atestamos que o Prof. Dr. RICARDO APARECIDO DE MORAES, RG nº 46.803.031-1, expedido pela SSP/SP, coorienta o discente abaixo relacionado, em Programa stricto sensu desta Unidade Universitária:

Programa: Física

DISCENTE	CURSO	INÍCIO	SITUAÇÃO
JULIO CESAR MONTEIRO DOS SANTOS	MESTRADO ACADÊMICO	24/03/21	EM ANDAMENTO

Guaratinguetá, 27 de setembro de 2021.

4.12 Comprovante de participação em banca de defesa de Mestrado - Julio Cesar Monteiro dos Santos

A T E S T A D O

Atestamos que o Prof. Dr. **Ricardo Aparecido de Moraes**, do(a) Departamento de Matemá tica / Faculdade de Engenharia de Guaratinguetá UNESP, participou em 09 de maio de 2022, como COORIENTADOR e MEMBRO CONVIDADO da Comissão Examinadora da DEFESA DE DISSERTAÇÃO de JULIO CESAR MONTEIRO DOS SANTOS, discente regular do Programa de Pós-Graduação em Física, Curso de Mestrado Acadêmico, cujo trabalho se intitula **Fluxo de Material para o Disco Circumplanetário Necessário para a Formação de Satélites de Planetas Gigantes**. A Comissão Examinadora foi constituída pelos seguintes membros:

1. Prof. Dr. ERNESTO VIEIRA NETO (Orientador - Participação Virtual)
 Departamento de Matemática / Faculdade de Engenharia de Guaratinguetá UNESP
2. Dr. RAFAEL RIBEIRO DE SOUSA (Participação Virtual)
 Departamento de Matemática / Faculdade de Engenharia de Guaratinguetá
3. Prof. Dr. FERNANDO VIRGILIO ROIG (Participação Virtual)
 Observatório Nacional

Guaratinguetá, 09 de maio de 2022.

Renata Pereira da Rocha Barbosa
Seção Técnica de Pós-graduação
Supervisora Técnica de Seção

4.13 Comprovante de participação em banca de qualificação de Doutorado - Tiago Francisco Lins Leal Pinheiro

A T E S T A D O

Atestamos que o Dr. **RICARDO APARECIDO DE MORAES**, do(a) Departamento de Matemática / Faculdade de Engenharia de Guaratinguetá, participou em 29 de setembro de 2022, como MEMBRO TITULAR da Comissão Examinadora do Exame de QUALIFICAÇÃO de TIAGO FRANCISCO LINS LEAL PINHEIRO, discente regular do Programa de Pós-Graduação em Física, Curso de Doutorado, cujo trabalho se intitula **Constraining the nature of the nature of the possible extrasolar PDS110b ring system** . A Comissão Examinadora foi constituída pelos seguintes membros:

1. Prof. Dr. RAFAEL SFAIR DE OLIVEIRA (Orientador - Participação Virtual)
   Departamento de Matematica / Faculdade de Engenharia de Guaratingueta
2. Dr. RICARDO APARECIDO DE MORAES (Participação Virtual)
   Departamento de Matemática / Faculdade de Engenharia de Guaratinguetá
3. Prof. Dr. GUSTAVO BENEDETTI ROSSI (Participação Virtual)
   Departamento de Matemática / Faculdade de Engenharia de Guaratinguetá

Guaratinguetá, 29 de setembro de 2022.

Rodrigo José Nunes
Seção Técnica de Pós-graduação
Supervisor Técnico de Seção

Referências Bibliográficas

Alvarado-Montes, J. A., Zuluaga, J. I., and Sucerquia, M. (2017). The effect of close-in giant planets' evolution on tidal-induced migration of exomoons. *MNRAS*, 471(3):3019–3027.

Barclay, T., Rowe, J. F., Lissauer, J. J., Huber, D., Fressin, F., Howell, S. B., Bryson, S. T., Chaplin, W. J., Désert, J.-M., Lopez, E. D., Marcy, G. W., Mullally, F., Ragozzine, D., Torres, G., Adams, E. R., Agol, E., Barrado, D., Basu, S., Bedding, T. R., Buchhave, L. A., Charbonneau, D., Christiansen, J. L., Christensen-Dalsgaard, J., Ciardi, D., Cochran, W. D., Dupree, A. K., Elsworth, Y., Everett, M., Fischer, D. A., Ford, E. B., Fortney, J. J., Geary, J. C., Haas, M. R., Handberg, R., Hekker, S., Henze, C. E., Horch, E., Howard, A. W., Hunter, R. C., Isaacson, H., Jenkins, J. M., Karoff, C., Kawaler, S. D., Kjeldsen, H., Klaus, T. C., Latham, D. W., Li, J., Lillo-Box, J., Lund, M. N., Lundkvist, M., Metcalfe, T. S., Miglio, A., Morris, R. L., Quintana, E. V., Stello, D., Smith, J. C., Still, M., and Thompson, S. E. (2013). A sub-Mercury-sized exoplanet. *Nature*, 494(7438):452–454.

Barnes, J. W. and O' Brien, D. P. (2002). Stability of satellites around close-in extrasolar giant planets. *ApJ*, 575:1087–1093.

Ben-Jaffel, L. and Ballester, G. E. (2014). Transit of exomoon plasma tori: New diagnosis. *ApJL*, 785:L30.

Bennett, D. P., Batista, V., Bond, I. A., Bennett, C. S., Suzuki, D., Beaulieu, J.-P., Udalski, A., Donatowicz, J., Bozza, V., Abe, F., Botzler, C. S., Freeman, M., Fukunaga, D., Fukui, A., Itow, Y., Koshimoto, N., Ling, C. H., Masuda, K., Matsubara, Y., Muraki, Y., Namba, S., Ohnishi, K., Rattenbury, N. J., Saito, T., Sullivan, D. J., Sumi, T., Sweatman, W. L., Tristram, P. J., Tsurumi, N., Wada, K., Yock, P. C. M., MOA Collaboration, Albrow, M. D., Bachelet, E., Brillant, S., Caldwell, J. A. R., Cassan, A., Cole, A. A., Corrales, E., Coutures, C., Dieters, S., Dominis Prester, D., Fouqué, P., Greenhill, J., Horne, K., Koo, J.-R., Kubas, D., Marquette, J.-B., Martin, R., Menzies, J. W., Sahu, K. C., Wambsganss, J., Williams, A., Zub, M., PLANET Collaboration, Choi, J. Y., DePoy, D. L., Dong, S., Gaudi, B. S., Gould, A., Han, C., Henderson, C. B., McGregor, D., Lee, C.-U., Pogge, R. W., Shin, I.-G., Yee, J. C., μFUN Collaboration, Szymański, M. K., Skowron, J., Poleski, R., Kozłowski, S., Wyrzykowski, Ł., Kubiak, M., Pietrukowicz, P., Pietrzyński, G., Soszyński, I., Ulaczyk, K., OGLE Collaboration, Tsapras, Y., Street, R. A., Dominik, M., Bramich, D. M., Browne, P., Hundertmark, M., Kains, N., Snodgrass, C., Steele, I. A., RoboNet Collaboration, Dekany, I., Gonzalez, O. A., Heyrovský, D., Kandori, R., Kerins, E., Lucas, P. W., Minniti, D., Nagayama, T., Rejkuba, M., Robin, A. C., and Saito, R. (2014). Moa-2011-blg-262lb: A sub-earth-mass moon orbiting a gas giant primary or a high velocity planetary system in the galactic bulge. *ApJ*, 785:155.

Blanco-Cuaresma, S. and Bolmont, E. (2017). Studying Tidal Effects In Planetary Systems With Posidonius. A N-Body Simulator Written In Rust. In *EWASS Special Session 4 (2017): Star-planet interactions (EWASS-SS4-2017)*.

Bolmont, E., Raymond, S. N., Leconte, J., Hersant, F., and Correia, A. C. M. (2015). Mercury-T: A new code to study tidally evolving multi-planet systems. Applications to Kepler-62. *A & A*, 583:A116.

Chodas, P. (2016). The Orbit and Future Motion of Earth Quasi-Satellite 2016 HO3. In *AAS/Division for Planetary Sciences Meeting Abstracts #48*, volume 48 of *AAS/Division for Planetary Sciences Meeting Abstracts*, page 311.04.

de la Fuente Marcos, C. and de la Fuente Marcos, R. (2016). Asteroid (469219) 2016 HO_3, the smallest and closest Earth quasi-satellite. *MNRAS*, 462(4):3441–3456.

Fox, C. and Wiegert, P. (2021). Exomoon candidates from transit timing variations: eight kepler systems with ttvs explainable by photometrically unseen exomoons. *MNRAS*, 501(2):2378–2393.

Greenberg, R. (1974). The role of saturn's oblateness in the mimas-tethys resonance. *Symposium - International Astronomical Union*, 62:71–76.

Heller, R., Rodenbeck, K., and Bruno, G. (2019). An alternative interpretation of the exomoon candidate signal in the combined kepler and hubble data of kepler-1625. *A & A*, 624:A95.

Hippke, M. (2015). On the detection of exomoons: A search in kepler data for the orbital sampling effect and the scatter peak. *ApJ*, 806:51.

Kipping, D., Bryson, S., Burke, C., Christiansen, J., Hardegree-Ullman, K., Quarles, B., Hansen, B., Szulágyi, J., and Teachey, A. (2022). An exomoon survey of 70 cool giant exoplanets and the new candidate Kepler-1708 b-i. *Nature Astronomy*, 6:367–380.

Kipping, D. M., Bakos, G. Á., Buchhave, L., Nesvorný, D., and Schmitt, A. (2012). The Hunt for Exomoons with Kepler (HEK). I. Description of a New Observational project. *ApJ*, 750(2):115.

Lewis, K. M., Ochiai, H., Nagasawa, M., and Ida, S. (2015). Extrasolar binary planets ii: Detectability by transit observations. *ApJ*, 805:27.

Moraes, R. A., Borderes-Motta, G., Winter, O. C., and Monteiro, J. (2022). On the stability of additional moons orbiting Kepler-1625 b. *MNRAS*, 510(2):2583–2596.

Moraes, R. A. and Vieira Neto, E. (2020). Exploring formation scenarios for the exomoon candidate kepler 1625b i. *MNRAS*, 495(4):3763–3776.

Oza, A. V., Johnson, R. E., Lellouch, E., Schmidt, C., Schneider, N., Huang, C., Gamborino, D., Gebek, A., Wyttenbach, A., Demory, B.-O., Mordasini, C., Saxena, P., Dubois, D., Moullet, A., and Thomas, N. (2019). Sodium and potassium signatures of volcanic satellites orbiting close-in gas giant exoplanets. *ApJ*, 885(2):168.

Rein, H. and Liu, S. F. (2012). REBOUND: an open-source multi-purpose N-body code for collisional dynamics. *A & A*, 537:A128.

Sharkey, B. N. L., Reddy, V., Malhotra, R., Thirouin, A., Kuhn, O., Conrad, A., Rothberg, B., Sanchez, J. A., Thompson, D., and Veillet, C. (2021). Lunar-like silicate material forms the Earth quasi-satellite (469219) 2016 HO_3 Kamo'oalewa. *Communications Earth and Environment*, 2(1):231.

Singer, K. N., Jolliff, B. L., and McKinnon, W. B. (2020). Lunar secondary craters and estimated ejecta block sizes reveal a scale-dependent fragmentation trend. *Journal of Geophysical Research: Planets*, 125(8):e2019JE006313.

Sucerquia, M., Ramírez, V., Alvarado-Montes, J. A., and Zuluaga, J. I. (2020). Can close-in giant exoplanets preserve detectable moons? *MNRAS*, 492(3):3499–3508.

Teachey, A., Kipping, D. M., and Schmitt, A. R. (2018). Hek. vi. on the dearth of galilean analogs in kepler, and the exomoon candidate kepler-1625b i. *AJ*, 155:36.